MASTERARBEIT | MASTER'S THESIS

Titel | Title

Genetic Insights into Sulfobacin Biosynthesis in *Flavobacterium johnsoniae*

verfasst von | submitted by

Theresa Heidi Villunger BSc

angestrebter akademischer Grad | in partial fulfilment of the requirements for the degree of

Master of Science (MSc)

Wien | Vienna, 2026

Studienkennzahl lt. Studienblatt | degree programme code as it appears on the student record sheet:	UA 066 838
Studienrichtung lt. Studienblatt | degree programme as it appears on the student record sheet:	Masterstudium Ernährungswissenschaften
Betreut von | Supervisor:	Univ.-Prof. Dipl.-Biol. Dr. Alexander Loy

Acknowledgements

First, I sincerely thank Prof. Alexander Loy for giving me the opportunity to pursue my master's thesis in his group and to be part of this interesting project. I am very grateful for the scientific discussions, constructive feedback, and the inspiring research environment he created.

I also want to express my gratitude to my direct supervisor, Sebastian Tanabe, for his continuous support throughout this project. His patience, guidance, dedication to discussing ideas and troubleshooting experiments were invaluable. Beyond the technical skills and microbiology knowledge that I gained, he taught me to think more critically and approach scientific questions with greater depth. I am truly thankful for his encouragement and constant support.

I would also like to thank all members of the Loy Group for the inspiring discussions during gorup meetings, the collaborative atmosphere, and the many moments of laughter that made everyday lab life so enjoyable.

I want to thank Clara Priemer for her support with the LC-MS/MS measurement and her helpful input.

I would also like to sincerely thank Lea Arneth for her help with primer design and for her support and companionship as my lab partner throughout this project.

Finally, I am deeply grateful to my fellow master's students, who were always ready to listen to both the successes and setbacks of lab life. A special thank you to Lea, Sara, and Max for their encouragement, support, and friendship throughout this journey.

Abstract

Sulfobacins are bacteria-derived bioactive sulfonolipids that suppress inflammation and macrophage polarization in the mammalian gut, indicating an immunomodulatory function. Moreover, they are essential for gliding motility in *Flavobacterium johnsoniae* and induce multicellularity in choanoflagellates. Sulfobacins are structurally related to ceramides, a subclass of sphingolipids characterized by a serine-derived amino alcohol backbone (sphinganine) that is N-acylated to a fatty acid. Ceramides act as bioactive signaling molecules in eukaryotes, and related sphingolipids are also produced by certain gut bacteria. Sulfobacins are formed by N-acylation of a capnine base, the sulfonated analog of sphinganine. The initial steps of this pathway involve the condensation of cysteate with an acyl-carrier protein catalyzed by cysteate acyl-ACP transferase (SulA) and the reduction of 3-ketocapnine to capnine by dehydrocapnine reductase. However, the enzymes required for the final synthesis of sulfobacins from capnine remain unknown. The aim of this thesis was to characterize the yet unknown genes involved in sulfobacin biosynthesis using *Flavobacterium johnsoniae*, a genetically accessible model organism. Comparative genomics of bacterial ceramide pathways suggested the presence of two cysteate synthase genes and a potential sulfobacin synthase gene catalyzing N-acylation of the capnine base. In addition, two putative monooxygenases were identified as candidate genes involved in the biosynthesis of a hydroxylated sulfobacin variant. To test the function of the proposed genes, markerless deletion and frameshift mutants of *F. johnsoniae* were generated. Lipid extracts from deletion mutants were analyzed by lipidomics, and gliding motility phenotypes were evaluated microscopically. Gliding motility was completely lost in the putative sulfobacin synthase mutant strain. Lipidomic profiling confirmed the absence of sulfobacins and accumulation of the precursor capnine in the sulfobacin synthase mutant, supporting the role of the deleted gene in sulfobacin biosynthesis. In contrast, monooxygenase mutants retained sulfonolipid production despite impaired motility. In conclusion, this work identifies a previously unknown key enzyme in sulfobacin biosynthesis, a putative sulfobacin synthase, which is essential for gliding motility in *F. johnsoniae.*

Contents

List of abbreviations

Abbreviation	Definition
ACP	acyl carrier protein
bp	base pairs
bCers	bacterial ceramide synthase
DES2	Sphingolipid delta(4)-desaturase/C4-monooxygenase
CerH	ceramide hydroxylase
CerR	ceramide reductase
CYE	casitone yeast extract
LB	lysogeny broth
LPS	lipopolysaccharide
PLP	pyridoxal phosphate
RIF 1	rosette inducing factor 1
RIF 2	rosette inducing factor 2
Spt	serine palmitoyltransferase
SulA	cysteate acyl-ACP transferase
Ta	annealing temperature
Tm	melting temperature
TLR4	toll like receptor 4

1. Introduction

This work aimed to elucidate sulfobacin biosynthesis pathway in *F. johnsoniae*. Sulfobacins are sulfonolipids found in bacterial membranes that exhibit immunomodulatory effects in the mammalian gut. Understanding how these compounds are produced enables the identification of bacterial taxa capable of their synthesis and facilitates the quantification of sulfobacins in the mammalian gut. Furthermore, this knowledge will provide a foundation for identifying the ecological niches in which sulfobacin-producing bacteria are present and whether sulfonolipids can exert their biological activity in these unique environments.

The human gastrointestinal tract harbors trillions of microorganisms consisting of bacteria, fungi, viruses, archaea and protozoa. Among these, bacteria constitute the dominant fraction of the gut microbiome, accounting for the majority of microbial biomass in the intestine. This microbial community exists in a symbiotic relationship with the host and is essential for human health (Safarchi et al., 2025, Sender et al., 2016). Disruptions in this balanced microbial ecosystem can lead to dysbiosis, which is characterized by a decrease in beneficial microbes and an increased abundance of pathogens. Gut microbiota dysbiosis has been associated with a wide range of diseases, including metabolic, inflammatory, and immune-mediated disorders. In chronic inflammatory diseases, such as inflammatory bowl disease, dysbiosis is a critical factor in development and progression of the disease (Safarchi et al., 2025). By driving changes in microbial community composition, dysbiosis is accompanied by alterations in the availability of microbial derived metabolites. Over the past two decades, a large body of research has demonstrated that metabolites generated by the gut microbiota can act as signaling molecules that influence immune cell development and homeostasis, the regulation of host energy metabolism, and maintenance of intestinal barrier integrity (Lavelle and Sokol, 2020). Such metabolites include short chain fatty acids, bile acid derivatives and bacterial membrane lipids. These compounds arise from diverse processes, such as microbial transformation of dietary components and *de novo* synthesis by bacteria (Lavelle and Sokol, 2020, Ryan et al., 2023). While research has largely focused on soluble microbial metabolites, such as short chain fatty acids and bile acid derivatives, increasing evidence suggests that bacterial membrane lipids contribute to intestinal homeostasis through structure-specific interactions with host cells and immune receptors (Older et al., 2024, An et al., 2014).

Membrane-associated lipids represent a highly diverse group of molecules and can be classified based on their chemical structure and biosynthetic origins (Ryan et al., 2023). Major lipid classes include glycerophospholipids, fatty acyls, glycerolipids, and sphingolipids, each composed of different subclasses (Liebisch et al., 2020). In the well studied model organism *Escherichia coli*, membranes are primarily composed of the glycerolphospholipids phosphatidylethanolamine, phosphatidylglycerol and cardiolipin, with posphatidylethanolamin representing the major lipid fraction (Raetz and Dowhan, 1990). However, bacterial membrane composition varies widely across taxa, and many bacteria synthesize structurally distinct lipids, including phosphorus-free membrane lipids (Ryan et al., 2023).

1.1. Sulfonolipids as a distinct class of bacterial membrane lipids

Among these lipid classes mentioned above, sulfonolipids represent a unique subclass of sphingolipids and belong to the group of amino acid–derived membrane lipids. While sphingolipids are ubiquitous in eukaryotic cellular membranes, their occurrence in bacteria seems to be restricted to members of the phylum Bacteroidota and certain Proteobacteria (Kawahara et al., 2000,Brown et al., 2019, Stankeviciute et al., 2022). Sphingolipids are characterized by a long-chain amino alcohol backbone, named sphinganine, that is amide-linked to a fatty acyl chain. After N-acylation of sphinganine, dihydroceramide forms the core structure of many bacterial sphingolipids and can undergo further modifications, including hydroxylation, branching of acyl chains, and the addition of diverse headgroups (Harrison et al., 2018). Beyond their structural role in membranes, eukaryotic sphingolipids act as important signaling molecules with central roles in regulating inflammation, immunity, autophagy, growth, and cell survival (Maceyka and Spiegel, 2014). Although the functions of sphingolipids in bacteria are not yet fully understood, studies in *Bacteroides* demonstrate that these lipids are essential for appropriate stress responses and bacterial persistence (An et al., 2011). Additionally, bacterial sphingolipids produced by gut strains have been shown to contribute to the maintenance of intestinal homeostasis by influencing the number and function of invariant natural killer T cells during early life. Proper regulation of these immune cells is important in limiting susceptibility to intestinal inflammation (An et al., 2014).

The structurally distinct subclass of sulfonolipids has attracted increasing interest in gut microbiome research, as these lipids are produced by certain gut bacteria and potentially have an immunomodulatory effect on the host (Ryan et al., 2023, Walker et al., 2017). Sulfonolipids are characterized by a long chain base, that contains cysteate rather than a serine-derived functional group typical for sphingolipids (Abbanat et al., 1985). Structurally, they are formed by N-acylation of capnine (2-amino-3-hydroxy-15-methylhexadecane-1-sulfonic acid), resulting in amphiphilic molecules with a conserved sulfonated backbone (White, 1984,Kamiyama et al., 1995). Structural diversity within this lipid class arises primarily from variations in the length and branching of the N-acyl chain, as well as from differences in hydroxylation and desaturation of the lipid backbone (Walker et al., 2017). To date, their occurrence appears to be re-

stricted to members of the phylum Bacteroidota, where they are represented by sulfobacins and related derivatives (Godchaux and Leadbetter, 1984, Alegado et al., 2012, Liu et al., 2022, Hou et al., 2022, Walker et al., 2017). Sulfobacins have been detected in the membrane of the *Cytophaga-Flavobacteria* group, the genus of *Capnocytophaga* and in gut associated genera, like *Alistipes* and *Odoribacter* (Abbanat et al., 1986, Radka et al., 2020, Walker et al., 2017). More recently, they have been isolated from the opportunistic pathogen *Chryseobacterium gleum* and the potentially food spoiling *Chryseobacterium capnotolerans* (Hou et al., 2022, Heidler von Heilborn et al., 2022).

Sulfobacin A and B were identified in *Flavobacterium sp.* (Kamiyama et al., 1995), followed shortly by the discovery of structurally related flavochristamides in marine isolates (Kohayashi et al., 1995). Sulfobacin B consists of a saturated C15 fatty acyl chain with iso-methyl branching, linked to an unmodified capnine base. Sulfobacin A and flavochristamides contain a C16 iso-branched acyl chain that is hydroxylated at C3. Flavochristamide A additionally contains a double bond at C4 of the capnine base, introducing a desaturation into the backbone (Kamiyama et al., 1995), Kohayashi et al., 1995). More recently, four additional sulfobacin variants were isolated and characterized in *Algoriphagus machipongonensis*, which were named sulfobacin C-F. Sulfobacin C differs from sulfobacin B by a one-carbon-shortened capnine backbone. Sulfobacin D represents a hydroxylated derivative of sulfobacin B, whereas sulfobacin E corresponds to the hydroxylated analog of sulfobacin C. In both compounds, the hydroxyl group is located at C2 of the acyl chain. Sulfobacin F combines C2 hydroxylation of the acyl chain and a C4 double bond within the capnine backbone (Beemelmanns et al., 2014). In addition, the rosette inducing factors RIF-1 and RIF-2 represent more complex sulfonolipids with increased degrees of hydroxylation and desaturation. In both molecules, the C15 acyl chain is hydroxylated at C3, while two hydroxyl groups are positioned on the capnine backbone. RIF-1 additionally contains a double bond in the capnine backbone (Alegado et al., 2012, Leichnitz et al., 2022). Together, these compounds illustrate substantial structural diversity within the sulfonolipid class, while maintaining a conserved capnine-based architecture.

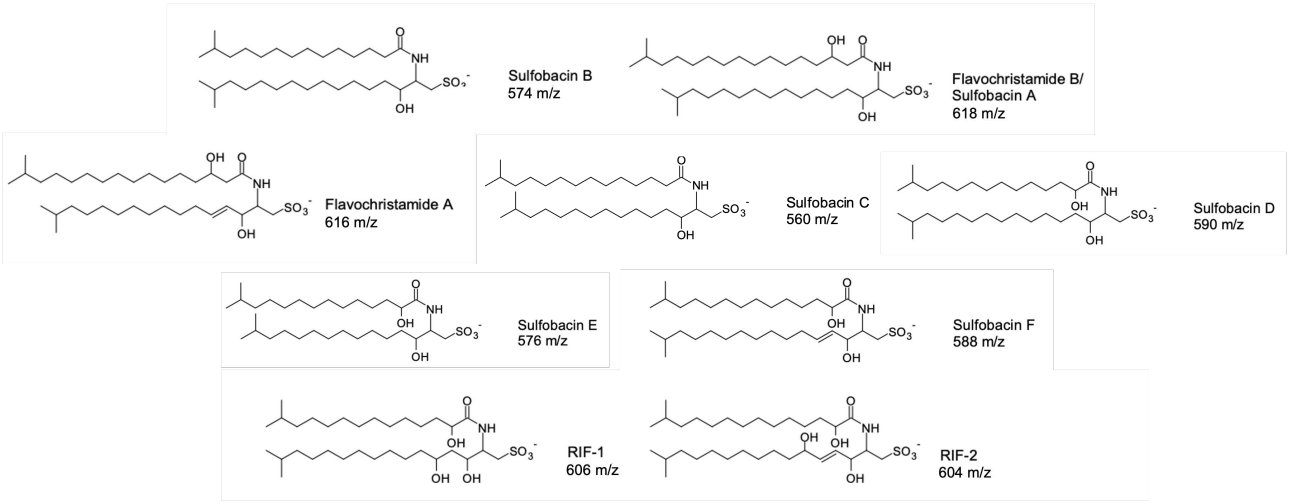

Figure 1.: **Structures and masses of the sulfobacins A-F, flavochristamide A, flavochristamide B and the rosette inducing factors RIF-1 and RIF-2** .

1.2. Sulfobacins as bioactive molecules

Among the best-characterized members of the sulfonolipid class are sulfobacin A and sulfobacin B, which have been associated with a variety of biological activities. Both were initially found during an antagonist screening for von Willebrand factor receptors, which play a central role in platelet aggregation and thrombosis in the host. In this context, sulfobacin A was demonstrated to inhibit platelet aggregation and blood clotting in *ex vivo* assays (Kamiyama et al., 1995).

In addition to these effects, emerging evidence suggests a role for sulfobacins in host–microbe immune interactions. Sulfobacin A and B have been shown to modulate host immune responses through interaction with Toll-like receptor 4 (TLR4) (Older et al., 2024). TLR4 is a key pattern recognition receptor activated by lipopolysaccharides (LPS), a key component of Gram-negative bacterial membranes, leading to nuclear factor-kappa B activation and the production of pro-inflammatory cytokines (Fitzgerald and Kagan, 2020). Mechanistically, sulfobacins act as antagonists of TLR4 signaling by binding to the TLR4 co-receptor myeloid differentiation factor 2, thereby displacing LPS and preventing receptor activation. This interaction results in a marked reduction of LPS-induced inflammatory signaling and suppresses macrophage polarization towards a pro-inflammatory M1 phenotype *in vitro* (Older et al., 2024). Consistent with these mechanistic findings, a negative correlation between sulfobacin production and colitis progression in a mouse model was reported, with sulfobacin A and B being significantly reduced in fecal samples of diseased mice compared to healthy controls (Older et al., 2024). These observations were further supported by a more recent study demonstrating that administration of sulfobacin B attenuated colitis severity in a mouse model of inflammatory bowel disease, providing functional evidence for its anti-inflammatory potential. Additionally, sulfobacins were detected in the bloodstream of mice, and subsequent analysis indicated that microbially derived sulfobacins can be transported systemically via

bacterial outer membrane vesicles, highlighting a potential mechanism by which gut-derived sulfobacins exert immunomodulatory effects beyond the intestinal lumen (Older et al., 2025). These observations suggest that sulfobacins can influence inflammatory processes in the mammalian gut, supporting their emerging role as microbially derived bioactive molecules.

Apart from mammalian immune modulation, sulfonolipids have also been implicated in host–microbe interactions in evolutionary distinct systems. The rosette inducing factors RIF-1 and RIF-2, produced by *Algoriphagus machipongonensis*, have been shown to induce multicellular rosette formation in choanoflagellates, the closest living relatives of animals (Alegado et al., 2012, Leichnitz et al., 2022). This process represents a regulated transition from a unicellular lifestyle to a coordinated multicellular organization and is therefore widely used as a model for studying mechanisms relevant to the evolution of animal multicellularity (Ros-Rocher et al., 2021). In a subsequent study, the effects of structural analogs of RIF-1 on rosette formation were investigated, including the sulfobacin variants C-F. None of these compounds induced the development of rosette colonies, suggesting a highly specific substrate-receptor interaction underlying RIF-1 activity (Beemelmanns et al., 2014). However, rosette-inducing capacity has been shown to be antagonized in a dose-dependent manner by sulfobacin D and F (Peng et al., 2023). To date, no biological activity has been reported for sulfobacin C and E, and their bioactive potential therefore remains to be explored (Beemelmanns et al., 2014).
Together, these findings identify sulfobacins as microbially derived bioactive molecules with diverse and highly structure-dependent effects on host physiology. Despite their emerging biological relevance, the molecular mechanisms underlying sulfobacin biosynthesis remain poorly understood.

1.3. Comparison of sphingolipid and sulfonolipid biosynthesis

Sulfonolipids exhibit structural similarities to sphingolipids. Both lipid classes are characterized by a long-chain base that is N-acylated with a fatty acid, resulting in amphiphilic molecules that contribute to membrane organization and bioactivity (Ryan et al., 2023). In bacteria, dihydroceramide represents the core structural unit for more complex sphingolipid species and consists of a sphingoid base N-acylated with a fatty acyl chain (Stankeviciute et al., 2022). Sulfobacin B represents the sulfonolipid counterpart of dihydroceramide consisting of a capnine-base that is N-acylated with an iso-methyl-branched fatty acid. (Kamiyama et al., 1995). Based on their structural similarities it has been suggested that sulfonolipid synthesis follows an analogous biosynthesis pathway to bacterial ceramides. In line with this, genes involved in sulfobacin biosynthesis have recently been identified based on sequence homology to enzymes involved in ceramide synthesis, providing genetic support for an analogous pathway of these lipids (Liu et al., 2022, Radka et al., 2022).

1.3.1. Biosynthesis of bacterial ceramides

Bacterial sphingolipid synthesis is well characterized and serves as a conceptual framework for understanding sulfobacin biosynthesis. The initial step of bacterial ceramide synthesis is catalyzed by serine palmitoyltransferase (Spt), which condenses L-serine with palmitoyl-CoA to yield 3-ketodihydrosphinganine (Ikushiro et al., 2003). Subsequent steps involve the action of a ceramide synthase and a ceramide reductase, ultimately yielding dihydroceramide. Although there is agreement on the identity of the bacterial enzymes involved in the pathway, the exact order of the chemical reactions leading to dihydroceramide formation remains debated. Two mechanisms have been proposed, with one following the well-known eukaryotic pathway for ceramide synthesis (*Figure 2*). Because the first step of sphingolipid biosynthesis is conserved between bacteria and eukaryotes, it has been suggested that subsequent reactions follow the same order. Based on the eukaryotic pathway 3-ketosphinganine is reduced to sphinganine by 3-keto-sphinganine reductase, following addition of the second acyl chain by ceramide synthase (Uchendu et al., 2024). Supporting this model, 3-ketosphinganine reductase has been identified and characterized in *Bacteroides thetaiotaomicron* (Lee et al., 2022). In contrast, studies in *Caulobacter crescentus* suggest that the addition of the second acyl chain precedes the reduction of the long-chain base. This hypothesis was supported by bioinformatic analysis, revealing that ceramide synthase and ceramide reductase show no obvious structural similarity with their eukaryotic counterparts. In this alternative pathway, 3-ketodihydrosphinganine is initially acylated by a bacterial ceramide synthase (bCerS), generating an oxidized ceramide intermediate. Subsequently, the oxidized ceramide is reduced by ceramide reductase (CerR) to yield dihydroceramide (Stankeviciute et al., 2022). Further support for this reaction order comes from the subcellular localization of the enzymes in *Caulobacter crescentus*. Spt and bCerS were found to be cytoplasmic proteins, whereas CerR resides in the periplasm. Considering that sphingolipids are transported to the outer membrane, this spatial organization is consistent with a model in which reduction occurs after addition of the acyl chain (Uchendu et al., 2024). Together, these findings suggest that two possible pathways for bacterial dihydroceramide synthesis exist (Lee et al., 2022;Uchendu et al., 2024). Beyond this core pathway, dihydroceramide can undergo species-specific modifications. In *C. crescentus*, this includes a hydroxylation occurring on C2 of the fatty-acyl chain by ceramide hydroxylase (CerH), producing α-hydroxy-ceramides (Stankeviciute et al., 2022). In eukaryotes and plants a common modification is the addition of a hydroxyl group at the C-4 position of the sphingoid base to form phytoceramides. In human tissue, this modification is made by the bifunctional enzyme DEGS2, which acts as a sphingolipid Δ^4-desaturase and a C4-monooxygenase (Rabionet et al., 2014).

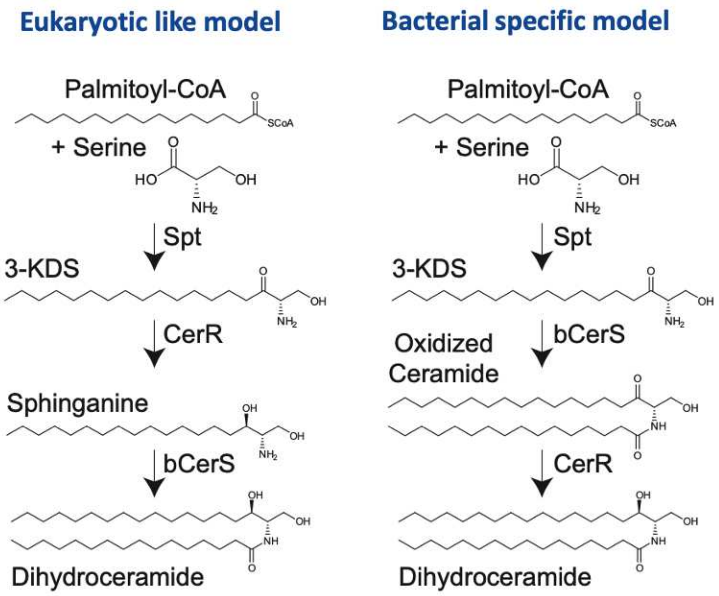

Figure 2.: **Proposed pathways for dihydroceramide synthesis.** Comparison of eukaryotic-like and a bacterial specific ceramide biosynthesis pathway. In the eukaryotic-like model, 3-ketodihydrosphingosine (3-KDS) is reduced to sphinganine prior to acylation by bacterial ceramide synthase (bCerS) to generate dihydroceramide. In the bacterial specific model, acylation precedes reduction, resulting in an oxidized ceramide intermediate before formation of dihydroceramide. Figure was adapted from Uchendu et al., 2024.

1.3.2. Biosynthesis of sulfobacins

In contrast to ceramide biosynthesis, the enzymatic pathway leading to sulfobacins has not yet been fully elucidated. While the formation of the capnine backbone is well described, the enzymatic steps to finally yield sulfobacins have not yet been experimentally confirmed. The known enzymes required for capnine formation include a cysteate synthase, a cysteate acyl-acyl carrier protein (acyl-ACP) transferase, and a 3-ketocapnine reductase (Liu et al., 2022; Radka et al., 2022).

In *Capnocytophaga* species, two proteins essential for sulfonolipid biosynthesis have been identified. CapA, a cysteate synthase, catalyzes the formation of cysteate from O-phospho-L-serine and sulfite using pyridoxal phosphate as a cofactor. The cysteate acyl-ACP transferase CapB subsequently catalyzes the condensation of cysteate with acyl-ACP to form 3-ketocapnine (Liu et al., 2022). Homologs of the CapB gene, encoding the cysteate acyl-ACP transferase *(sulA)*, have been identified in *Flavobacterium johnsoniae* and in the gut bacterium *Alistipes finegoldii*, suggesting that the core steps of sulfonolipid biosynthesis are conserved across different members of the phylum Bacteroidota (Vences-Guzmán et al., 2021; Radka et al., 2022). In *Flavobacterium johnsoniae* the gene fjoh_2419 was identified as a cysteate acyl-ACP transferase and shown to be essential for sulfonolipid production. The candidate gene fjoh_2419 was chosen based on sequence similarity to the serine palmitoyltransferase gene in *Sphingomonas wittichii*, which is responsible for the formation of sphinganine in sphingolipid synthesis (Raman et al., 2010). Deletion of fjoh_2419 completely abolished the synthesis of sulfobacin A and B, while genetic comple-

mentation in *E. coli* led to the production of a capnine like molecule. However, the product of the reaction was not structurally characterized (Vences-Guzmán et al., 2021). More recently, the cysteate acyl-ACP transferase from the gut commensal *Alistipes finegoldii* was biochemically and structurally characterized in detail. X-ray crystallographic analysis revealed that SulA closely resembles bacterial serine palmitoyltransferases (Radka et al., 2022). The final reduction to capnine is mediated by a 3-ketocapnine reductase, CapC, which was identified in *Ornithobacterium rhinotracheale* (Liu et al., 2022). Following capnine formation, N-acylation with different fatty acids leads to the generation of structurally diverse sulfonolipids, such as sulfobacin B and derivates (Radka et al., 2022). Based on structural analogies to ceramides, it has been proposed that the conversion of capnine to sulfobacin B and its hydroxylated variant sulfobacin D is mediated by enzymes functionally analogous to the bacterial ceramide synthase CerS and the eukaryotic sphingolipid delta(4)-desaturase/C4-monooxygenase DES2 (Uchendu et al., 2024, Rabionet et al., 2014).

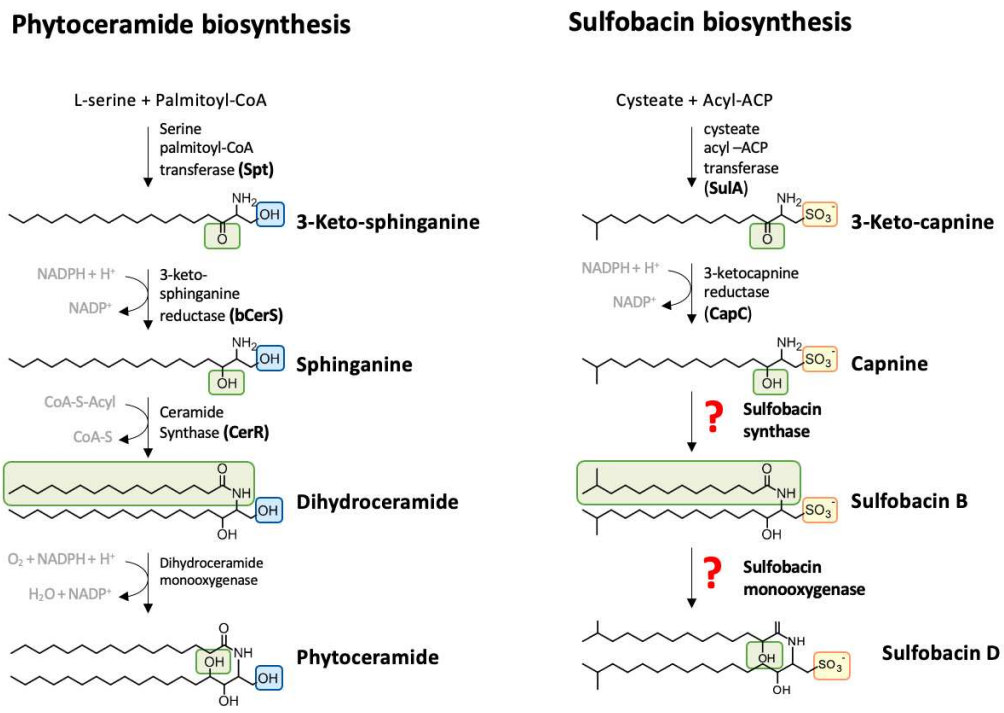

Figure 3.: **Comparison of phytoceramide synthesis and proposed sulfobacin biosynthesis pathway.** In the phytoceramide pathway, L-serine and palmitoyl-CoA are condensed by palmitoyltransferase to form 3-keto-sphinganine, which is reduced to sphinganine by 3-keto-sphinganine reductase. Sphinganine is subsequently acylated by ceramide synthase to generate dihydroceramide, which is hydroxylated by a monooxygenase to yield phytoceramide. In the sulfobacin synthesis pathway, cysteate and acyl-ACP are condensed by cysteate acyl-ACP transferase to form 3-keto-capnine, which is reduced by 3-keto-capnine reductase to capnine. Capnine is further converted into sulfobacin B and D through putative sulfobacin synthase and monooxygenase reactions (Uchendu et al., 2024, Rabionet et al., 2014, Liu et al., 2022).

1.4. Model organism *Flavobacterium johnsoniae*

Flavobacterium johnsoniae is a Gram-negative, obligate aerobe and rod-shaped member of the phylum Bacteroidota. In the last decades, *F. johnsoniae* has become an important model organism for studying

bacterial gliding motility (McBride, 2004). In contrast to well-characterized motile bacteria that rely on flagella or type IV pili, *F. johnsoniae* exhibits gliding motility over solid surfaces via a distinct mechanism that depends on the movement of motility adhesions along the outer membrane. Cells glide rapidly at rates of 2–4 µm/s along their long axis and produce colonies with thin spreading edges (McBride, 2004, Jarrell and McBride, 2008). The development of *F. johnsoniae* as a model organism has been facilitated by its genetic accessibility. Established methods for random and targeted mutagenesis enable functional genetic analysis of motility-associated and metabolic pathways (Braun et al., 2005, Mcbride and Kempf, 1996). In addition, *F. johnsoniae* has a unique membrane composition, where sulfonolipids account for up to 20% of total membrane lipids. These sulfonolipids, including sulfobacins have been shown to be essential for gliding motility. In this context, *F. johnsoniae* has previously been used as a model organism to study sulfobacin biosynthesis pathway (Abbanat et al., 1986, Vences-Guzmán et al., 2021).

1.4.1. Gliding motility in *F. johnsoniae*

Several studies have shown that more than 20 genes are required for gliding motility in *F. johnsoniae* (Braun et al., 2005, Nelson et al., 2008, Shrivastava et al., 2012, Johnston et al., 2018). Many of these *gld* and *spr* genes are unique to members of the phylum Bacteroidota, suggesting that gliding motility in *F. johnsoniae* and related species evolved independently from other bacterial locomotion systems (Braun et al., 2005).

Gliding motility in *F. johnsoniae* is tightly linked to the type IX secretion system, a protein export pathway that transports proteins across the cytoplasmic membrane, through the periplasm, and across the outer membrane to the cell surface. The type IX secretion system is composed of multiple conserved components and is essential for the secretion of the surface adhesins SprB and RemA, which are critical for motility. Proteins named GldK, GldL, GldM, GldN, SprA, SprE, and SprT are required for the secretion of both adhesins (Johnston et al., 2018). In contrast, SprF is required for the secretion of the adhesin SprB but not RemA, whereas PorV is specifically required for RemA secretion (Nelson et al., 2008, Shrivastava et al., 2012). The motility adhesions SprB and RemA are secreted to the cell surface, where they attach as large filamentous proteins (Shrivastava et al., 2015). The exact mechanism by which these adhesions are attached to the outer membrane is unknown. During gliding motility, SprB and RemA interact transiently with the solid substratum, providing traction required for cell movement. These adhesins are propelled along the cell surface along an apparently helical track by components of the gliding motility machinery, such that adhesion of SprB to the surface results in forward translocation of the cell (Johnston et al., 2018, Shrivastava et al., 2015). Although the detailed molecular mechanism of force generation is not fully understood, experimental evidence indicates that the gliding motor has a rotary component. In a previous study, *F. johnsoniae* cells tethered to glass via the adhesin SprB rotated around a fixed point. Subsequent measurements of rotation speed and torque suggested a rotary motor powered by a proton motive force,

which drives the movement of motility adhesions along the cell surface (Shrivastava et al., 2015).

1.4.2. Sulfonolipids as determinants of gliding motility

In addition to this complex gliding machinery, *Flavobacterium johnsoniae* has a unique bacterial membrane composition. The membranes of *F. johnsoniae* are composed of ornithine lipids, the phospholipid phosphatidylethanolamine, sulfonolipids, glycine lipids and seringlycine lipids (flavolipin) (Vences-Guzmán et al., 2021). Among these, sulfobacins are of particular interest because they have been directly linked to gliding motility. The connection between sulfobacins and motility was first demonstrated by Abbanat et al., 1986. Mutants deficient in cysteate formation were unable to synthesize sulfobacins and exhibited a gliding defect. Addition of the sulfobacin precursor L-cysteate restored both sulfobacin synthesis and motility. D-cysteate did not restore gliding motility, suggesting a stereo specific effect of cysteate in sulfonolipid synthesis. Although the genetic basis of these mutants was unknown at the time, these experiments provided early evidence that sulfobacins are essential for gliding motility (Abbanat et al., 1986). A more recent study identified a cysteate-fatty acyl transferase gene fjoh_2419 in *F. johnsoniae*, which is required for synthesis of the sulfobacin precursor capnine. Deletion of cysteate-fatty acyl transferase (fjoh_2419) resulted in loss of sulfobacin production and an immobile phenotype, while expression of the gene in *E. coli* led to the production of a capnine like molecule (Vences-Guzmán et al., 2021). Why sulfonolipids are required for gliding motility remains unknown. However, these findings demonstrate that sulfonolipis are not merely structural membrane components but are required for the function of the gliding motility machinery in *F. johnsoniae*. As sulfonolipid deficiency leads to a detectable loss of gliding motility, *F. johnsoniae* provides a suitable model organism in which mutations in sulfonolipid biosynthesis genes can be identified by phenotypic screening and subsequently characterized at the molecular and biochemical level (Abbanat et al., 1986, Vences-Guzmán et al., 2021).

1.5. Purpose of this work

As introduced above, sulfobacins are a bioactive class of sulfonolipids whose functions extend from bacterial physiology to interactions with the host. Increasing evidence suggests that these microbially derived lipids contribute to immune modulation and signaling in the gastrointestinal tract of mammals, including humans. Despite their potential biological relevance, the biosynthetic pathway responsible for sulfobacin production remains incompletely understood. Although the synthesis of the precursor capnine has been described, a comprehensive genetic and biochemical framework elucidation how these lipids are produced is still lacking.

The aim of this thesis was to elucidate the sulfobacin biosynthesis pathway in *Flavobacterium johnsoniae* by combining genetic, phenotypic, and biochemical approaches. In particular, this thesis sought to address the following research questions:

1. Which gene encodes the enzyme responsible for cysteate synthesis in *F. johnsoniae*?
2. Which enzyme catalyzes the N-acylation step required for the formation of sulfobacin B?
3. Is the hydroxylation of sulfobacins mediated by a monooxygenase?

To answer these questions, candidate genes potentially involved in sulfobacin synthesis were targeted for markerless gene deletions and frameshift mutations in *F. johnsoniae*. Mutants exhibiting defects in gliding motility were further analyzed for alterations in sulfonolipid production using liquid chromatography–tandem mass spectrometry.

By identifying genes required for sulfobacin biosynthesis, this work contributes to the genetic characterization of sulfobacin production and provides a foundation for future studies investigating sulfobacin-producing gut strains and the biological functions of these lipids.

2. Materials and Methods

2.1. Materials

2.1.1. Chemicals

Chemicals were purchased from Thermo Fisher Scientific (Waltham, MA, USA) and Sigma Aldrich (St. Louis, MO, USA). The enzymes used were acquired from New England Biolabs (NEB) (Ipswich, MA, USA) and primers were purchased from biomers.net (Ulm, Germany).

2.1.2. Kits

Table 1.: Used Kits

Kit	Uilization	Producer
Simplex® Easy DNA Extraction Kit	DNA extraction	GEN-IAL® GmbH (Troisdorf, Germany)
innuPREP PCRpure Kit	PCR purification	IST Innuscreen GmbH (Berlin, Germany)
InnuPREP Gel Extraction Kit	DNA gel extraction	AJ Innuscreen GmbH (Berlin, Germany)
NEBuilder® HiFi DNA Assembly	DNA assembly	New England Biolabs (Ipswich, MA, USA)
Monarch® Spin Plasmid Miniprep Kit	plasmid isolation	New England Biolabs (Ipswich, MA, USA)

2.1.3. Devices and Software

Table 2.: Used devices

Device	Producer
Biological Safety Cabinet Class II	LAMSYSTEMS GmbH (Berlin, Germany)
VWR Orbital Shaker 10000-1 ADV	VWR International GmbH (Leuven, Belgium)
T100™ Thermal Cycler	Bio-Rad (Munich, Germany)
Horizontal Gel System	Thermo Fisher Scientific (Waltham, USA)
PowerPac™ Basic Power Supply	Bio-Rad (Munich, Germany)
Gel Doc XR+ Gel Documentation System	Bio-Rad (Munich, Germany)
Centrifuge 5804 R	Eppendorf (Hamburg, Germany)
MiniSpin® Mini Centrifuge	Eppendorf (Hamburg, Germany)
Digital block thermostat LLG-uniBLOCKTHERM	LLG-Labware
Photometer	Thermo Fisher Scientific (Waltham, USA)
THUNDER EPI microscope	Leica Microsystems GmbH (Vienna, Austria)
SONOREX ultrasonic bath	Bandelin electronic GmbH & co. KG (Berlin, Germany)
Freeze dryer Alpha 1-4 LSCbasic	Martin Christ (Osterode, Germany)

Table 3.: Used software

Software	Function	Source
ApE	*in silico* cloning	https://jorgensen.biology.utah.edu/wayned/ape/
NEBuiler Assembly Tool	*in silico* cloning	https://nebuilder.neb.com/
KEGG Genome	Gene sequences	https://www.genome.jp/kegg/genome/
Clustal Omega	Multiple sequence alignment	https://www.ebi.ac.uk/jdispatcher/msa/clustalo
Reverse Complement	sequencing analysis	https://reverse-complement.com/
RStudio	statistical analysis	Scientific and Educational Software
Microsoft Office	Editing pictures	Microsoft Corporation
Skyline	LC/MS Analysis	https://skyline.ms/home/software/Skyline/

2.1.4. Strains, Plasmid and Primers

Table 4.: Used strains

Strain	Genotype	Reference
E. coli 10 β	Δ(ara-leu) 7697 araD139 fhuA ΔlacX74 galK16 galE15 e14- ϕ80dlacδM15 recA1 relA1 endA1 nupG rpsL (StrR) rph spoT1 Δ(mrr-hsdRMS-mcrBC)	New England Biolabs (Ipswich, MA, USA)
E. coli S17-1 λ pir	(F-) RP4-2-Tc::Mu aphA::Tn7 recA λpir lysogen	Ferrières et al., 2010
F. johnsoniae UW101	wild type	McBride et al., 2009

Table 5.: Used plasmid

Plasmid	Feature	Reference
pYT313	*oriT, pompA, sacB, ermF, bla, oriV*	Zhu et al., 2017

Table 6.: primers used for screening

Primer	Sequence (5' $\rightarrow$ 3')	T_a (°C)	T_m (°C)	Reference
SacB_fwd	CGCTTGAGGTACAGCGAAGTG	40	55	Lea Arneth, unpublished
SacB_rev	GAACATCAACGGTGTAGAG	40	42	Lea Arneth, unpublished

Table 7.: Primers used for markerless deletions

Primer	Sequence (5' overlap/ANNEAL 3')	T_{a} (°C)	T_{m} (°C)	Reference
fjoh1748_up_fwd	attcgggggatcctctagagGGATCCGTTGGCTTAAC	58	74	Sebastian Tanabe, unpublished
fjoh1748_up_rev	gaagtgagcagcaacggcgcGAGCCGTGTTATTCATAATTG	58	79	Sebastian Tanabe, unpublished
fjoh1748_down_fwd	aattatgaataacacggctcGCGCCGTTGCTGCTC	68	75	Sebastian Tanabe, unpublished
fjoh1748_down_rev	gattacgccaagcttgcatgCCCCAGGCATATTCGGC	68	79	Sebastian Tanabe, unpublished
fjoh1927_up_fwd	attcgggggatcctctagagTACAAGGTGATGATATTGCG	50	67	This study
fjoh1927_up_rev	ggattaaagttttatttataagcctaCATTTTATTTAAGTTTAATGTGG	50	59	This study
fjoh1927_down_fwd	ccacattaaacttaaataaaatgTAGGCTTATAAATAAAACTTTAATCC	56	58	This study
fjoh1927_down_rev	gattacgccaagcttgcaTGCTTATGTTGGTTTTGATGC	56	67	This study
fjoh2419_up_fwd	attcgggggatcctctagagGTTACAGGCGATTTAGAGTC	60	72	Sebastian Tanabe, unpublished
fjoh2419_up_rev	cgaaacgtctactgttgtacGTTCCCTTATTGTCCTGAATTC	60	71	Sebastian Tanabe, unpublished
fjoh2419_down_fwd	gaattcaggacaataagggaACGTACAACAGTAGACGTTTCG	60	71	Sebastian Tanabe, unpublished
fjoh2419_down_rev	gattacgccaagcttgcatgCTAGATTATGACGCCTCTGG	60	75	Sebastian Tanabe, unpublished
fjoh2421_up_fwd	attcgggggatcctctagagCTTCTAACGCAACGGCAAAC	66	77	Sebastian Tanabe, unpublished
fjoh2421_up_rev	ttattctccgcttaAGGAACCCAATATGGATTGTC	66	67	Sebastian Tanabe, unpublished
fjoh2421_down_fwd	gacaatccatattgggttccttaagcGGAGAATAATGCTATTCACTTAC	66	73	Sebastian Tanabe, unpublished
fjoh2421_down_rev	gattacgccaagcttgcatgGGACAATAAGGGACCTTTAG	66	74	Sebastian Tanabe, unpublished

fjoh2557_up_fwd	attcgggggatcctctagagAATGCAGAACGATATACTGG	65	72	Sebastian Tanabe, unpublished
fjoh2557_up_rev	cagtcgtcgcGTGGGGTGTTACCTATTAACTC	65	68	Sebastian Tanabe, unpublished
fjoh2557_down_fwd	atgttttagagttaataggtaacaccccacGCGACGACTGGATGAATG	68	76	Sebastian Tanabe, unpublished
fjoh2557_down_rev	gattacgccaagcttgcatgCCACAACATTACCTGCATC	68	76	Sebastian Tanabe, unpublished
fjoh4604_up_fwd	aaaattcgggggatcctGCGTAACACAGCCGATGTC	60	76	Lea Arneth, unpublished
fjoh4604_up_rev	catggagggattcgaaccttAACACATGATTTCAAATC	60	70	Lea Arneth, unpublished
fjoh4604_down_fwd	gatttgaaatcatgtgTTAAGGTTCGAATCCCTCCATG	60	70	Lea Arneth, unpublished
fjoh4604_down_rev	gcttgcatgcctgcaggtcGACGGTTATTATAACGATTC	60	75	Lea Arneth, unpublished

Table 8.: primers used for frameshift mutations

Primer	Sequence (5' overlap/ANNEAL 3')	T_{a} (°C)	T_{m} (°C)	Reference
fjoh1748_up_fwd	attcgggggatcctctagagGGATCCGTTGGCTTAAC	56	74	Sebastian Tanabe, unpublished
fjoh1748_up_gen_rev	gcatacactattctcagaatTTCCGGCATCCAGATCTTCG	56	67	This study
fjoh1748_gen_down_fwd	gcgattaagttgggtaacgcGAATTATTCGTTTTACAGAGC	54	66	This study
fjoh1748_down_rev	gattacgccaagcttgcatgCCCCAGGCATATTCGGC	54	79	Sebastian Tanabe, unpublished
fjoh4604_up_fwd	aaaattcgggggatcctGCGTAACACAGCCGATGTC	60	76	Sebastian Tanabe, unpublished
fjoh4604_up_gen_rev	gcatacactattctcagaatATGTCGATATCCCAATCTGGC	60	65	This study
fjoh4604_gen_down_fwd	gcgattaagttgggtaacgcTAAACAAAGTGACATTATCAGG	55	64	This study
fjoh4604_down_rev	gcttgcatgcctgcaggtcGACGGTTATTATAACGATTC	55	75	Sebastian Tanabe, unpublished
TC_fwd	ATTCTGAGAATAGTGTATGC	55	56	This study
TC_rev	GCGTTACCCAACTTAATCGC	55	60	This study

2.2. Molecular biological methods

2.2.1. Genomic DNA isolation

Genomic DNA was purified using the Simplex Easy DNA Extraction Kit according to the manufacturer's instructions. Cell material from bacterial colonies served as the starting material for the extraction. DNA was eluted in 100 µl or 50 µl of buffer and stored at 4 °C.

2.2.2. Polymerase chain reaction

Polymerase chain reaction was used to amplify double-stranded copies of specific DNA sequences (Mullis et al., 1986). PCR reactions were setup in a total volume of 25 µl according to the manufacturer's instructions for the polymerase used. Different annealing temperatures were tested for each primer pair, and elongation times were adjusted as needed. The Q5 high-fidelity polymerase was used to generate PCR products for cloning and to amplify long genomic regions that exceed 5 kb (*Table 9*). Taq-Polymerase was only used to verify successful plasmid transfer (*Table 10*). The reactions were set up on ice and transferred to a thermo cycler immediately after the polymerase was added.

Table 9.: Standard mixture for a PCR reaction with Q5 polymerase

Component	25 µl reaction
5x Q5 Reaction Buffer	5 µl
10 µM Forward Primer	1,25 µl
10 µM Reverse Primer	1,25 µl
10 mM dNTPs	0,5 µl
gDNA	0,5–1 µl
Q5 highfidelity DNA polymerase	0,25 µl
rH_2O	add to 25 µl

Table 10.: Standard mixture for a PCR reaction with Taq polymerase

Component	25 µl reaction
10X ThermoPol Reaction Buffer	2,5 µl
10 µM Forward Primer	0,5 µl
10 µM Reverse Primer	0,5 µl
10 mM dNTPs	0,5 µl
gDNA	0,5–1 µl
Taq DNA Polymerase	0,125 µl
rH_2O	add to 25 µl

Table 11.: PCR Cycler program for Q5 Polymerase

Temperature	Time	Step	
98°C	3 min	Initial denaturation	x 1
98°C	20 sec	Denaturation	x 32
55 - 68°C?	30 sec	Annealing	x 32
72°C	1 - 1,5 min/kB	Elongation	x 32
72°C	5 min	Final elongation	x 1
12°C	∞ min	Storage	

Table 12.: PCR Cycler program for Taq Polymerase

Temperature	Time	Step	
95°C	3 min	Initial denaturation	x 1
95°C	30 sec	Denaturation	x 32
40	30 sec	Annealing	x 32
68°C	1 min/kB	Elongation	x 32
68°C	5 min	Final elongation	x 1
12°C	∞ min	Storage	

2.2.3. Agarose gel electrophoresis

DNA fragments were separated by size using agarose gel electrophoresis (Vogelstein and Gillespie, 1979). The gel was prepared using 1% or 0,5% agarose dissolved in Tris-base, acetic acid, and EDTA buffer (TAE buffer). For this, 1 g of agarose was heated in 100 ml TAE buffer until dissolved. To stain DNA fragments, GelRed® was added to the hot unpolymerized gel at a ratio of 1:1000.

Electrophoresis was performed at 100 V until an adequate separation of DNA fragments was achieved. Depending on the concentration of the PCR product, the sample volume was adjusted and diluted with rH_2O if needed. For loading the gel, 1 µl purple loading dye (New England Biolabs) was added to 5 µl of sample, allowing visualization of the migration front. A 1 kb DNA ladder (Thermo Fisher Scientific) was used as a molecular size reference.

2.2.4. PCR purification

PCR amplification products were purified using the innuPREP PCRpure Kit according to the manufacturer's instructions. Purified PCR fragments were eluted in 20 µl rH_2O and stored at -20 °C.

2.2.5. Agarose gel DNA purification

DNA fragments were purified using the innuPREP Gel Extraction Kit. All steps were performed according to the manufacturers instructions. Purified DNA was dissolved in 20 µl of elusion buffer and stored at - 20 °C.

2.2.6. Restriction digest

Restriction digest of circular DNA fragments was performed at 37°C for 1 hour by adding a buffer and 1 or 2 suitable restriction enzymes (*Table 13*). For DNA assembly the reaction was heat inactivated at 65°C for 20 minutes. To confirm successful plasmid assembly, restriction enzymes generating specific fragment patterns were selected. In this case heat inactivation was not needed. Together with a control digest, the cut DNA fragments were separated using agarose gel electrophoresis.

Table 13.: Standard digest for plasmids

Component	Volume for plasmid digest	Volume for control digest
DNA	5 µl	2 µl
rCutSmart Buffer	2 µl	2 µl
Each restriction enzyme	1 µl	1 µl
rH_2O	add to 20 µl	add to 20 µl

2.2.7. DNA Assembly

For plasmid assembly, the NEBuilder HiFi DNA Assembly kit was used. This kit, based on the principles of Gibson Assembly, enables joining of multiple DNA fragments with a plasmid vector in a single, isothermal reaction. The master mix includes a set of enzymes that function in the same buffer. An exonuclease generates single-stranded 3' overhangs to allow annealing of fragments with overlapping sequences. The polymerase fills in resulting gaps within each annealed fragment and a DNA ligase seals the remaining nicks to produce an intact assembled plasmid. All fragments used share a 20-40bp overlap with each other and the ends of the linearized plasmid backbone.

For successful DNA assembly and cloning, the manufacturers protocol was adapted. The reaction was setup on ice by first incubating approximately 0,015 pmol of each fragment in a 10 µl reaction for 2 hours at 50 °C (*Table 14*). This step enables the fusion of the fragments into one single fragment. From this reaction, 5 µL were used for the final assembly with additional master mix and 10.25 ng of linearized vector (*Table 15*). The complete assembly reaction was incubated for another 2 hours at 50 °C before transformation into *E. coli* 10 β. The final reaction contained 0,0021 pmol of the vector with 3,5-fold molar excess of each insert. A negative control without inserts was prepared in a total volume of 5 µl. For this, 0,0021 pmol of vector was mixed with 2,5 µl master mix. rH_2O was added to reach a final volume of 5µl, and the reaction incubated for 2 hours at 50 °C before transformation into *E. coli* 10 β.

Table 14.: Reaction mixture for fusion of DNA fragments

Component	Volume (µl)	pmol
2x NEBuilder HiFI DNA Assembly Master Mix	5 µl	
Each Fragment	variable	0,01-0,02 pmol
rH_2O	add to 10 µl	

Table 15.: Reaction mixture for DNA assembly with linearized vector

Component	25 µl reaction	pmol
reaction with fused inserts	5µl	0,005 - 0,01 pmol
2x NEBuilder HiFI DNA Assembly Master Mix	2,5 µl	
pYT-313 vector	variable	0,002 pmol
rH_2O	add to 10 µl	

To calculate the number of pmol of each fragment the following formula was used: $\mathrm{pmol} = \frac{m(\mathrm{ng}) \times 1000}{\mathrm{bp} \times 650\mathrm{Da}}$

2.2.8. Plasmid DNA isolation

Plasmid DNA was isolated using the Monarch® Spin Plasmid Miniprep Kit following the manufacturer's protocol. This method uses standard cell suspension, alkaline lysis of the cells and a subsequent neutralization step to avoid plasmid degradation. Cell components with a higher molecular weight precipitate, while the plasmids remain dissolved. In the next step precipitated cellular debris is centrifuged and the supernatant containing the plasmids is transferred to a spin column. DNA binds to the silica matrix, while subsequent washing steps remove any remaining protein, RNA and salt, allowing elusion of concentrated plasmid DNA. DNA was eluted in 50µl rH_2O and stored at -20 °C until use.

2.2.9. DNA sequencing

For DNA sequencing samples were sent to Microsynth AG. For this purpose, plasmids were diluted with rH_2O in a volume of 15µl to a concentration of 40-80 ng/µl.

2.3. Microbiological Methods

2.3.1. bacterial cultivation

E. coli strains were cultured in liquid or on solid lysogeny broth (LB) (*Table 16*) (Bertani, 1951). *F. johnsoniae* wiltype and mutant strains were cultured in liquid or on solid casitone-yeast-extract medium (CYE) (*Table 18*) (Mcbride and Kempf, 1996). Cultures were generally grown over night with *E. coli* strains incubating at 37 °C and *F. johnsoniae* at 27 °C. Liquid cultures were shaken at 180 rpm. For LB agar plates, 1,5 % agar was added prior to autoclaving, whereas 2% agar was used for CYE plates. Antibiotics were added after sterilization. For counter selection purposes, CYE medium was enriched with 5% sucrose before autoclaving. Motility medium agar plates were prepared for phenotypic analysis of *F. johnsoniae* mutant strains (Vences-Guzmán et al., 2021). LTY medium agar plates were prepared for the phenotypic characterization of *F. johnsoniae* mutant strains, which are potentially deficient in cysteate biosynthesis, to limit exogenous cysteate availability (Abbanat et al., 1986).

Table 16.: Medium for *E.coli* cultivation

Component	LB-Medium
LB-Medium	25 gl^{-1}
Nuclease-free water	1 L
Agar	1.5 % (w/v)

Table 17.: LTY Medium for phenotypic analysis of *F. johnsoniae* mutant strains

Component	LTY-Medium
Yeast	0,5 gl^{-1}
Triptone	0,5 gl^{-1}
Agar-Agar	1,8 % (w/v)

Table 18.: Medium for *F. johnsoniae* cultivation

Component	CYE-Medium
Casitone	10 gl^{-1}
Yeast	5 gl^{-1}
Magnesium sulfate	8 mM
Tris buffer (pH = 7.5)	10 mM
Nuclease-free water	1 L
Agar-Agar	2 % (w/v)
Sucrose	5 % (w/v)

Table 19.: Motility Medium for phenotypic analysis of *F. johnsoniae* mutant strains

Component	Motility-Medium
Casitone	3,3 gl^{-1}
Yeast	1,7 gl^{-1}
Tris buffer (pH = 7.5)	3,3 mM
Nuclease-free water	1 L
Agar	1,5 % (w/v)
Sucrose	5 % (w/v)

Table 20.: Antibiotics for cultivation

Antibiotic	Concentration	Solvent	Used for
Ampicillin	100 µg ml^{-1}	rH_2O	LB-Medium
Erythromycin	25 µg ml^{-1}	mol. grade ethanol	CYE-Medium
Tetracycline	10 µg ml^{-1}	rH_2O	CYE-Medium

2.3.2. Preparation of chemical competent cells

Chemical competent *E. coli* cells were prepared using the $CaCl_2$ method (Dagert and Ehrlich, 1979). For this an overnight preculture was inoculated in 70 ml of LB medium at a ratio of 1:100 (v/v). The culture was grown at 37°C and 180 rpm. Optical denisty (OD_{600}) was measured hourly until it reached an OD_{600} = 0,6. For $CaCl_2$ treatment, subsequent steps were performed on ice with cooled solutions. Cells were harvested by centrifugation at 400 × g for 10 minutes at 4 °C. Supernatant was discarded and the cell pellet resuspended in 10,5 ml $CaCl_2$/$MgSO_4$ solution (70 mM $CaCl_2$, 20 mM $MgSO_4$). After a 40 minute incubation on ice, cells were harvested again (400 × g, 10 min, 4 °C) and resuspended in 3,5 ml $CaCl_2$/$MgSO_4$ solution. After another 40 minute incubation on ice, 875 µl of cold sterile glycerol was added and mixed. 200 µl aliquots of cell suspension were prepared and frozen at -70 °C.

2.3.3. Transformation of cells

Plasmids were introduced into competent *E. coli* cells by heat shock transformation (Hanahan et al., 1991). For this method, competent *E. coli* cells were defrosted on ice. For transformations with isolated plasmids, 1 µl of Plasmid DNA was mixed with 100 µl of cells and incubated on ice for 30 minutes. For cloning proce-

dures, the entire DNA-assembly reaction was mixed with the same volume of cells and likewise incubated on ice. Heat shock was performed at 42 °C for 90 seconds, following a 2 minute incubation on ice and the addition of 800 µl LB medium. After 1 hour of incubation at 37 °C the cells were pelleted at 1000 $\times g$, resuspended and plated onto LB agar plates containing suitable antibiotics for selection. The plates were incubated at 37°C overnight to develop colonies of transformed cells.

2.3.4. Conjugative transfer

Transfer of the suicide plasmid into *F. johnsoniae* was enabled by conjugation. The *E. coli* donor strain used was *E. coli* S17-1 λ pir. Conjugation was performed as previously described, using erythromycin to select for successful conjugative transfer (Mcbride and Kempf, 1996). For this purpose, the bacterial strains were grown overnight, with *E. coli* incubated at 37 °C and *F. johnsoniae* at 27 °C. CYE agar plates were treated with 100 µl of 1 M $CaCl_2$ solution and dried before spotting the cells. One milliliter of each culture was centrifuged for 1 minute at 5000 rpm. The *F. johnsoniae* pellet was resuspended in 50 µl of CYE medium. The *E. coli* strain was washed with 1 ml of CYE to remove any residual antibiotics. *E. coli* cells were pelleted (1 min, 5000 rpm) and resuspended in 50 µl of CYE. To prepare the control, 25 µl of the *F. johnsoniae* suspension was spotted onto a CYE agar plate. For conjugative transfer, the strains were mixed at a 1:1 ratio to a total volume of 50 µl. The cell suspension was then spotted onto CYE agar plates. After overnight incubation at 27 °C, *F. johnsoniae* cells were scraped off the plates and resuspended in 2 ml CYE liquid medium. One hundred microliters of control cell suspension was plated onto CYE agar containing 25 µg/ml of erythromycin. The suspension containing *F. johnsoniae* cells post-conjugation was further diluted 10^{-1}-10^{-5}. 100 µl of each dilution was then plated onto CYE agar containing 25 µg/ml of erythromycin. Plates were incubated for 2-3 days at 27 °C to select for successful conjugative transfer.

2.3.5. Markerless deletion and frameshift mutation strategy

Markerless in-frame deletions and frameshift mutations were generated using homologous recombination. A markerless deletion strategy has previously been applied to generate mutants of *F. johnsoniae* (Vences-Guzmán et al., 2021). In this method, a specific gene is removed without disrupting the open reading frame of neighboring genes. A frameshift mutation disrupts the open reading frame by inserting foreign DNA into the coding sequence. Unlike in-frame deletions, this type of mutation can cause downstream polar effects when genes located downstream of the target gene are oriented in the same direction. To generate in-frame deletion mutants, a suicide plasmid carrying a selection marker, a counter-selection marker, and upstream and downstream flanking regions of the target gene is introduced into *F. johnsoniae*. An antibiotic resistance gene is used as a selection marker. The counter selection marker carries a genetic element that is harmful to the organism under specific conditions, which allows negative selection. The homologous regions included in the suicide plasmid determine the chromosomal sites at which homologous recombination occurs. Mutant generation relies on two homologous recombination

events. The selection and counter selection markers enable the identification of clones in which these recombination steps have taken place. During the first crossing over event, either the up- or downstream region of the plasmid aligns with the homologous region on the chromosome, allowing the integration of the plasmid. To verify successful plasmid integration, positive clones are selected using the selection marker. To trigger the second homologous recombination event, cells with integrated plasmid are grown in liquid medium without selection pressure. The outcome of the second crossing over depends on which flanking region is used for recombination. Recombination at the flanking region that was not used during the first crossing over produces the desired mutant allele. If the recombination takes place between the same region as during the first crossing over, the wild type is restored. Counter selection is then used to screen for successful mutants, which is further confirmed using PCR. For frameshift mutations an additional resistance marker was inserted between the flanking regions. In addition, the up- and downstream fragments carried the first and second half of the target gene sequence.

For this work, the pYT313 suicide vector was used, which carries the erythromycin resistance gene (*ermf*) as a selection marker and the *sacB* gene for counter selection. The *sacB* gene encodes for levan sucrase, which catalyzes the synthesis of levan from sucrose. This exopolysaccharide is toxic to gram negative bacteria and leads to cell death at high concentrations (Steinmetz et al., 1983). Depending on the type of mutation, suitable DNA fragments were assembled into the vector via gibson assembly.

Markerless gene deletion

To delete a gene, up- and downstream fragments of approximately 2500 bp were generated using PCR and assembled into the pYT313 vector. The suicide plasmid was introduced into *F. johnsoniae* by conjugative transfer from *E coli* S17-1 λ pir. After conjugation, colonies were transferred onto CYE plates supplemented with erythromycin, as well as plates supplemented with 5% sucrose. The plates were incubated for 2-3 days at 27°C. Positive clones were selected by erythromycin resistance, and the presence of the SacB gene was confirmed by PCR. To trigger the second homologous recombination event, positive clones were inoculated in CYE liquid medium and grown for 1-2 days without selection pressure. A serial dilution of the culture was prepared ranging from 10^{-1} - 10^{-10}. Subsequently, 100 µl of the 10^{-5} - 10^{-10} dilutions were plated onto CYE agar plates supplemented with 5% sucrose to select for a successful second homologous recombination event. The plates were incubated for 2-3 days at 27°C. To distinguish a deletion mutant from a wild type, colonies were transferred onto motility medium agar plates, allowing analysis of gliding motility. Deletion mutants were further verified by PCR of the targeted genomic region.

Frameshift mutation

To generate a frameshift mutation the pYT313 vector was assembled with three fragments. The upstream fragment consisted of approximately 2500 bp upstream of the target gene and the first half of the gene. Likewise, the downstream fragment contained 2,500 bp downstream of the target gene together with the

second half of the gene. A tetracycline resistance cassette (*tet(Q)*) was inserted between the two flanking regions. Following conjugation, the first homologous recombination occurs, leading to integration of the plasmid into the chromosome within the target gene. Cells carrying the plasmid were selected by erythromycin and tetracycline resistance. For this purpose, positive clones were transferred onto CYE plates containing erythromycin and inoculated in CYE liquid medium supplemented with tetracycline. Plates and cultures were incubated for 2-3 days. The presence of the *sacB* gene was confirmed by PCR and phenotypic changes assessed on motility medium agar plates. To induce the second homologous recombination event, single recombinants were grown in liquid medium for 1-2 days without antibiotics. Serial dilutions (10^{-5} - 10^{-10}) were plated onto CYE agar containing 5% sucrose and incubated for 2-3 days at 27°C. Successful excision of the plasmid backbone resulted in retention of the *tet(Q)* cassette within the target gene, thereby generating a frameshift mutation. Mutants were identified by tetracycline resistance and erythromycin sensitivity. A successful mutation was further confirmed by amplifying the targeted genomic region by PCR.

2.3.6. Growth experiment

To assess whether growth is affected by the gene deletion, *F. johnsoniae* wild type and deletion mutants were grown in CYE liquid media at 27 °C over 26-30 hours. For this purpose, each overnight preculture was inoculated 1:100 into 50 ml of CYE liquid medium in biological triplicates. OD_{600} measurements were taken every 2 hours over a period of 10 hours and at 1-2 additional time points the following day.

2.3.7. Microscopy

For microscopic analysis, overnight precultures of *F. johnsoniae* wild type and mutant strains were inoculated 1:100 into 5 ml CYE liquid medium. After reaching an OD_{600} = 0,6, three 1µl drops of each culture were spotted onto motility medium agar plates and dried. To assess differences in the gliding phenotype, colonies were imaged hourly over a 15 hour period. Imaging was performed using a transmitted light brightfield (TL-BF) illumination with a 6.3x objective on a Leica THUNDER EPI widefield microscope (Leica Microsystems GmbH). Time-lapse image series were acquired using an intensity mode of 50 with an exposure time of 10 ms.

2.4. Biochemical Methods

2.4.1. Lipid Extraction

For lipidomic analysis, lipids of *F. johnsoniae* cells were extracted using a modified protocol of Bligh and Dyer, 1959. To obtain a suitable amount of cell material, overnight precultures were inoculated 1:100 into 5 ml CYE liquid medium supplemented with cysteaste (1 mg/ml). After 6 hours of cultivation at 27 °C, cells were harvested and lyophilized overnight. Once the pellet was completely dry, it was resuspended in 1 ml of methanol. The samples were transferred to an iced sonication bath and lysed for 1 hour, following a 2

hour incubation at room temperature. To separate cell debris from methanol, samples were centrifuged for 15 minutes at maximum $\times g$. 800 µl of the supernatant was transferred to a glass vial and evaporated overnight using a nitrogen evaporator. Dried lipids were diluted in methanol to a lipid concentration of 1-2 mg/ml. This solution was further diluted to a lipid concentration of 50 µg/ml and centrifuged at 14000 $\times g$ for 20 minutes. This step ensures that insoluble impurities separate from the methanolic lipid phase. For LC-MS/MS analysis, 150 µl of the supernatant was transferred to a glass vial. All eppendorf tubes and glass vials used were weighed before adding the samples to calculate wet weight of the cell pellets, and dry weight of the cell pellets and lipids.

2.4.2. Liquid chromatography-tandem mass spectrometry

Liquid chromatography-tandem mass spectrometry (LC-MS/MS) was used to identify sulfobacins and intermediates produced by *F. johnsoniae* and mutant strains. The LC-MS/MS protocol used was adapted from Peng et al., 2023. Lipid extracts were analyzed using a UHPLC system equipped with a reversed-phase C8 column, enabling separation of lipid species based on hydrophobicity. Following chromotographic separation, analytes were ionized and detected using an Orbitrap mass spectrometer operated in negative ion mode with MS/MS ion fragmentation. Structural characterization of sulfobacins and related intermediates was achieved based on accurate mass measurements and fragmentation patterns. Analysis of raw data was performed using Skyline software (MacLean et al., 2010).

3. Results

3.1. Identification of putative sulfobacin synthesis genes

Genes potentially involved in sulfobacin biosynthesis were identified based on sequence homology to characterized enzymes of bacterial ceramide and sphingolipid biosynthesis pathways. In the absence of detectable homologs, assignments were supported by protein family classification. A KEGG-based BLAST analysis with the known cysteate synthase gene in *Chryseobacterium gleum* identified two candidate genes fjoh_2557 and fjoh_1927, potentially encoding a cysteate synthase in *F. johnsoniae* (Hou et al., 2022). Both genes are annotated as cystathion β-synthases and showed significant matches with E-values of 0.0 and 2×10^{-129}. The putative sulfobacin synthase gene fjoh_2421 was identified by homology to the ceramide synthase of *Caulobacter crescentus* (Stankeviciute et al., 2022). Sequence comparison showed 82% coverage, an E-value of 3×10^{-24}, and 23.9% sequence identity. For identification of potential monooxygenases, a BLAST search was performed to find DES2 homologs (Mizutani et al., 2004). However, no homolog was detected in *F. johnsoniae*. Therefore, the identification of fjoh_4604 and fjoh_1748 as putative monooxygenases was based on protein family comparison. Like DES2, both proteins belong to the family of fatty acid desaturases and therefore could be involved in the hydroxylation of sulfobacins.

3.2. Establishment of a tool box for deletion or mutation of sulfobacin synthesis genes

In order to construct plasmids for the markerless deletion and frameshift mutation strategy, primers were designed using Clone Manager 9 and NEBuilder. For the markerless deletion of genes in *F. johnsoniae*, a deletion system has successfully been established previously (Zhu et al., 2017). In addition, a frameshift mutation strategy has been described in Wilkinson et al., 2006. In this work, these systems were adapted to perform deletion and disruption of selected target genes with a modified protocol. The suicide vector pYT313, originally developed for chromosomal gene deletions in *Z. galactanivorans* (Zhu et al., 2017), was used to generate suicide plasmids for deletion and disruption of genes in *F. johnsoniae*. It encodes an origin of replication (*oriV*) functional in *E. coli* and an origin of transfer (*oriT*), enabling conjugative transfer from *E. coli*S17-1 λ pir. For selection and counter selection, the pYT313 vector carries the ampicillin resistance gene (*bla*), the erythromycin resistance gene (*ermF*) and the *sacB* gene. The *bla* gene confers ampicillin resistance on *E. coli* and allows selection for plasmid acquisition during cloning. The erythromycin

resistance gene (*ermF*) is recognized and expressed in *F. johnsoniae*, but not in *E. coli*. Erythromycin resistance was used as a selection marker, while the *sacB* gene enabled counter selection in *F. johnsoniae*. For markerless deletions, upstream and downstream fragments of the target gene were amplified. These fragments included the start and/or stop codon of the target gene. For insertional mutations, the amplified fragments included the gene region to be disrupted. To construct insertional mutation plasmids, a tetracycline resistance cassette (*tet(Q)*) was amplified and incorporated into the assembly. The pCP23 plasmid, which carries the tetracycline resistance gene (*tet(Q)*) served as a template.

Fragments were assembled into the vector using Gibson Assembly. For this purpose, the fragments were designed with overlapping homologous ends to each other and to the linearized plasmid backbone. Overlaps were 20-30 bp in size for each construct. The pYT313 vector was linearized using the restriction sites *Sal*I and *Sph*I. These restriction sites were suitable for six constructs. Plasmids targeting fjoh_4604, were linearized with the restriction enzymes *Sal*I and *Xba*I.

3.2.1. Suicide plasmid design for fjoh_1927

The gene fjoh_1927, potentially encoding for a cysteate synthase in *F. johnsoniae* is located downstream of starch-binding outer membrane protein biosynthesis genes. The upstream fragment contained 2459 bp and included the start codon of fjoh_1927. The 2459 bp downstream fragment started one basepair after the last codon of fjoh_1927. The resulting plasmid, pYT313-1927_madel, was used for allelic exchange at the fjoh_1927 locus. A schematic representation of the plasmid is shown in *Figure 4*.

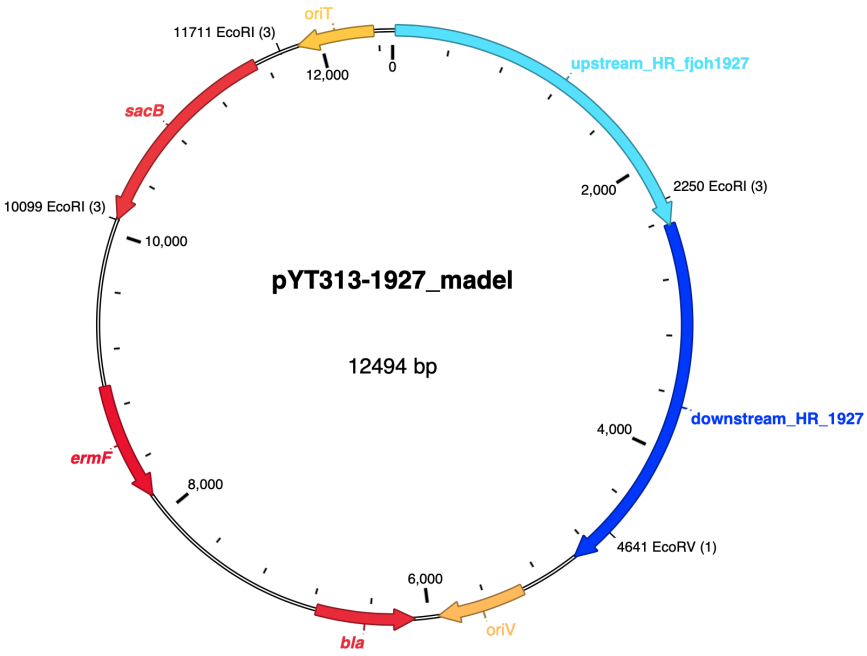

Figure 4.: **Plasmid map of pYT313-1927_madel**. Arrows indicate protein-coding genes and their orientation. Arrowheads shown for non-coding elements (*oriT*, *oriV*, and the upstream and downstream homologous regions) do not represent biologically relevant directionality. This figure was created with ApE.

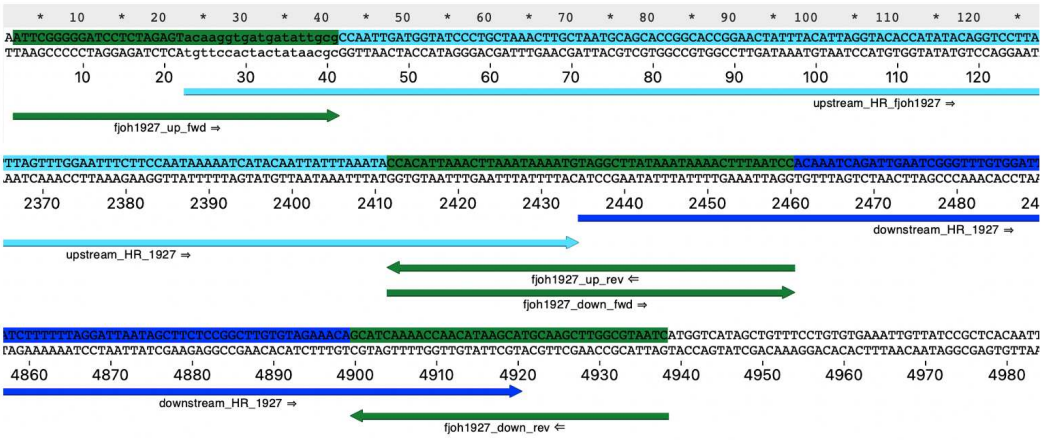

Figure 5.: **Primer binding sites of pYT313-1927_madel.** Arrows indicate orientation of the primers. Arrowheads shown for the upstream and downstream homologous regions do not represent biologically relevant directionality. This figure was created with ApE.

3.2.2. Suicide plasmid design for fjoh_2557

The second putative cysteate synthase gene fjoh_2557 is located downstream of a C-terminal processing peptidase gene and upstream of a oligopeptidase gene. The 2220 bp upstream fragment included 79 bp of the fjoh_2557 gene. The downstream fragment was 2170 bp in size and contained the last 58 bp of the target gene. An overview of the pYT313-2557_madel plasmid is presented in *Figure 6*.

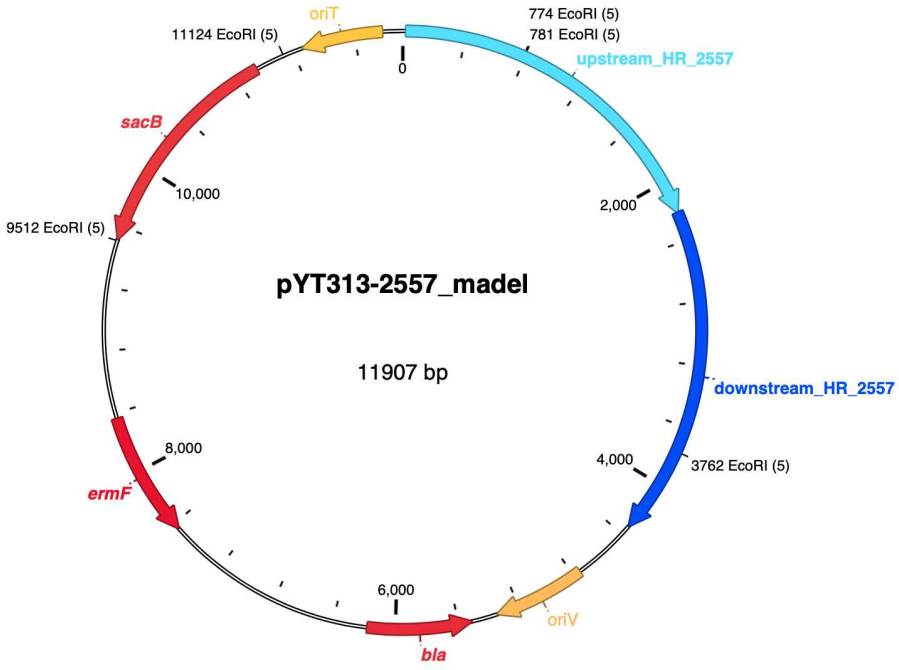

Figure 6.: **Plasmid map of pYT313-2557_madel**. Arrows indicate protein-coding genes and their orientation. Arrowheads shown for non-coding elements (*oriT*, *oriV*, and the upstream and downstream homologous regions) do not represent biologically relevant directionality. This figure was created with ApE.

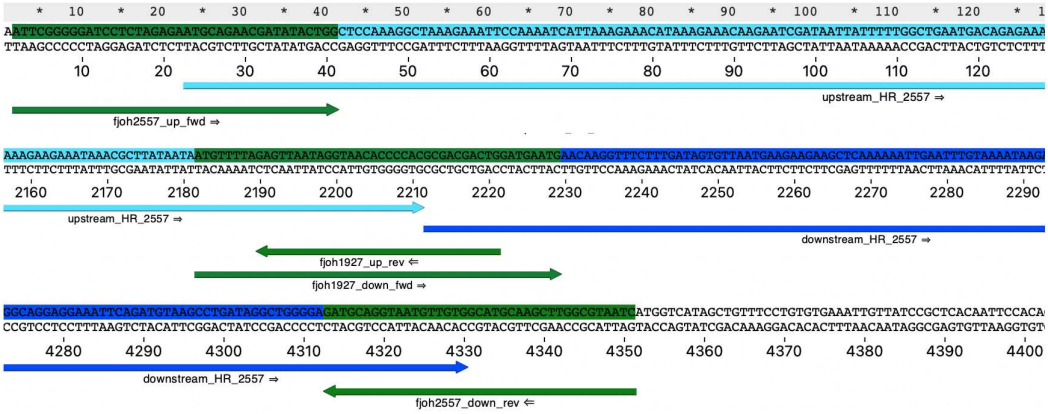

Figure 7.: **Primer binding sites of pYT313-2557_madel.** Arrows indicate orientation of the primers. Arrowheads shown for the upstream and downstream homologous regions do not represent biologically relevant directionality. This figure was created with ApE.

3.2.3. Suicide plasmid design for fjoh_2419

The gene fjoh_2419 encodes the cysteate acyl-ACP transferase (SulA) and is located upstream of a nitrite reductase gene. The plasmid pYT313-2419_madel contained a 2119 bp upstream and 2722 bp downstream homologous region. Flanking regions included 43 bp and 25 bp of the *sulA* gene. A schematic representation of the suicide plasmid required for markerless deletion of fjoh_2419 is shown in *Figure 8*.

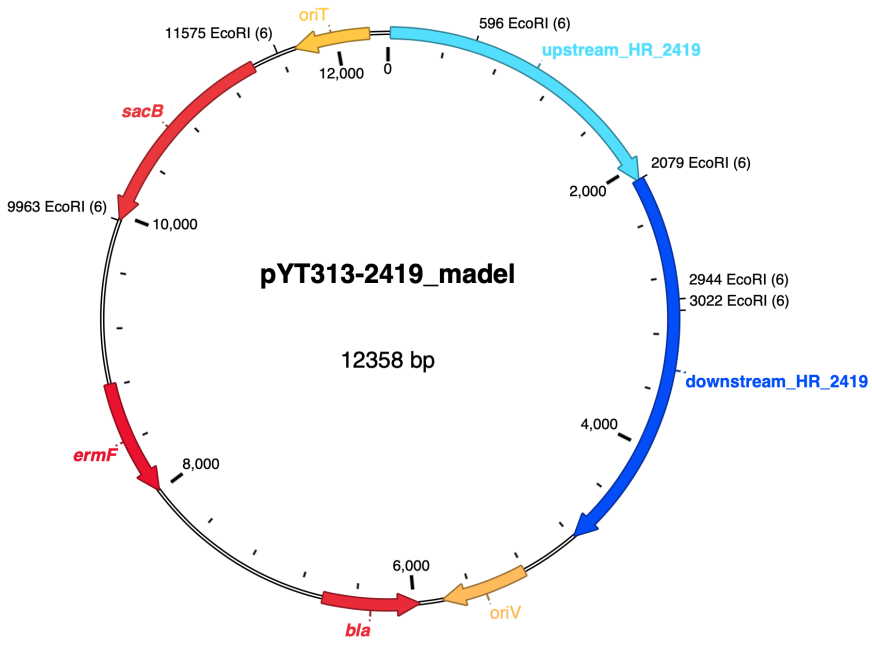

Figure 8.: **Plasmid map of pYT313-2419_madel**. Arrows indicate protein-coding genes and their orientation. Arrowheads shown for non-coding elements (*oriT*, *oriV*, and the upstream and downstream homologous regions) do not represent biologically relevant directionality. This figure was created with ApE.

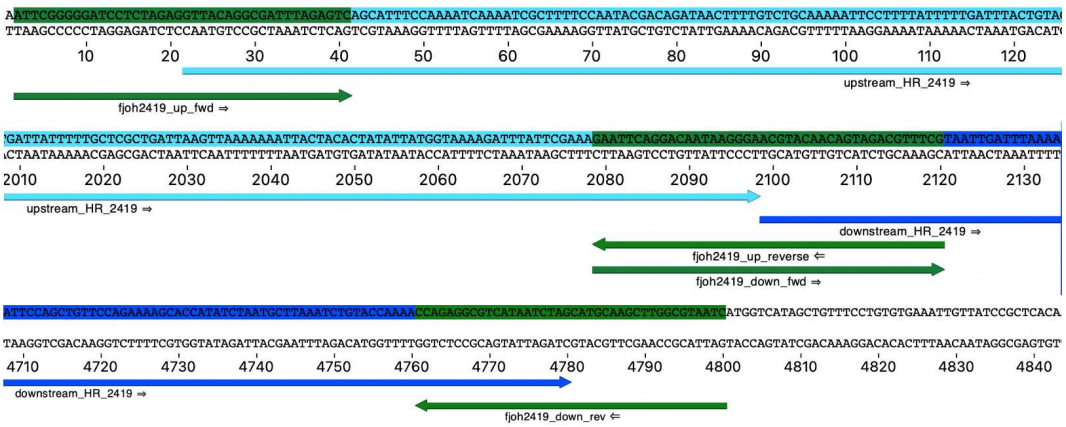

Figure 9.: **Primer binding sites of pYT313-2419_madel.** Arrows indicate orientation of the primers. Arrowheads shown for the upstream and downstream homologous regions do not represent biologically relevant directionality. This figure was created with ApE.

3.2.4. Suicide plasmid design for fjoh_2421

The putative sulfobacin synthase gene is located upstream of the *sulA* gene. The 2154 bp upstream fragment included 95 bp of the fjoh_2421 gene. The downstream fragment was 2058 bp in size and contained the last 84 bp of the target gene. A schematic representation of the pYT313-2421_madel required for the markerless deletion of fjoh_2421 is shown in *Figure 10*.

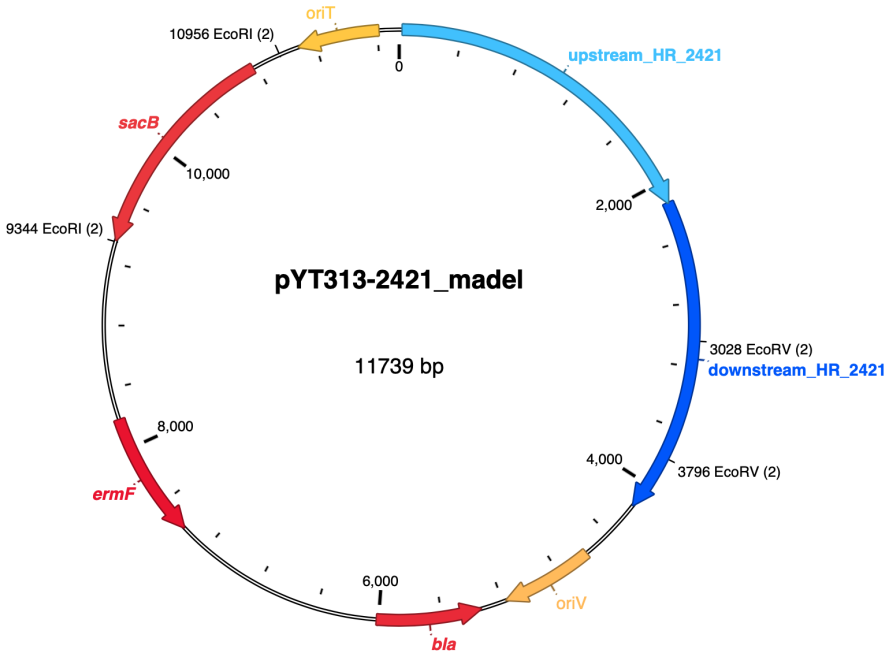

Figure 10.: **Plasmid map of pYT313-2421_madel**. Arrows indicate protein-coding genes and their orientation. Arrowheads shown for non-coding elements (*oriT*, *oriV*, and the upstream and downstream homologous regions) do not represent biologically relevant directionality. This figure was created with ApE.

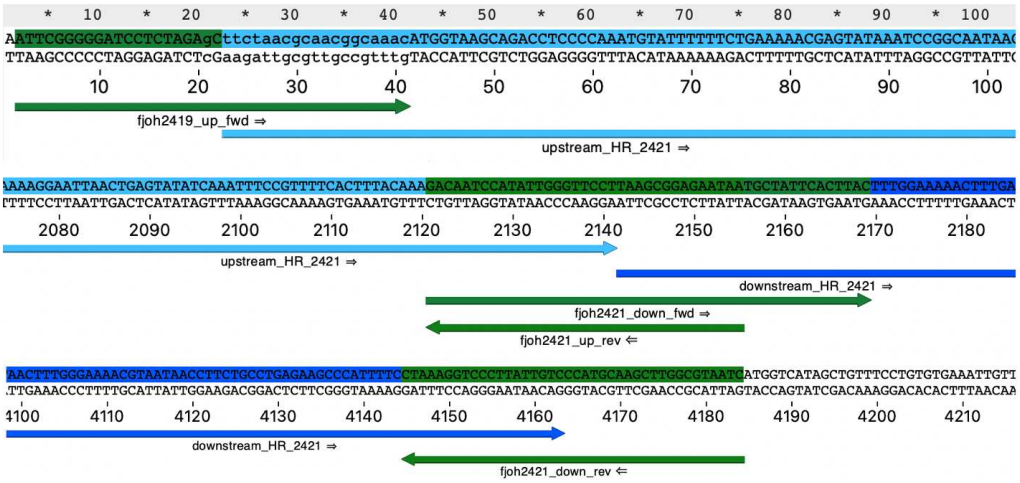

Figure 11.: **Primer binding sites of pYT313-2421_madel.** Arrows indicate orientation of the primers. Arrowheads shown for the upstream and downstream homologous regions do not represent biologically relevant directionality. This figure was created with ApE.

3.2.5. Suicide plasmids design for fjoh_1748

The putative monooxygenase gene (fjoh_1748) is located downstream of an aspartate aminotransferase gene and upstream of the methyltransferase gene (*gidB*). The upstream homologous region comprised 2295 bp and included the first 16 bp of the fjoh_1748 coding sequence. The downstream homologous region was 2523 bp in length and started 47 bp upstream of the fjoh_1748 stop codon. A schematic representation of the pYT313-1748_madel plasmid is shown in *Figure 12*.

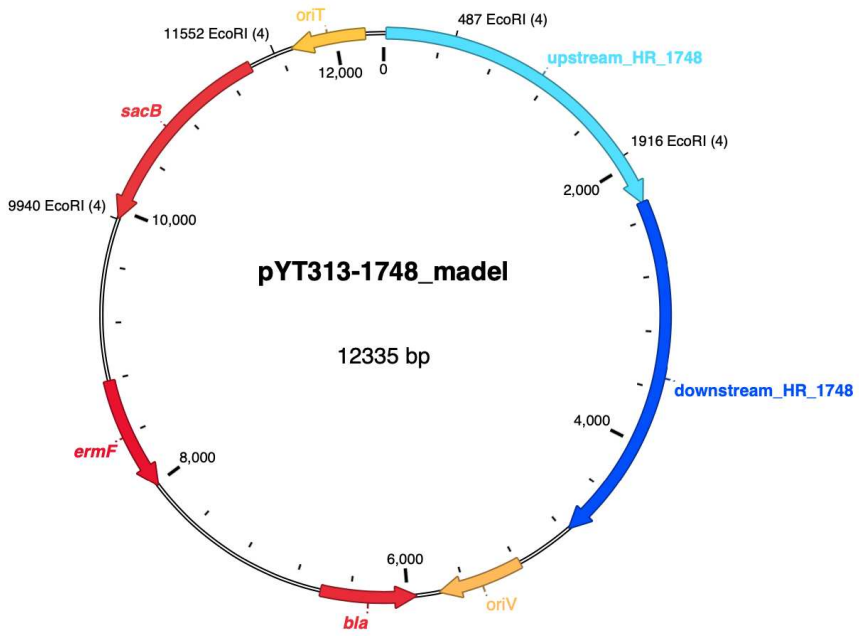

Figure 12.: **Plasmid map of pYT313-1748_madel**. Arrows indicate protein-coding genes and their orientation. Arrowheads shown for non-coding elements (*oriT*, *oriV*, and the upstream and downstream homologous regions) do not represent biologically relevant directionality. This figure was created with ApE.

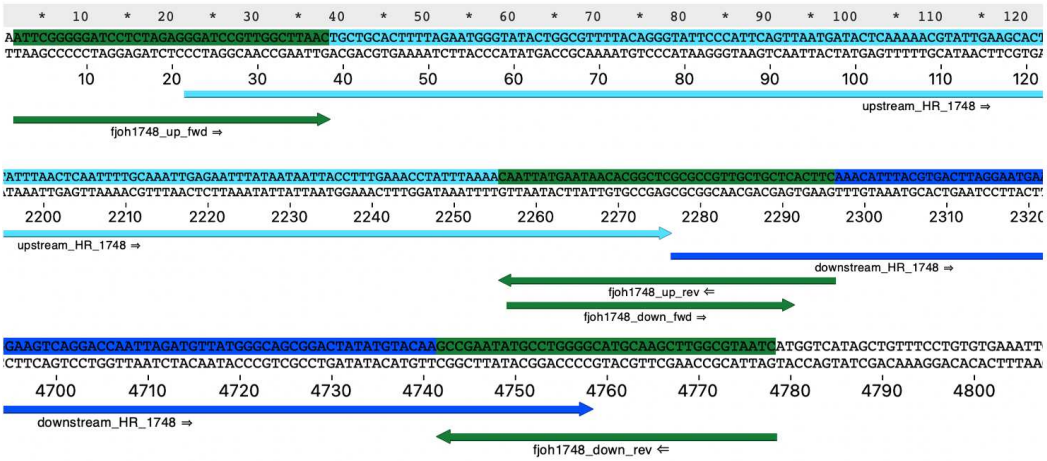

Figure 13.: **Primer binding sites of pYT313-1748_madel.** Arrows indicate orientation of the primers. Arrowheads shown for the upstream and downstream homologous regions do not represent biologically relevant directionality. This figure was created with ApE.

In addition to the markerless deletion construct, a suicide plasmid for insertional mutagenesis of fjoh_1748 was designed. For this purpose, the homologous fragments carried the gene to be disrupted. The upstream region comprised 2713 bp and contained the first 433 bp of the fjoh_1748 coding sequence. The downstream region contained 3102 bp and carried the second half of the gene, which was 665 bp in size. A tetracycline resistance cassette (*tet(Q)*), with a length of 3505 base pairs, was assembled between the two fragments. An overview of the pYT313-1748_TC plasmid is presented in *Figure 14*.

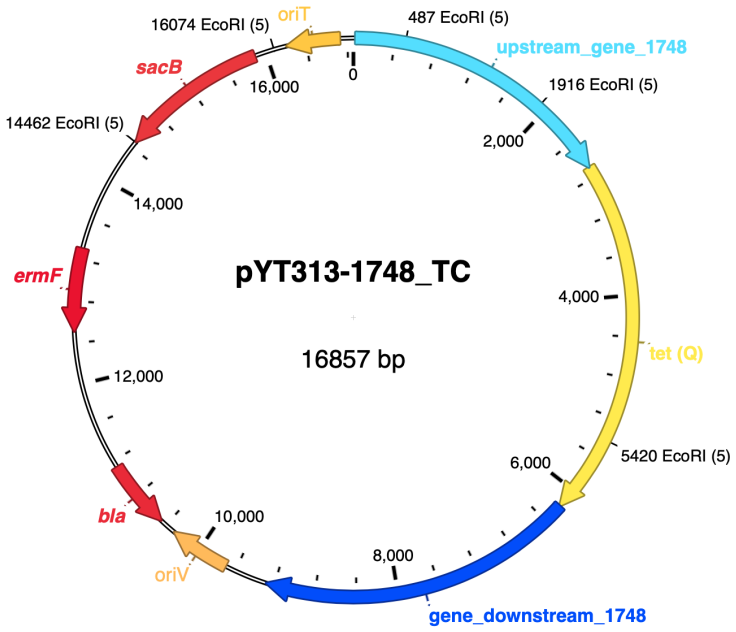

Figure 14.: **Plasmid map of pYT313-1748_TC**. Arrows indicate protein-coding genes and their orientation. Arrowheads shown for non-coding elements (*oriT*, *oriV*, and homologous gene regions) do not represent biologically relevant directionality. This figure was created with ApE.

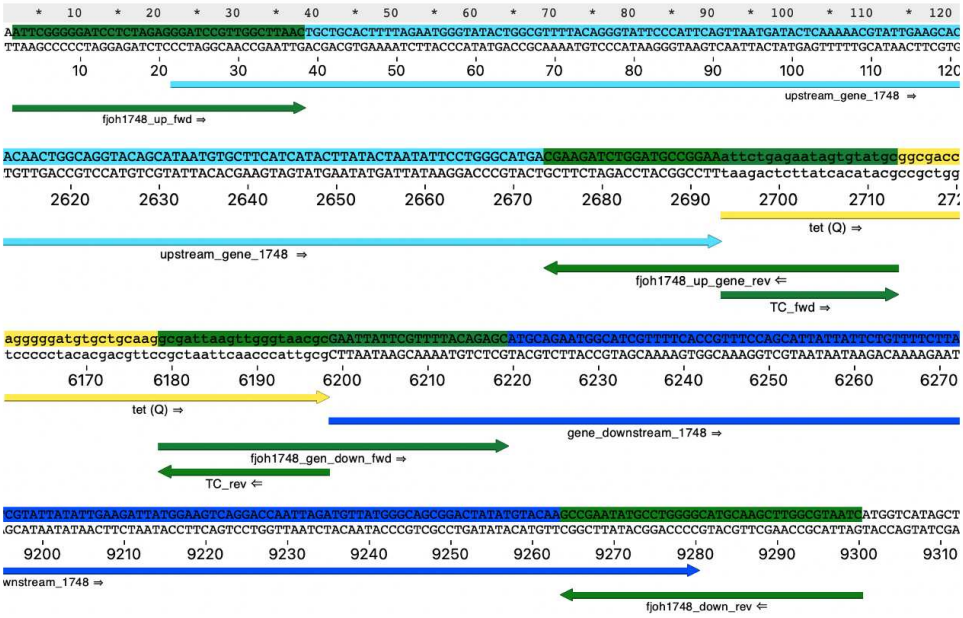

Figure 15.: **Primer binding sites of pYT313-1748_TC.** Arrows indicate orientation of the primers. Arrowheads shown for the upstream and downstream homologous regions do not represent biologically relevant directionality. This figure was created with ApE.

3.2.6. Suicide plasmids design for fjoh_4604

The second putative monooxygenase gene (fjoh_4604) is located downstream of a gene encoding an outer membrane phospholipase A-like protein and upstream of a peptidase family M15D-like protein. The upstream homologous region comprised 2678 bp and included the first 6 bp of the fjoh_4604 coding sequence. The downstream homologous region was 2400 bp in length and started 1 bp upstream of the fjoh_4604 stop codon. A schematic representation of the suicide plasmid required for allelic exchange at the fjoh_4604 locus is shown in *Figure 16*.

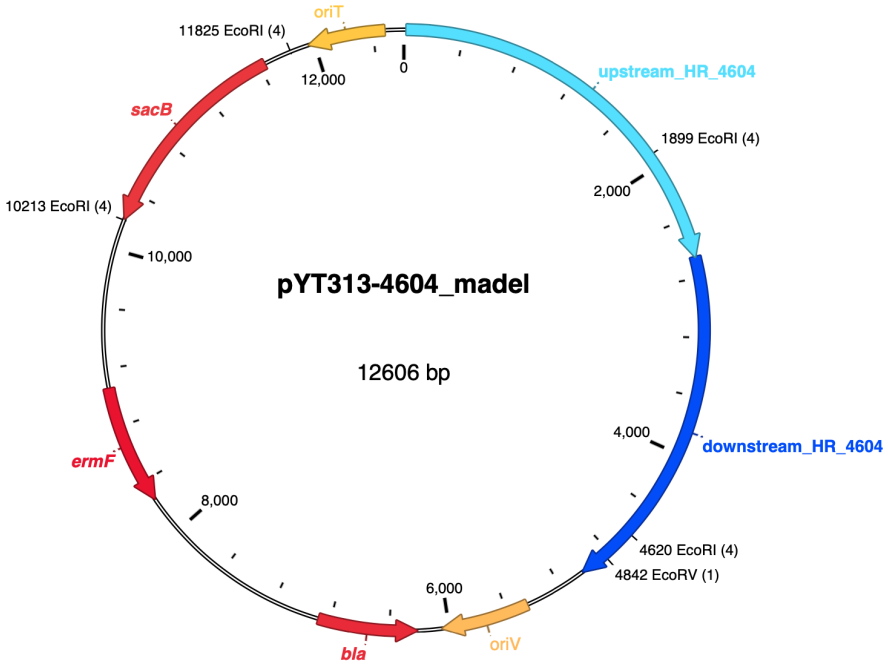

Figure 16.: **Plasmid map of pYT313-4604_madel**. Arrows indicate protein-coding genes and their orientation. Arrowheads shown for non-coding elements (*oriT*, *oriV*, and the upstream and downstream homologous regions) do not represent biologically relevant directionality. This figure was created with ApE.

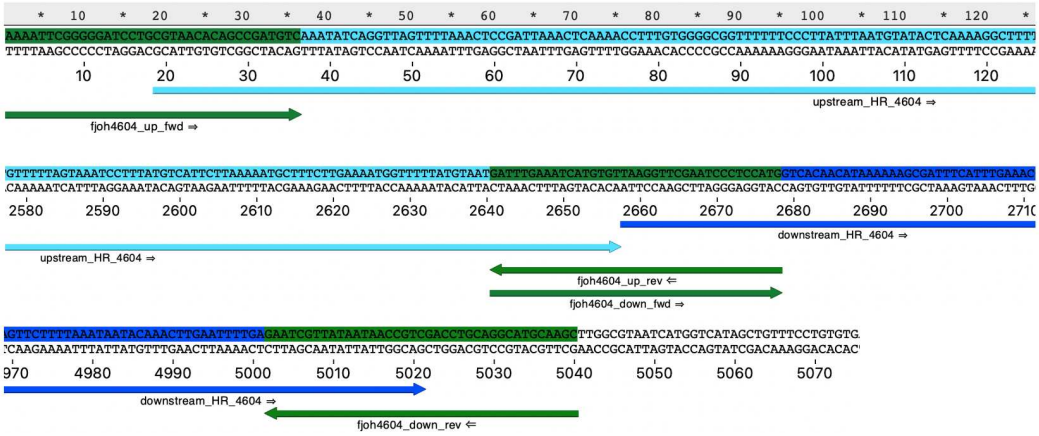

Figure 17.: **Primer binding sites of pYT313-4604_madel.** Arrows indicate orientation of the primers. Arrowheads shown for the upstream and downstream homologous regions do not represent biologically relevant directionality. This figure was created with ApE.

In addition to pYT313-4604_madel, a suicide plasmid for insertional mutagenesis of fjoh_4604 was designed.

The upstream region comprised 3144 bp and the first 473 bp of the fjoh_4604 coding sequence. The downstream region contained 3088 bp and carried the second half of the gene, which was 688 bp in size. A tetracycline resistance cassette, *tet(Q)*, with a length of 3,505 base pairs, was assembled between the two fragments. A schematic representation of the pYT313-4604-TC is shown in *Figure 18*.

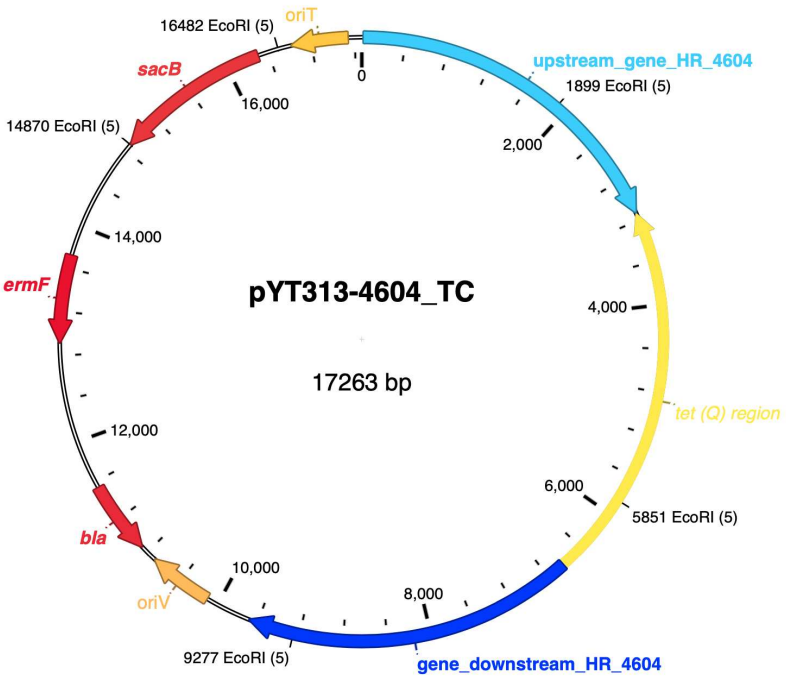

Figure 18.: **Plasmid map of pYT313-4604_TC**. Arrows indicate protein-coding genes and their orientation. Arrowheads shown for non-coding elements (*oriT*, *oriV*, and homologous gene regions) do not represent biologically relevant directionality. This figure was created with ApE.

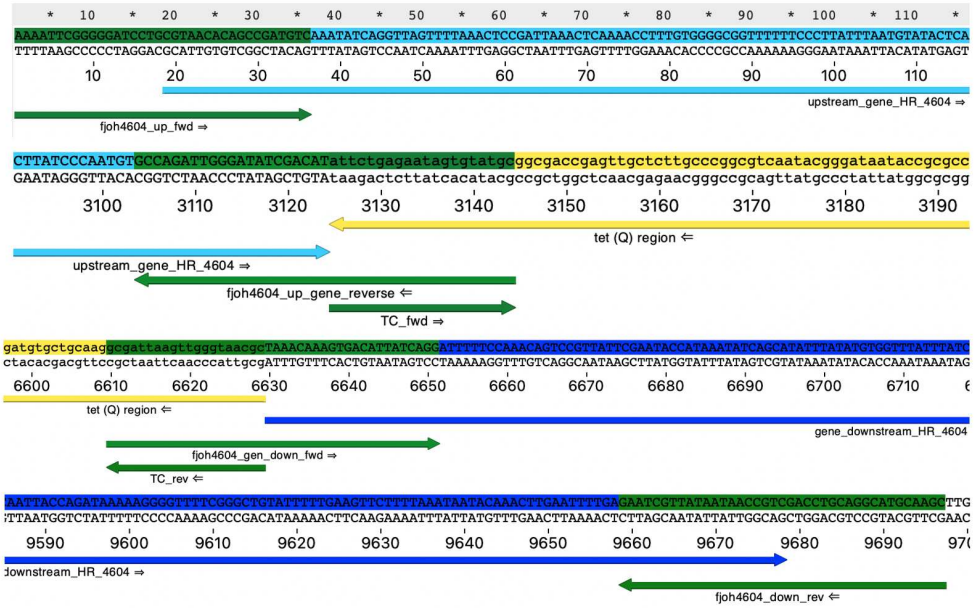

Figure 19.: **Primer binding sites of pYT313-4604_TC.** Arrows indicate orientation of the primers. Arrowheads shown for the upstream and downstream homologous regions do not represent biologically relevant directionality. This figure was created with ApE.

3.3. Deletion of the target genes

3.3.1. Suicide plasmid construction

For molecular cloning the up and downstream fragments of the respective genes were amplified by PCR using the Q5 Polymerase. The optimal annealing temperatures were calculated considering the overlap, which does not anneal during the first PCR cycle. The up_fwd and up_reverse primers were used to amplify the upstream fragment, while down_fwd and down_reverse primers were used to generate the downstream fragment of the gene to be deleted.

To amplify the fjoh_1748 fragments, an optimal annealing temperature of 58 °C was determined for the downstream fragment and 68 °C for the upstream fragment. The fjoh_1927 upstream primers showed highest efficiency at 50°C and downstream primers at 56°C. For the upstream and downstream fragment of fjoh_2419 and fjoh_4604 an annealing temperature of 60 °C was used. The amplification of both fjoh_2421 fragments was optimal at 66 °C. The upstream fragment of fjoh_2557 was amplified at 65 °C, while the downstream fragment was amplified at 68 °C. All fragments were separated by agarose gel electrophoresis using a 1% agarose gel. The expected fragment size ranged from 2100 bp to 2730 bp (*Figure 20* & *Figure 21*).

Table 21.: Expected size of each fragment in basepairs

target locus	upstream fragment (bp)	downstream fragment (bp)
fjoh_1748	2295	2523
fjoh_1927	2459	2527
fjoh_2419	2119	2722
fjoh_2421	2141	2069
fjoh_2557	2220	2170
fjoh_4604	2678	2400

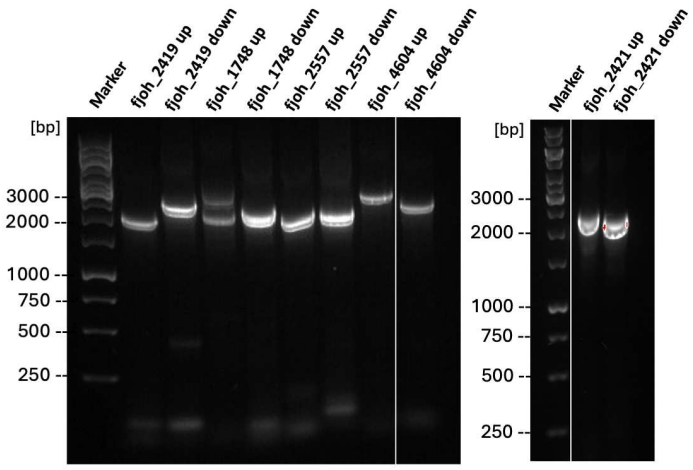

Figure 20.: **PCR fragments** from the amplification of the upstream and downstream regions of fjoh_1748, fjoh_2419, fjoh_2421, fjoh_2557, fjoh_4604. 1kb gene ruler was used as a marker

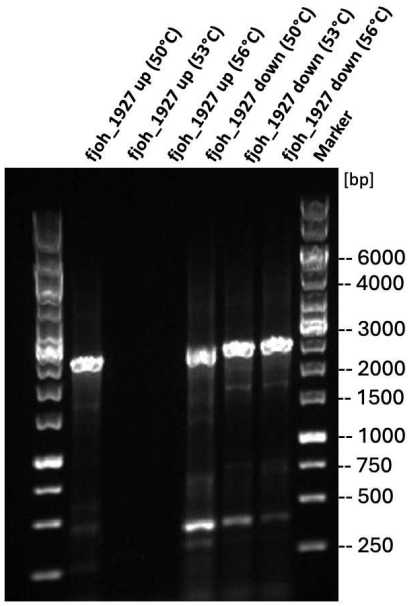

Figure 21.: **PCR fragments** from the amplification of the upstream and downstream regions of fjoh_1927 at different annealing temperatures. 1kb gene ruler was used as a marker

The PCR products were purified using the innuPREP PCRpure Kit, with the exception of the fjoh_1748 upstream fragment. As an unspecific fragment was amplified at 3000 bp, gel extraction was performed on the 2000 bp fragment. To assemble the suicide plasmid with up and downstream fragments of fjoh_1748, fjoh_1927, fjoh_2419, fjoh_2421 and fjoh_2557, the pYTT313 vector was digested with *Sal*I-HF and *SpH*I-HF. To generate the fjoh_4604 suicide plasmid the pYT313 vector was digested with *Sal*I-HF and *Xba*I. The fragments were assembled into the pYT313 vector via the NEBuilder HiFi DNA Assembly Kit. The protocol was adapted since no clones with correct insertions were obtained following the manufacturers instructions. For successful plasmid assembly incubation time was extended from 1 to 4 hours. Instead of 50-100 ng of vector, as recommended by the manufacturer, 10,25 ng of vector were used for the assembly reaction. Additionally a 1:3,5 vector to insert ratio was required for the reaction, which contrasts with the 1:2 ratio recommended by New England Biolabs. Plasmids were transferred into *E. coli* 10β by heat shock transformation and positive clones were selected for ampicillin resistance. A negative control without inserts was prepared to estimate the amount of background colonies obtained after transformation. Plasmids from 3-4 obtained clones were isolated and digested with suitable restriction enzymes to confirm correct assembly. The chosen restriction enzymes cut at multiple sites on the assembled plasmid, resulting in a distinct fragment pattern for each construct. The plasmids pYT313-2419_madel, -2557_madel were digested with *Eco*RI (*Figure 22*). The constructs pYT313-1748_madel, pYT313-1927_madel, pYT313-2421_madel and pYT313-4604_madel were digested with *Eco*RI and *Eco*RV (*Figure 24* & *Figure 23*). An empty pYT313 vector digested with the same restriction enzymes served as a control. Digestion with *Eco*RI alone, as well as *Eco*RI and *Eco*RV, resulted in 2 fragments of 1612 and 5998 bp, since *Eco*RV has no restric-

tion site in the empty pYT313.

Table 22.: Patterns for restriction digest after successful assembly of up- and downstream fragments.

Plasmid	Enzymes	patterns for fragment sizes (bp)					
pYT313-2419_madel	*Eco*RI	6994	1612	1483	1376	864	78
pYT313-2421_madel	*Eco*RI and *Eco*RV	5546	3820	1612	768		
pYT313-2557_madel	*Eco*RI	5750	2982	1612	1557		
pYT313-1748_madel	*Eco*RI and *Eco*RV	7317	1612	1424	1270	707	
pYT313-1927_madel	*Eco*RI and *Eco*RV	5456	3033	2394	1612		
pYT313-4604_madel	*Eco*RI and *Eco*RV	5369	2721	2680	1612	224	

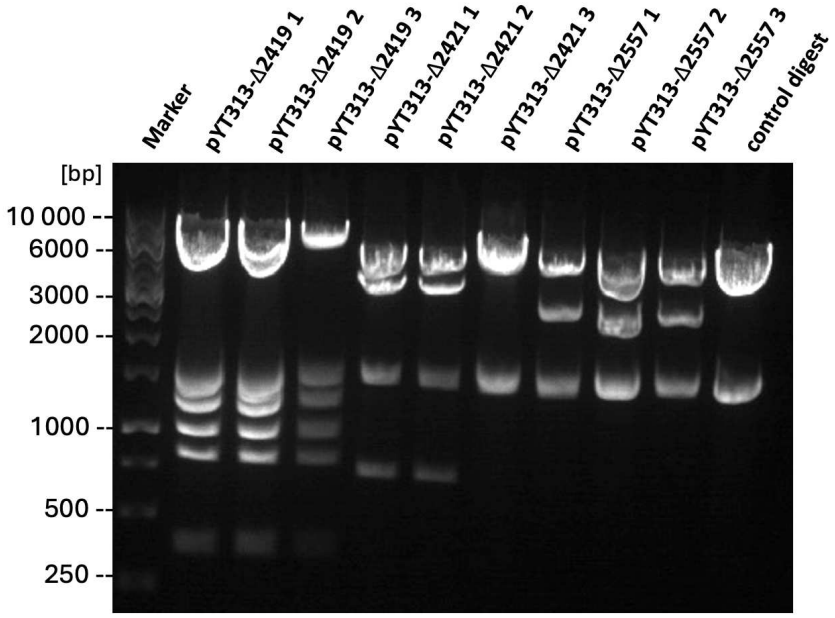

Figure 22.: **Restriction enzyme digest** from plasmids isolated after gibson assembly of pYT313-2419_madel, pYT313-2421_madel and pYT313-2557_madel

All pYT313-2419_madel constructs showed one fragment between 6000 - 8000 bp depending on the intensity of the band. Additionally 5 fragments with a size smaller than 2000 bp were observed, which correspond the expected sizes. For pYT313-2421_madel the first two clones showed a distinct fragment pattern with 2 fragments around 5000 and 4000 bp, one at 1500 bp and one at 750 bp. Restriction enzyme digest of pYT313-2557_madel constructs resulted in three DNA fragments of the size 5000 bp, 2500 bp and 1600 bp (*Figure 22*). Correct molecular cloning for constructs isolated from clone 1 of pYT313-2419_madel, -2421_madel and -2557_madel was confirmed by sequencing the downstream fragment.

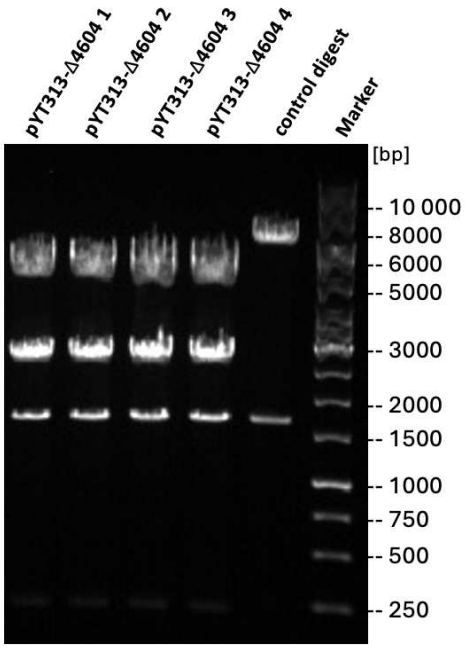

Figure 23.: **Restriction enzyme digest** from plasmids isolated after Gibson assembly of pYT313-4604_madel

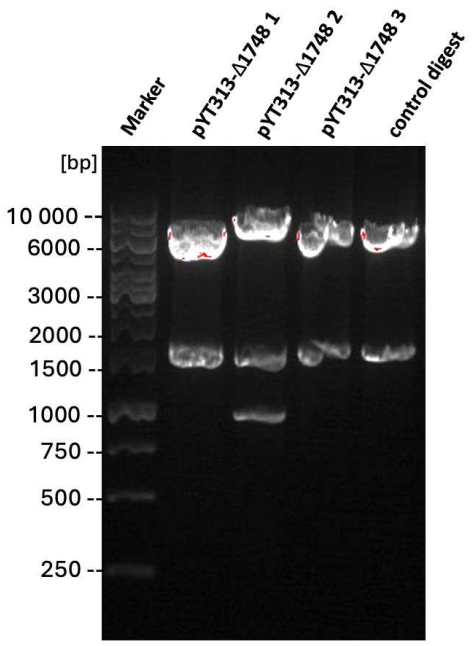

Figure 24.: **Restriction enzyme digest** from plasmids isolated after Gibson assembly of pYT313-1748_madel

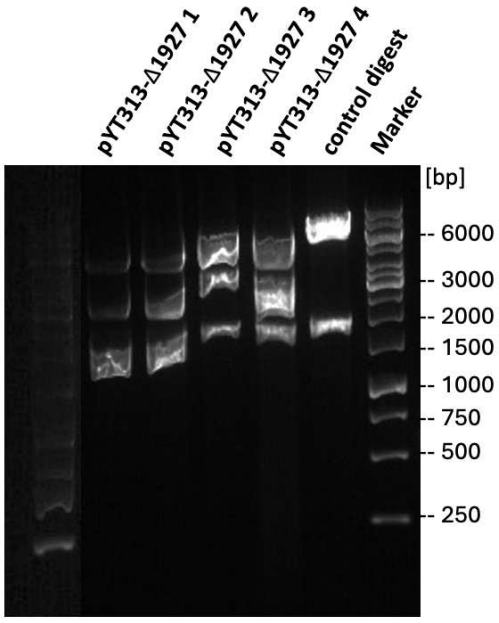

Figure 25.: **Restriction enzyme digest** from plasmids isolated after gibson assembly of pYT313-1927_madel

For potential pYT313-4604_madel constructs, four bands were observed for all clones at roughly 5500 bp, 3000 bp, 1700 bp, and 250 bp. The fragment pattern therefore correlates with the expected fragment sizes

(*Figure 23*). Correct molecular cloning was successfully verified by sequencing the downstream fragment of the construct obtained from clone 3 for pYT313-4604_madel.

For pYT313-1748_madel constructs, restriction digest of clone 2 revealed DNA fragments migrating at approximately 8000 bp, 1500 bp and 1000 bp (*Figure 24*). Based on comparison to the control digest the fragments of approximately 8000 bp and 1500 bp correspond to the expected fragments of 7317 bp and 1612 bp. In contrast, the fragment observed at approximately 1000 bp did not match the expected additional fragments of 1424 bp, 1270 bp, or 707 bp. Despite this discrepancy, sequencing of the downstream region of the construct from clone 2 was successful, confirming the presence of the downstream fragment. As correct insertion of this fragment requires compatible ligation sites, this result supports proper assembly of the construct. The construct obtained from clone 2 was used for subsequent experiments.

Restriction digest of potential pYT313-1927_madel plasmids revealed three detectable DNA fragments for clone 4. One fragment migrated at approximately 4000 bp and a second slightly below 2000 bp. The third band was observed between 2000 bp and 3000 bp. The smallest fragment corresponds to the expected 1612 bp fragment, as it co-migrates with the expected 1612 bp fragment in the control digest. The largest fragment migrated at 4000 bp, which is smaller than the expected fragment of 5456 bp fragment. The remaining expected fragments of 3033 bp and 2394 bp could not be clearly distinguished, as the band observed appeared diffuse and extended over approximately 1000 bp (*Figure 25*). Despite this, sequencing of the downstream region of the construct from clone 4 was successful, confirming the presence of the downstream fragment. Given that correct insertion of the downstream fragment requires complementary ligation sites from the upstream fragment and plasmid backbone, this supports proper assembly of the construct. Clone 4 was selected for further analysis.

3.3.2. Deletion of genes in *F. johnsoniae* wild type

To elucidate sulfobacin biosynthesis pathway, several genes proposed to be involved in the pathway were targeted for markerless deletion in *F. johnsoniae* wild type. This included a potential cysteate synthase gene (fjoh_2557), a putative sulfobacin synthase gene (fjoh_2421) and two potential monooxygenase genes (fjoh_1748 and fjoh_4604). All deletion mutants were successfully generated except for the second potential monooxygenase gene fjoh_1748, for which no deletion mutant was obtained. In addition the previously reported *sulA* gene (fjoh_2419) encoding for cysteate acyl-ACP transferase was deleted. The resulting *sulA* mutant served as a sulfobacin-deficient and immobile control strain.

To introduce a markerless deletion, two homologous recombination events are required. During the first homologous recombination, the plasmid integrates into the genome of the respective organism. During the second homologous recombination, either the first recombination event is reverted, or the plasmid is lost together with the target gene. The selection and counter selection marker are used to identify clones in which these recombination events have taken place (subsection 2.3.5). The suicide plasmids were in-

troduced into *F. johnsoniae* by conjugative transfer from *E. coli* S17-1 λ pir (subsection 2.3.4). To select for successful plasmid transfer, serial dilutions of *F. johnsoniae* cells were plated onto erythromycin containing plates. Growth was observed for all constructs on the selective plates up to a dilution of 10^{-4}, with colony numbers decreasing at higher dilutions. Colony growth was compared between undiluted plates and undiluted control plates. Growth on the control plates was reduced, but not completely absent. These clones were considered to be spontaneous resistant to erythromycin. To distinguish between clones with an integrated plasmid and spontaneous resistant clones, 50 colonies were transferred onto CYE-erythromycin plates and CYE plates containing 5% sucrose. Expression of the *sacB* gene led to the production of a white, glossy layer on top of colonies that carry the plasmid. This product was most likely levan. Clones that grew on the erythromycin plates and showed a white coating on the sucrose containing plate were considered to be single recombinants. Presence of the *sacB* gene was confirmed by amplifying a 650 bp fragment of the *sacB* gene from the pYT313 plasmid. An empty pYT313 plasmid served as a positive control.

Levan production was observed for *F. johnsoniae* clones carrying pYT313-1748_madel, pYT313-2419_madel, pYT313-2421_madel and pYT313-2557_madel. From the conjugation plates of pYT313-1748_madel, pYT313-2419_madel and pYT313-2557_madel, DNA of 1 positive clone was isolated and the presence of the *sacB* gene confirmed by PCR (*Figure 26* & *Figure 27*).

F. johnsoniae cells potentially carrying pYT313-4604_madel did not produce levan in the presence of sucrose. However, growth on erythromycin plates was still observed. In this case DNA from two erythromycin resistant clones was isolated and tested for *sacB*. Subsequent gel electrophoresis resulted in a 650 bp fragment for both clones, confirming the presence of the *sacB* gene (*Figure 28*).

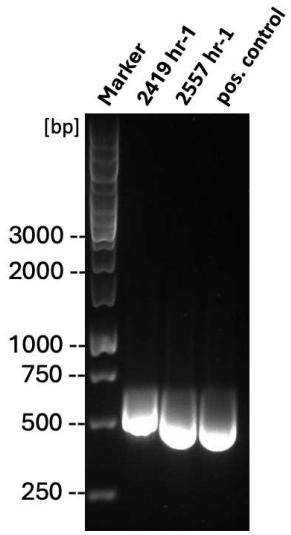

Figure 26.: **PCR ampflication of *sacB*** (650 bp) to confirm genomic integration of the suicide vector pYT313-2419_madel for the deletion of fjoh_2419 **(2419 hr-1)** and pYT313-2557_madel for the deletion of fjoh_2557 **(2557 hr-1)**. The pYT313 plasmid was used as a psositive control. Gene Ruler 1 kb ladder was used as marker.

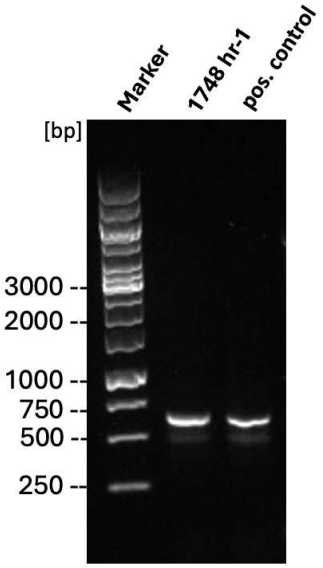

Figure 27.: **PCR ampflication of *sacB*** (650 bp) to confirm genomic integration of the suicide vector pYT313-1748_madel for the deletion of fjoh_1748 **(1748 hr-1)**. An empty pYT313 vector served as a positive control. Gene Ruler 1 kb ladder was used as marker.

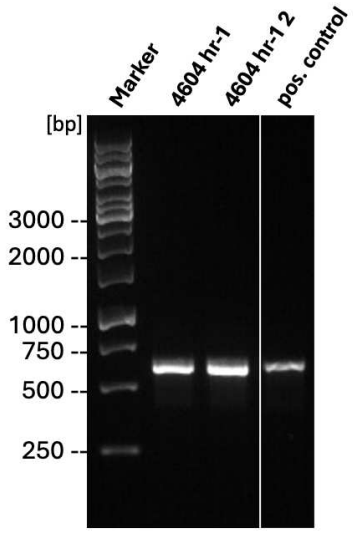

Figure 28.: **PCR ampflication of *sacB*** (650 bp) to confirm genomic integration of the suicide vector pYT313-4604_madel for the deletion of fjoh_4604 **(4604 hr-1, 4604 hr-1 2)**. The pYT313 plasmid served as a positive control. Gene Ruler 1 kb ladder was used as marker.

The single recombinants obtained were grown without selection pressure to induce the second homologous recombination. Dilutions of these cultures were plated onto CYE agar plates containing sucrose and further incubated. To screen for successful deletion mutants, 50-100 clones were transferred onto sucrose containing agar plates and motility medium agar plates. Clones that grew on sucrose containing

agar plates without producing levan were considered to have lost the plasmid. To distinguish between a wild type and mutant strain, gliding phenotypes were analyzed on motility medium agar plate. Successful deletion of the gene was verified by amplifying the targeted genomic region. The same genomic region of the wild type served as a control. For this, the upstream forward and downstream reverse primers of the respective genes were used. Compared to the wild type control, deletion mutants were expected to generate a smaller PCR product. In this case, only the flanking regions of the target gene were amplified. A consistent upward shift of DNA fragments relative to the DNA ladder was observed during agarose gel electrophoresis. Pre-staining agarose gels with GelRed is known to alter DNA migration, as documented by the manufacturer of the DNA ladder used. Therefore, fragment size estimation was based on comparison with the corresponding wild type control rather than relying exclusively on the DNA ladder.

To generate a Δ2421 mutant, 100 clones were screened for deletion, four of which exhibited an immobile phenotype on motility agar. DNA was isolated from these four clones, and PCR was performed to amplify the fjoh_2421 region. The targeted genomic region of the wild type consists of 5267 bp, with the fjoh_2421 gene being 1119 bp in size. Accordingly, a successful deletion results in a PCR product of 4148 bp. Agarose gel electrophoresis of the PCR products revealed a fragment of approximately 6000 bp for the wild type and a fragment of approximately 4500 bp for all four clones. These results confirm successful deletion of the putative sulfobacin synthase gene (fjoh_2421) in all four clones (*Figure 29*).

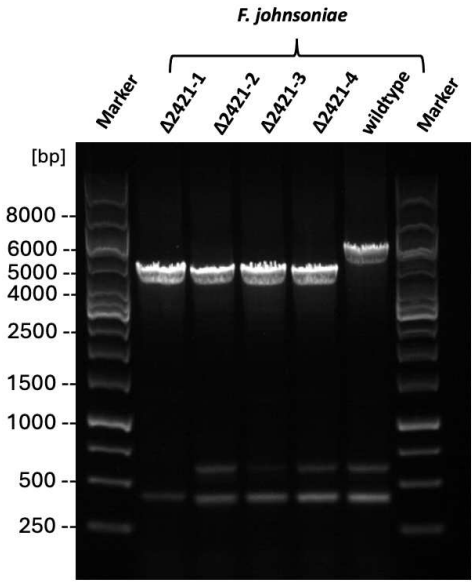

Figure 29.: **Screening for fjoh_2421 deletion in *F.johnsoniae***. For individual clones the fjoh_2421 region was amplified. *F. johnsoniae* wild type served as a control. Gene Ruler 1 kb ladder was used as marker.

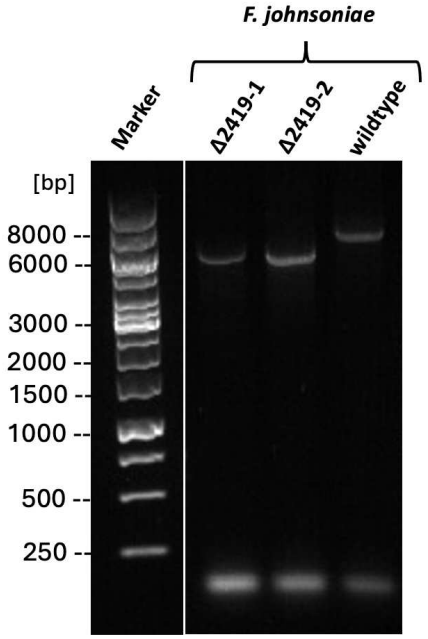

Figure 30.: **Screening for fjoh_2419 deletion in *F.johnsoniae***. For individual clones the fjoh_2419 region was amplified. *F. johnsoniae* wild type served as a control. Gene Ruler 1 kb ladder was used as marker.

For deletion of the *sulA* gene (fjoh_2419), two out of 100 clones revealed an immobile phenotype on motil-

ity agar. Deletion of the fjoh_2419 is expected to result in a PCR fragment 1260 bp smaller than the 6078 bp wild type region. PCR of the two immobile clones followed by agarose gel electrophoresis resulted in fragments of approximately 8000 bp for the wild type and a fragment slightly larger than 6000 bp for both clones. Despite aberrant DNA migration, the observed size difference between wild type and mutants corresponded to the expected reduction, confirming successful deletion of the *sulA* gene (*Figure 30*).

For potential Δ2557 clones, growth on sucrose plates and gliding on motility medium agar plates was observed for all 50 clones. DNA of 10 clones was isolated and the fjoh_2557 region analyzed using PCR. The wild type fjoh_2557 region yields a PCR product of 5411 bp, while deletion of the 1041 bp gene is expected to result in a 4370 bp fragment. Agarose gel electrophoresis revealed a fragment slightly above 8000 bp for the wild type and fragments right below 8000 bp in three of the ten clones. The relative reduction in fragment size compared to the wild type control corresponded to the expected deletion of fjoh_2557. Therefore, these three clones were identified as Δ2557 mutants (*Figure 31*). For the deletion of the potential monooxygenase fjoh_4604, one out of 50 clones displayed an altered phenotype. Although gliding motility was not completely lost, it was markedly impaired on motility agar plates. PCR was performed for this clone. The expected fragment size of a Δ4604 mutant is 5078 bp, while the wild type region spans 6239 bp. Agarose gel electrophoresis resulted in a fragment of approximately 10 000 bp for the wild type and 8000 bp for the mutant clone. The expected size difference is consistent with the expected deletion size, confirming the deletion of fjoh_4604 (*Figure 32*).

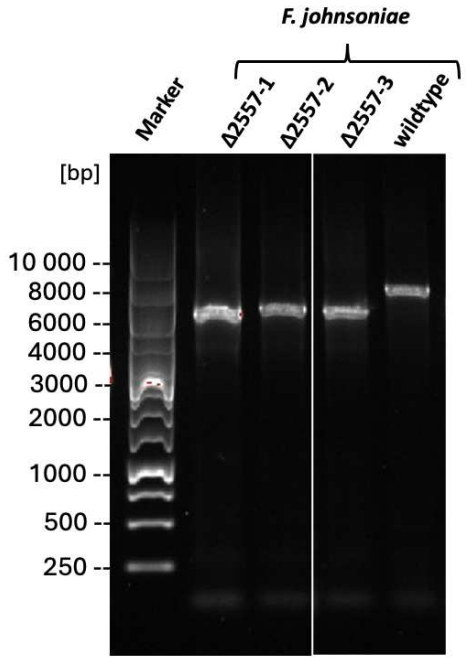

Figure 31.: **Screening for fjoh_2557 deletion in *F.johnsoniae***. For individual clones the fjoh_2557 region was amplified. *F. johnsoniae* wild type served as a control. Gene Ruler 1 kb ladder was used as marker.

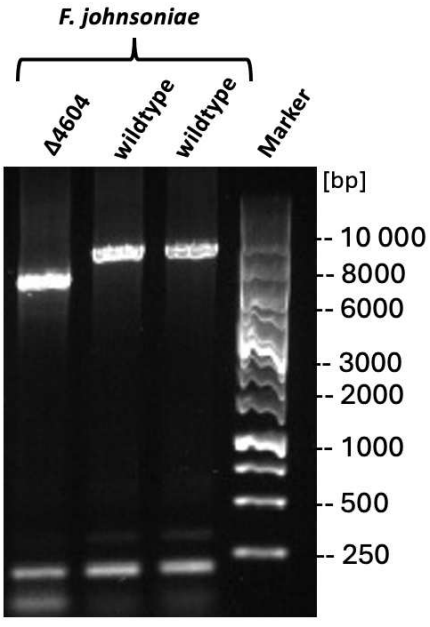

Figure 32.: **Screening for fjoh_4604 deletion in *F.johnsoniae***. For individual clones the fjoh_2557 region was amplified. *F. johnsoniae* wild type served as a control. Gene Ruler 1 kb ladder was used as marker.

To generate a knockout of fjoh_1748, a *sacB* positive clone was grown without selection pressure for 2 days. No altered phenotype was observed for 50 clones on motility medium agar plates. PCR was performed for all 50 clones. However, PCR amplicons resulted in fragments the same size as the wild type control. The procedure was repeated once, but again no Δ1748 mutants were obtained. For this construct, the second homologous recombination was considered to have reversed the first recombination event or to not have taken place at all. Therefore, deletion of fjoh_1748 was not successful.

3.3.3. Deletion of fjoh_1927 in *F. johnsoniae* Δ2557 mutant strain

As deletion of the putative cysteate synthase gene fjoh_2557 did not result in loss of motility, the Δ2557 mutant strain was targeted for deletion of fjoh_1927, another gene potentially involved in cysteate synthesis. For this purpose, the pYT313-1927_madel suicide plasmid was introduced into *F. johnsoniae* Δ2557 by conjugative transfer from *E. coli* S17-1 λ pir (subsection 2.3.4. To select for successful conjugative transfer, *F johnsoniae* Δ2557 cells were diluted and plated onto erythromycin plates. However, the selection process resulted in a bacterial lawn for all dilutions on the selective plates. Consequently, no single colony could be isolated for screening on sucrose plates to assess *sacB* activity. Therefore, conjugative transfer of pYT313-1927_madel and generation of a double mutant strain were unsuccessful under the conditions tested.

3.4. Introduction of frameshift mutations in fjoh_1748 and fjoh_4604

3.4.1. Suicide plasmid construction

For molecular cloning the targeted genomic regions of fjoh_1748 and fjoh_4604 were amplified by PCR using the Q5 polymerase. The up_fwd and up_gen_reverse primers were used to amplify the upstream fragment, which carries the first half of the gene to be disrupted. The downstream fragment containing the second half of the target gene was generated using down_fwd and gen_down_reverse primers. The tetracycline resistance cassette *tet(Q)* was amplified using the TC_fwd and TC_reverse primes. The pCP23 plasmid, which carries the tetracycline resistance gene *tet(Q)* served as a template.

Annealing temperatures were calculated considering the 20 bp overlap of each primer and tested. To amplify the fragments for the fjoh_1748 mutation, an annealing temperature of 56 °C was determined to be optimal for the upstream fragment, and 54 °C for the downstream fragment. Generation of upstream and downstream fragments for the fjoh_4604 construct was most efficient at an annealing temperature of 60 °C. Amplification of the tetracycline resistance cassette *tet(Q)* was observed at 55°C. An upward shift of the fragments and incomplete separation of the DNA ladder were observed in gel (B) (*Figure 33*). Although absolute migration was affected, the relative size differences between the amplicons were consistent with the expected sizes.

Table 23.: Expected size of each fragment in basepairs

DNA fragment	size (bp)
fjoh_1748 upstream_gen	2671
fjoh_1748 gen_downstream	3082
fjoh_4604 upstream_gen	3107
fjoh_4604 gen_downstream	3051
tetracycline resistance cassette	3503

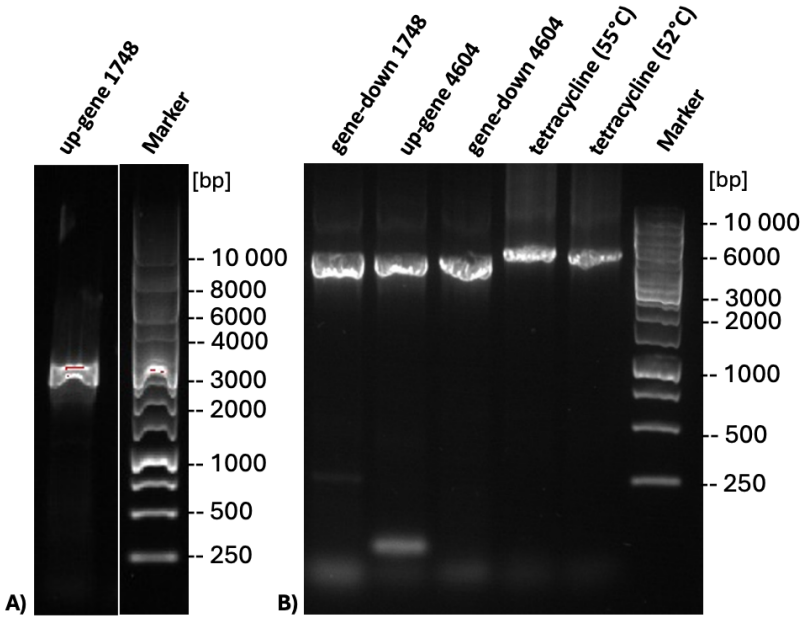

Figure 33.: **PCR fragments** of the upstream region of fjoh_1748 **(A)** and PCR amplicons from downstream regions of fjoh_1748, up and downstream region of fjoh_4604 and the tetracycline resistance gene **(B)**. In gel (B) an upward shift of the fragments and incomplete separation of the DNA ladder were observed. 1kb gene ruler was used as a marker.

PCR reactions of the amplified fragments were purified using the innuPREP PCRpure Kit. For assembly of the suicide plasmid pYT313-1748_TC, the pYTT313 vector was digested using the restriction enzymes *Sal*I-HF and *SpH*I-HF. To generate the suicide plasmid for disruption of fjoh_4604, the pYT313 vector was digested with *Sal*I-HF and *Xba*I. The purified PCR fragments were assembled into the pYT313 vector via the NEBuilder HiFi DNA Assembly Kit, using 10,25 ng of vector with 3,5-fold molar excess of each insert. A negative control without inserts was prepared for both assemblies. Following transformation into *E.coli* 10β, colony growth was observed for both constructs, while the negative controls yielded approximately half the number of colony forming units. Plasmid DNA from four clones was isolated for each construct and digested with *EcoR*I. An empty pYT313 vector served as a negative control. Expected fragment sizes of the control digest were 1612 bp and 5998 bp.

Table 24.: Patterns for restriction digest after successful assembly of upstream and downstream fragments, and tetracycline resistance cassette (*tet(Q)*) with pYT313.

Plasmid	Enzymes	patterns for fragment sizes (bp)				
pYT313-1748_TC	*Eco*RI	9042	3504	1612	1429	1269
pYT313-4604_TC	*Eco*RI	5593	3952	3426	2680	1612

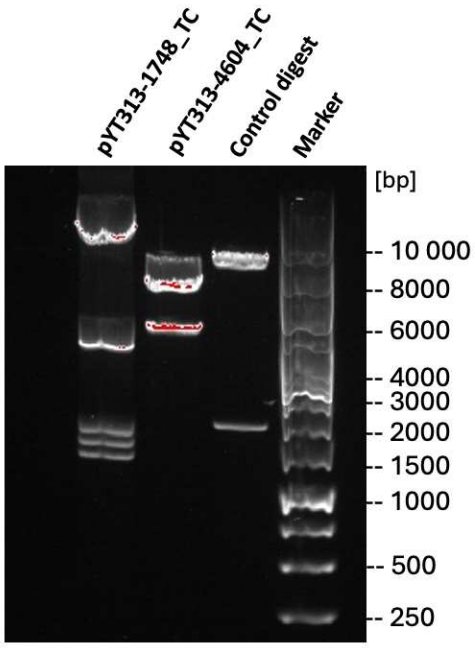

Figure 34.: **Restriction enzyme digest** from plasmids isolated after gibson assembly of pYT313-1748_TC and pYT313-4604_TC. A consistent upward shift in fragment migration relative to the DNA ladder was observed. 1kb gene ruler was used as a marker.

Agarose gel electrophoresis of one clone per construct revealed distinct fragment patterns compared to the control digest. The restriction enzyme digest of pYT313-1748_TC construct resulted in five fragments, including one fragment larger than 10 000 bp, one fragment of roughly 5000 bp, and three fragments ranging between 1500 and 2000 bp (*Figure 34*). Although absolute fragment migration deviated from the DNA ladder, relative band pattern was consistent with correct assembly. Correct molecular cloning was confirmed by sequencing the downstream region of fjoh_1748 and the tetracycline resistance gene *tet(Q)* of pYT313-1748_TC. For the pYT313-4604_TC construct two bands were observed, which correspond to the expected fragments at 5593 bp and 3952 bp (*Figure 34*). However, three additional bands were expected at 3426 bp, 2680 bp, and 1612 bp. Sanger sequencing of the downstream region of fjoh_4604 did not yield interpretable sequencing data, suggesting that errors during the assembly process occurred. Therefore, assembly of the pYT313-4604_TC construct was not successful.

3.4.2. Disruption of the open reading frame of fjoh_1748

As no Δ1748 deletion mutant could be obtained, the putative monooxygenase gene proposed to be involved in the hydrxoylation of sulfobacins, was targeted for a frameshift mutation. This mutation strategy was based on two homologous recombination events, resulting in the insertion of a tetracycline resistance gene *tet(Q)* into the target gene and thereby disrupting it's open reading frame.

For this purpose, the suicide plasmid pYT313-1748_TC was introduced into *F. johnsoniae* by conjugative transfer from *E. coli* S17-1 λ pir (subsection 2.3.4. To select for successful conjugative transfer, serial dilutions of *F. johnsoniae* cells were plated onto erythromycin containing plates. Growth was observed for the pYT313 construct up to a dilution of 10^{-2}. Colony growth on control plates indicated the presence of spontaneous resistant clones without an integrated plasmid. To distinguish cells that have successfully undergone conjugation from spontaneous resistant clones, 50 clones were transferred onto CYE erythromycin plates and motility medium agar plates. As integration of the suicide plasmid into the target locus already disrupts the open reading frame, phenotypic analysis on motility medium agar plates was performed at this stage. All 50 erythromycin resistant clones exhibited an immobile phenotype. Two of these clones were inoculated in liquid medium supplemented with tetracycline and growth was observed after two days of incubation. Genomic DNA of erythromycin and tetracycline resistant clones was isolated and tested for the *sacB* gene by PCR. Erythromycin and tetracycline resistant clones that exhibited impaired mobility and carried the *sacB* gene were considered to have successfully integrated the plasmid into the target gene (*Figure 35*).

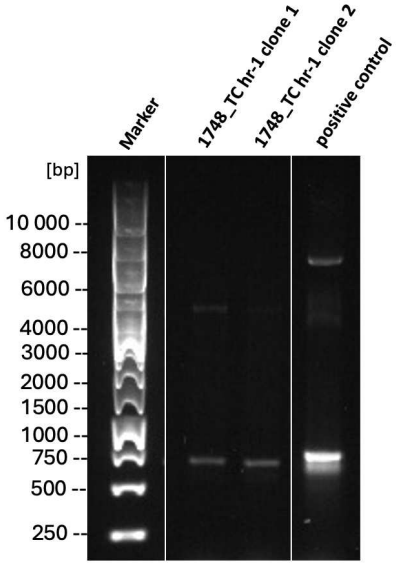

Figure 35.: **PCR ampflication of *sacB*** (650 bp) to confirm genomic integration of the suicide plasmid pYT313-1748_TC for the disruption of fjoh_1748 **(1748_TC hr-1 clone 1-2)**. As positive control the pYT313 plasmid was used as a template. Gene Ruler 1 kb ladder was used as marker.

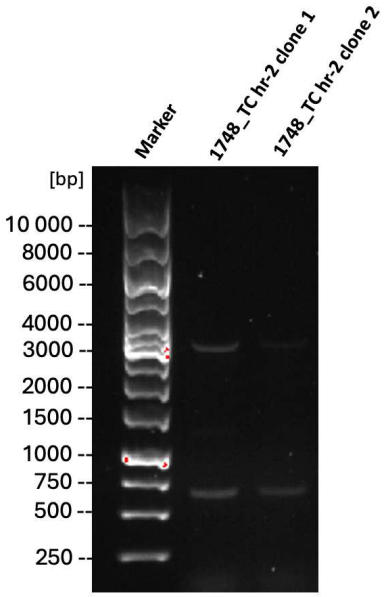

Figure 36.: **PCR ampflication of *sacB*** (650 bp) to confirm retention of the suicide plasmid pYT313-1748_TC after incubation without selection pressure **(1748_TC hr-2 clone 1-2)**. Gene Ruler 1 kb ladder was used as marker.

To induce the second homologous recombination event, a single recombinant was grown in liquid medium without selection pressure for two days. Dilutions of this culture were plated onto sucrose containing plates, and 50 clones that did not produce levan were transferred onto motility medium agar plates. All 50 clones again exhibited an immobile phenotype. To determine whether the second homologous recombination event had occurred, all clones were transferred onto erythromycin plates. Erythromycin resistant clones were considered to be single recombinants. Growth was observed for all clones on the erythromycin plate, indicating that the second homologous recombination event had not taken place. Genomic DNA of two clones was isolated and tested for the presence of the *sacB* gene by PCR. The *sacB* gene was detected in both clones, further confirming that the plasmid was still present (*Figure 36*). The entire procedure was repeated once, but a successful second homologous recombination was not achieved. As the initial homologous recombination event results in gene disruption, a single crossover mutant was used for downstream experiments.

3.5. Deletion of the putative sufobacin synthesis gene fjoh_2419, fjoh_2421 and fjoh_4604 does not affect growth in liquid medium

The mutant strains Δ2419, carrying a deletion in the cysteate acly-ACP transferase gene, Δ2421, lacking the putative sulfobacin synthase gene, and Δ4604 with a deletion in a potential monooxygenase gene, were grown in liquid medium to analyze whether gene deletion affected their growth. *F. johnsoniae* wild type served as a control. OD_{600} measurements were taken for three biological triplicates of each mutant strain and the wild type control.

Growth rates were calculated as the slope of linear regressions of log-transformed OD_{600} values over time during the exponential growth phase for each biological replicate. The exponential growth phase was defined as the period between 2 hours and 8 hours of cultivation, during which log-transformed OD_{600} values increased linearly, confirming exponential growth. Slopes were compared between wild type and mutant strains using Welch's two-sample t-test. The mean growth rate of the wild type strain was 0.494 ± 0.003 h^{-1}. Comparable growth rates where observed for the Δ2419 (0.501 ± 0.02 h^{-1}) and Δ2421 mutant strains (0.502 ± 0.008 h^{-1}), as seen in *Figure 37* and *Figure 38*. The Δ4604 mutant also exhibited a similar growth rate of 0.499 ± 0.01 h^{-1} (*Figure 39*). No significant differences in growth rates were observed between wild type and Δ2419 (*P* value = 0,61), Δ2421 (*P* value = 0,19) and Δ4604 (*P* value = 0.84) mutant strains.

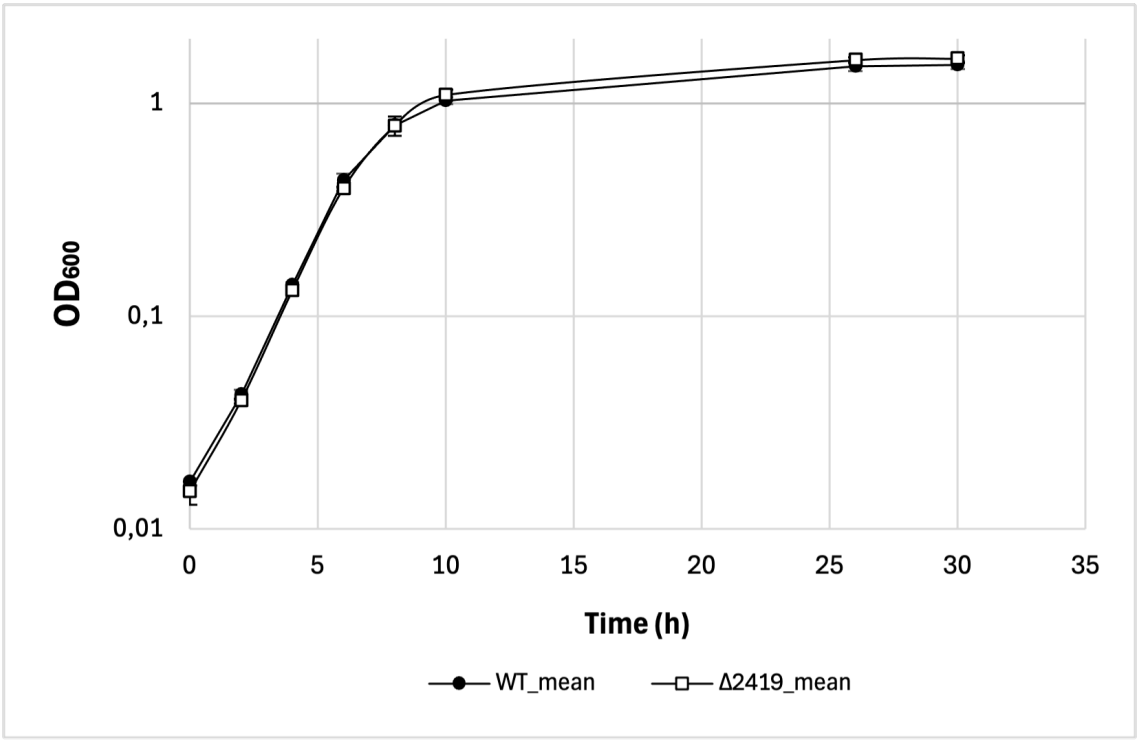

Figure 37.: **Growth** of *F. johnsoniae* Δ2419 and *F. johnsoniae* wild type under aerobic conditions at 27 °C. Data for Δ2419 and wild type represent the average of three independent biological replicates. Error bars indicate standard deviation and are smaller than the symbol size for most time points.

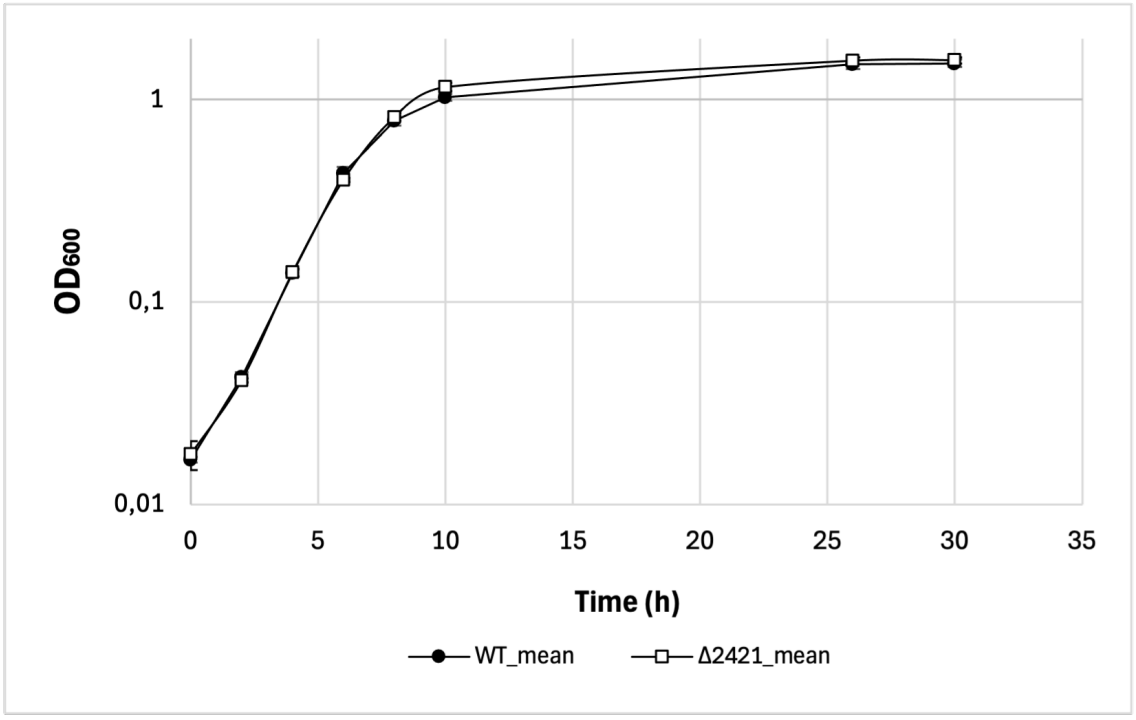

Figure 38.: **Growth** of *F. johnsoniae* Δ2421 and *F. johnsoniae* wild type under aerobic conditions at 27 °C. Data for Δ2421 and wild type represent the average of three independent biological replicates. Error bars indicate standard deviation and are smaller than the symbol size for most time points.

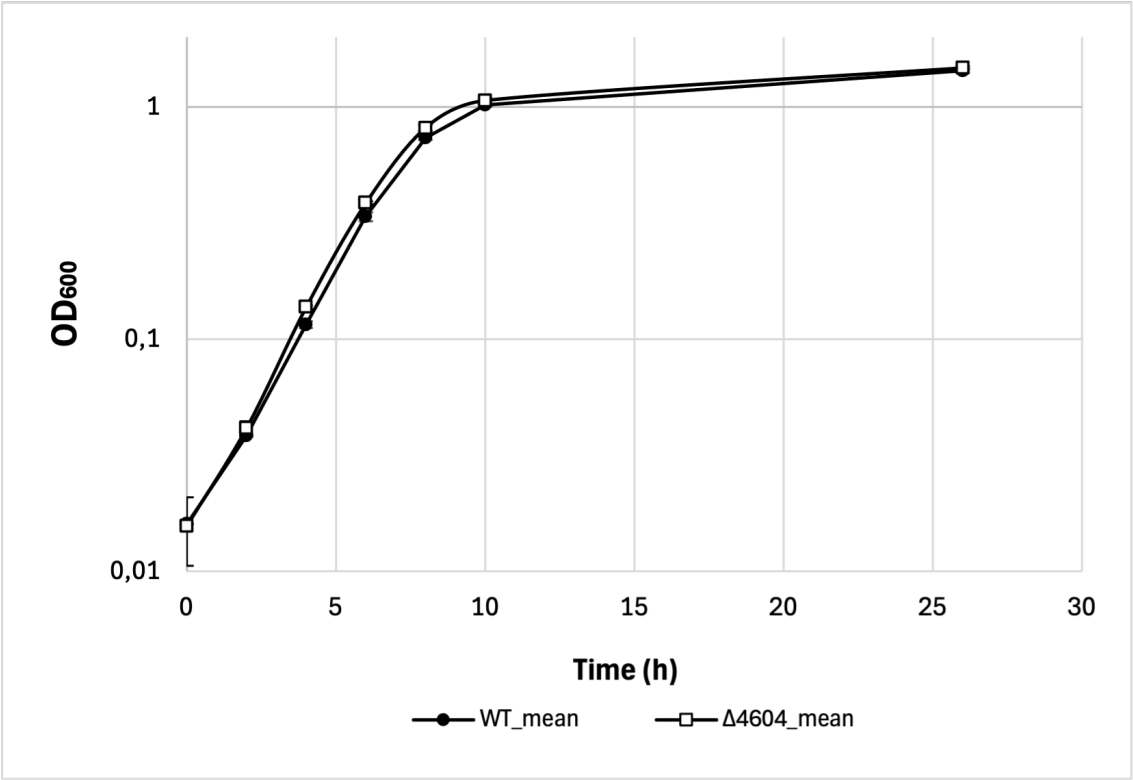

Figure 39.: **Growth** of *F. johnsoniae* Δ4604 and *F. johnsoniae* wild type under aerobic conditions at 27 °C. Data for Δ4604 and wild type represent the average of three independent biological replicates. Error bars indicate standard deviation and are smaller than the symbol size for most time points.

3.6. Deletion of fjoh_2419, fjoh_2421 and fjoh_4604 and disruption of fjoh_1748, but not fjoh_2557 impairs gliding motility of *F. johnosoniae*

To analyze gliding motility of the mutant strains, cultures were imaged hourly over a 15 hour period on motility medium agar plates. The only exception was the mutant strain potentially involved in cysteate synthesis Δ2557, which was imaged on LTY agar plates. LTY is a minimal medium, which has previously been used to identify cysteate deficient mutant strains (Abbanat et al., 1985). *F. johnsoniae* wild type served as a mobile control, while the *sulA* mutant strain (Δ2419) served as an immobile and sulfobacin deficient control. Deletion of Δ2419 has previously been reported to affect gliding motility in *F. johnsoniae* (Vences-Guzmán et al., 2021).

Gliding motility of *F. johnsoniae* wild type was analyzed over a 15 hour period to serve as a mobile control. The wild type colony exhibited gliding motility, which was observed by the formation of dendritic structures at the edges of the colony (*Figure 40*). This colony morphology is consistent with previously described gliding motility patterns in *F. johnsoniae* (McBride, 2004, Sato et al., 2021).

For microscopic analysis of Δ2557, colonies were imaged on LTY agar plates. As shown in *Figure 41*, deletion of Δ2557 did not result in loss of motility, as dendritic formations developed at the colony margins

after 15 hours of imaging.

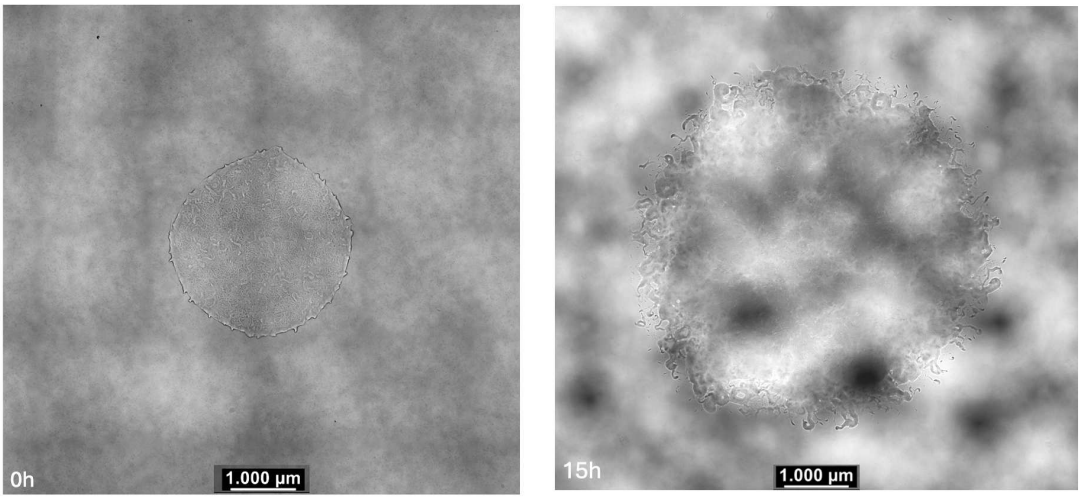

Figure 40.: **Microscopic imaging of a wild type colony** on a motility agar plate before and after 15 hours of time lapse series. Gliding motility of the colony can be seen by the formation of thin spreading edges after 15 hours of incubation.

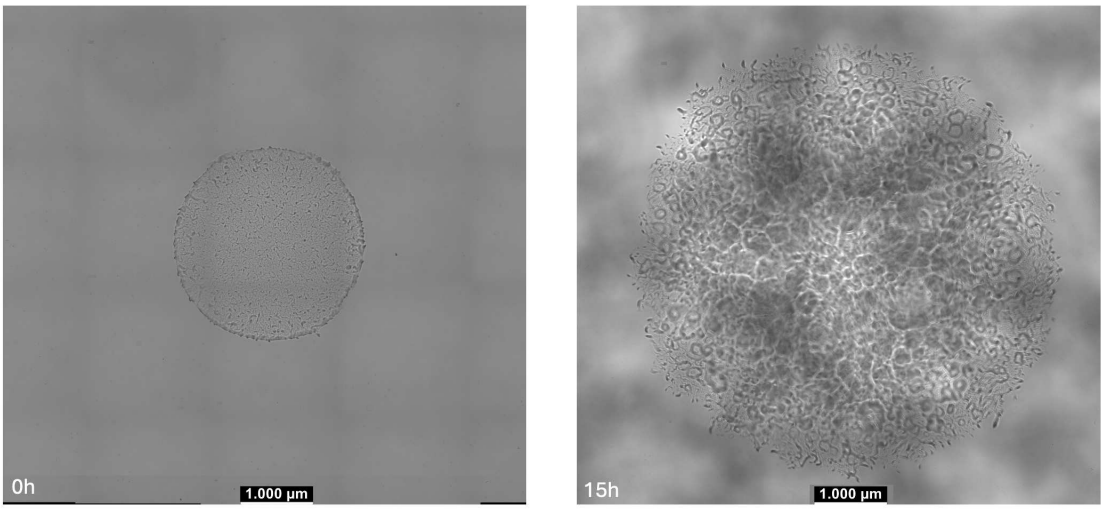

Figure 41.: **Microscopic imaging of a Δ2557 colony** on a LTY agar plate before and after 15 hours of time lapse series. Δ2557 strain exhibited a mobile phenotype during analysis.

Imaging of the cysteate acyl-ACP transferase (*sulA*) deficient strain (Δ2419) confirmed the absence of gliding motility, as no dendritic formations were observed after 15 hours of imaging and the colony remained compact with clean edges (*Figure 42*).

Deletion of the putative sulfobacin synthase gene (Δ2421) resulted in a phenotype similar to the *sulA* deficient Δ2419 mutant strain. No visible gliding motility was observed over 15 hours of imaging (*Figure 43*).

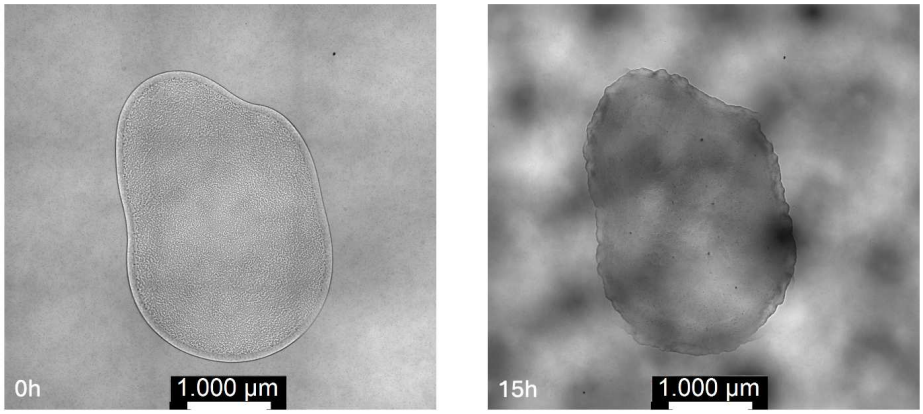

Figure 42.: **Microscopic imaging of a Δ2419 colony** on a motility agar plate before and after 15 hours of time lapse imaging. Δ2419 mutant strain exhibited an immobile phenotype during analysis.

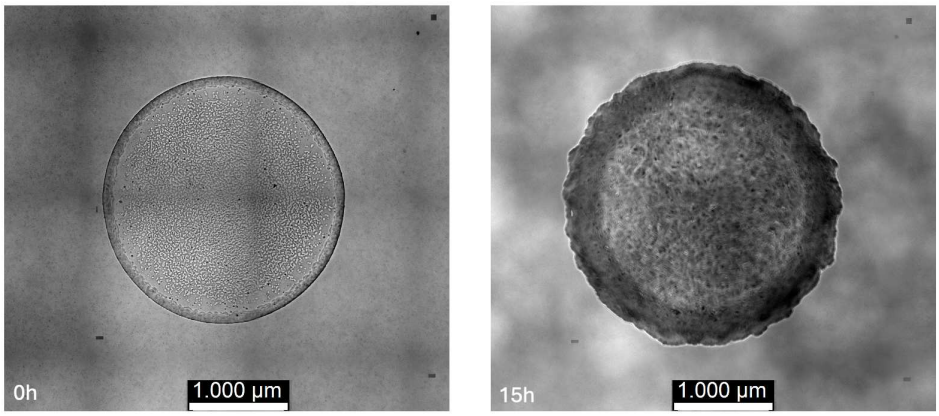

Figure 43.: **Microscopic imaging of a Δ2421 colony** on a motility agar plate before and after 15 hours of time lapse imaging. Δ2421 mutant strain exhibited an immobile phenotype during analysis.

The absence of a potential monooxygenase gene (fjoh_4604), resulted in impaired gliding ability. Compared to the wild type control, colony expansion and gliding was less, but not completely absent in the Δ4604 mutant strain (*Figure 44*). This can be seen by the formation of dendritic arms at the edges of the Δ4604 colony after 15 hours of imaging (*Figure 45*).

Time lapse imaging of the single crossover mutant with a disruption in a putative monooxygenase gene fjoh_1748 revealed an immobile phenotype comparable to the Δ2419 mutant strain. In addition, growth appeared impaired, as colony density did not visibly increase over the 15 hour observation period. (*Figure 46*).

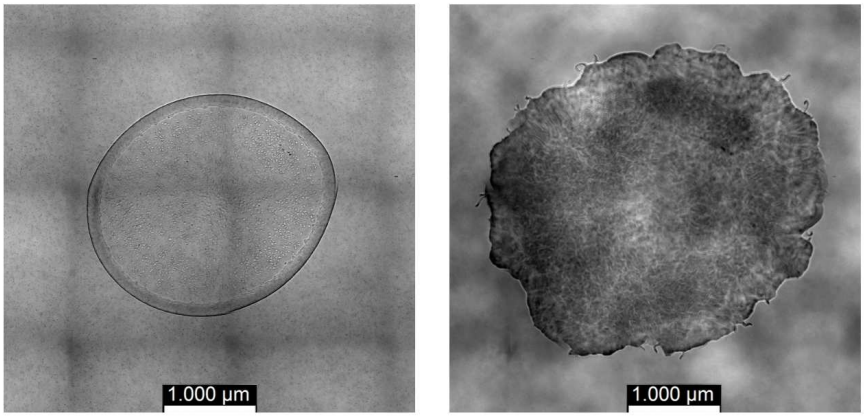

Figure 44.: **Microscopic imaging of a Δ4604 colony** on a motility agar plate before and after 15 hours of time lapse imaging. Δ4604 mutant strain exhibited impaired gliding motility during analysis.

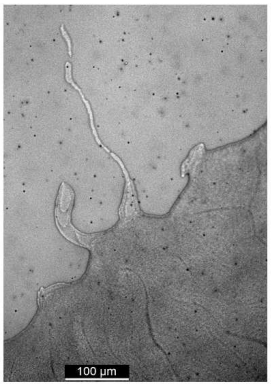

Figure 45.: **Formation of dendrite like structures in Δ4604 colony**, indicating gliding motility.

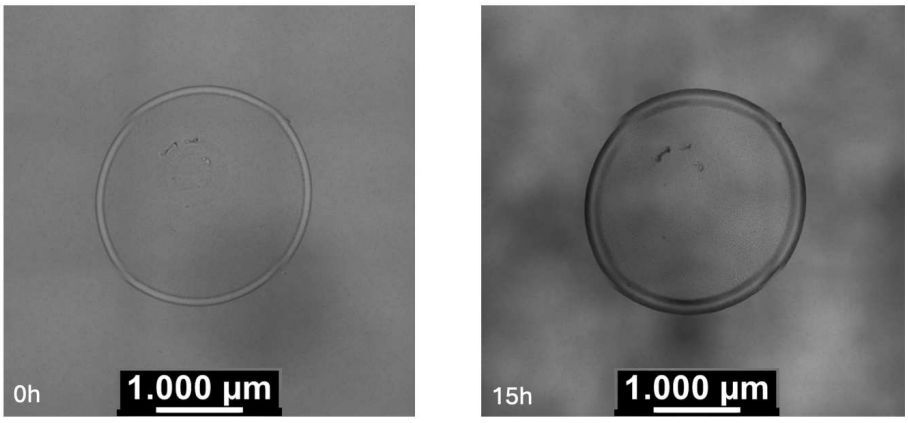

Figure 46.: **Microscopic imaging of a mutant with a single crossover disruption in fjoh_1748** on a motility agar plate before and after 15 hours of time lapse imaging. Fjoh_1748 disruption mutant strain exhibited an immobile phenotype and impaired growth during analysis.

3.7. Lipidomic profiling of *F. johnsoniae* wild type and mutant strains

To analyze whether the mutations affected sulfobacin biosynthesis, liquid chromatography-tandem mass spectrometry (LC-MS/MS) was performed for mutant strains deficient in gliding. Raw LC-MS/MS data were analyzed using Skyline. Structural assignment was based on accurate mass to charge ratios (m/z), retention times, and characteristic MS/MS fragmentation of the capnine backbone at m/z 350.2457 and 333.2102 and the sulfonate ion at m/z 80.9652. The detection limit for each lipid species was defined as twice the signal intensity measured in the corresponding blank.

3.7.1. Lipidomic analysis of *F. johnsoniae* wild type revealed the presence of eight major sulfonolipids

LC–MS analysis of lipid extracts from *F. johnsoniae* revealed a complex mass spectral profile containing several masses for known sulfobacins and their precursors capnine and 3-ketocapnine (*Figure 47*). Masses corresponding to the precursors 3-ketocapnine (m/z 349.2253) and capnine (m/z 350.2372) were detected at 10.2 and 10.6 minutes, but were present only in very low abundance. In total, eight sulfonolipid species were detected, including sulfobacin A, sulfobacin B, and sulfobacin D, together with five unknown sulfonolipids with precursor ions at m/z 686.4645, 604.4608, 588.4662, 588.4589 and 588.4298.

Signals corresponding to sulfobacin A (m/z 618.4768) and Sulfobacin B (m/z 574.4501) were observed at a retention time of 15.2 minutes. An additional signal was observed with a mass to charge ratio of 590.4451 eluting at 14.43 minutes, which is consistent with LC-MS data of sulfobacin D. MS/MS analysis of these compounds revealed fragment ions at m/z 350.2372 and 333.2102, corresponding to capnine fragments. In addition, the compound at m/z 590.4451 exhibited a fragment ion at 80.9652 m/z, consistent with a sulfonate moiety.

Furthermore, five unassigned masses were detected. The compound at m/z 604.4608 was detected at a retention time of 15,02 minutes and exhibited the same fragment ions as the compound associated with sulfobacin D, suggesting the presence of a capnine backbone. A compound with a precursor ion at m/z 686.4645 eluted at 16.61 minutes, and two closely related masses at m/z 588.4589 and 588.4662 were detected at retention times of 15.76 and 15.62 minutes, respectively. MS/MS spectra of the compounds at m/z 686.4645 and 588.4662 contained the fragment ion at m/z 350.2372, suggesting the presence of a capnine-derived moiety. Another compound was detected at m/z 588.298 and a retention time of 14.25, but fragmentation data were not obtained.

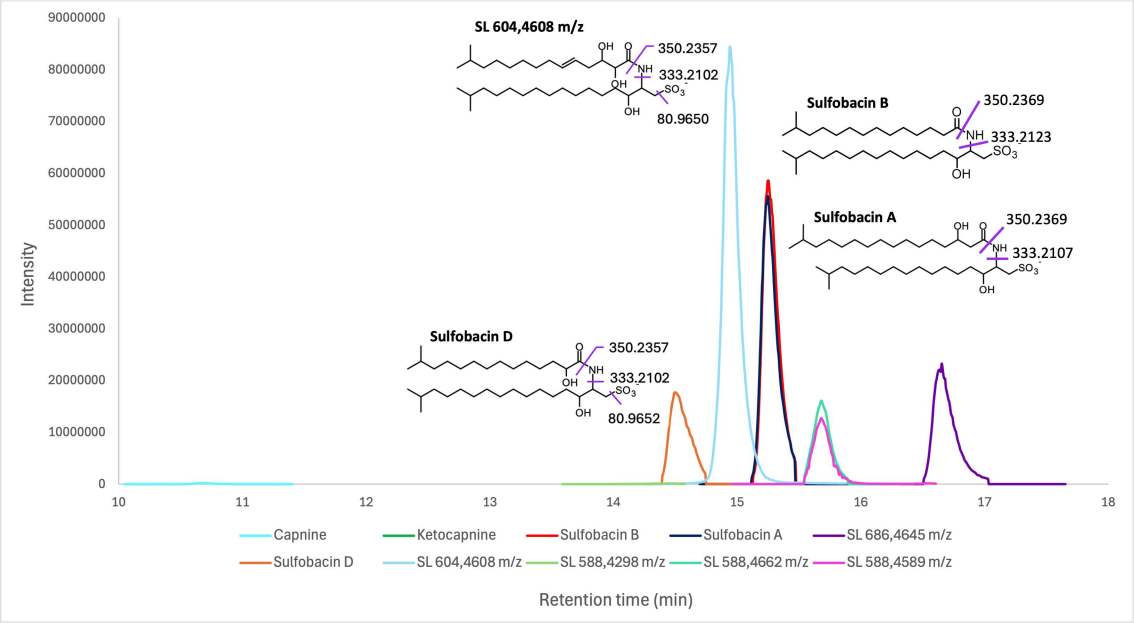

Figure 47.: **Lipidomic analysis of *F. johnsoniae* wild type** revealed a complex sulfonolipid profile. Known sulfobacins A, B and D were detected at retention times of 15,2 min (A and B) and 14,43 min (D). In addition, five unassigned sulfonolipid species were observed with precursor ions at m/z 686.4645, 604.4608, 588.4662, 588.4589, and 588.4298. MS/MS fragmentation of sulfobacins A, B, and D yielded characteristic capnine fragment ions at m/z 350.2372 and 333.2102. Sulfobacin D additionally showed a sulfonate fragment at m/z 80.9652. The sulfonolipid species m/z 604.4608 exhibited fragmentation patterns consistent with a capnine backbone. Although not shown in this figure, fragmentation of sulfonolipid species m/z 686.4645 and 588.4662 revealed fragmentation ions at 350.2372.

3.7.2. Deletion of cysteate acyl transferase fjoh_2419 revealed the absence of sulfonolipids

Deletion of fjoh_2419, previously identified as the cysteate acyl transferase gene was characterized by the absence of sulfonolipids, but accumulation of the sulfonolipid precursor capnine (m/z = 350,2372, 10,65 minutes). A mass for 3-ketocapnine was detected at m/z 349.2253 and a retention time of 10.79 minutes, but was found only in low abundance (*Figure 48*).

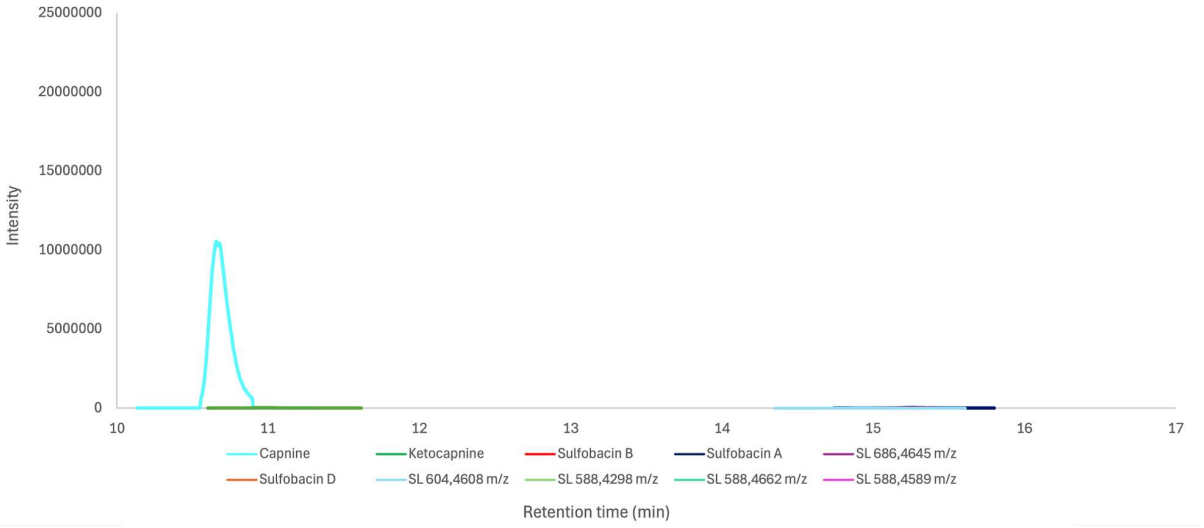

Figure 48.: **Lipidomic analysis of Δ2419.** LC-MS analysis of lipid extracts from the Δ2419 revealed the absence of sulfonolipids. Instead accumulation of the precursor capnine (m/z 350.2372) was detected at a retention time of 10.65 min. No signals corresponding tp sulfobacins or ther sulfonolipid species observed in the wild type were detected.

3.7.3. Deletion of the putative sulfobacin synthase fjoh_2421 resulted in an accumulation of the precursor capnine and absence of sulfonolipids

The chromatogram of the putative sulfobacin synthase Δ2421 mutant strain is characterized by a prominent signal at a retention time of 10.7 min, corresponding to the precursor molecule capnine (m/z = 350,2372). A mass corresponding to 3-ketocapnine (m/z = 349.2253) was detected at a retention time of 10.2 minutes. Signals for mature sulfonolipids were not detected, indicating that fjoh_2421 is required for sulfonolipid biosynthesis downstream of capnine formation (*Figure 49*).

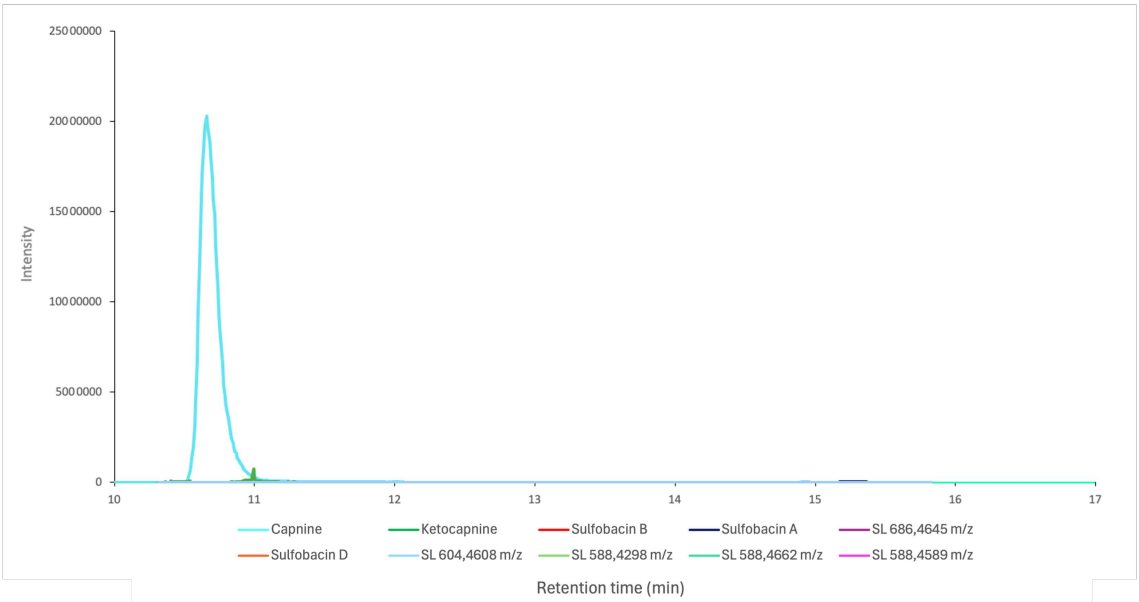

Figure 49.: **Lipidomic analysis of Δ2421.** The chromatogram of Δ2421 mutant strain displayed a dominant peak corresponding to capnine (m/z 350.2372) at a retention time of 10.7 minutes. Mature sulfonolipid species detected in the wild type were absent.

3.7.4. LC-MS/MS analysis of the potential monooxygenase mutant strains (fjoh_4604 and fjoh_1748) revealed the presence of all sulfonolipids detected in the wild type

Lipidomic analysis of the Δ4604 strain and the mutant with a single crossover disruption in fjoh_1748 revealed mass spectral profiles comparable to the chromatogram obtained from the wild type (*Figure 50* and *Figure 51*). Signals corresponding to 3-ketocapnine (m/z 349.2253) and capnine (m/z 350.2372) were present in low abundance in both strains. Mass signals and fragmentation patterns consistent with sulfobacin A (m/z 618.4768), sulfobacin B (m/z 574.4501), and sulfobacin D (m/z 590.4451) were detected in both mutant strains at retention times comparable to those observed in the wild type. Fragmentation patterns for these lipid species were characteristic for capnine fragment ions at m/z 350.2372 and 333.2102. The lipid species corresponding to sulfobacin D also showed a sulfonate fragment at m/z 80.9652. In addition, masses with precursor ions at m/z 604.4608, 588.4662 and 588.4589 were detected in both mutants. MS/MS spectra of m/z 604.4608 contained the three characteristic fragment ions for a capnine backbone (m/z 350.2372, 333.2102 and 80.9652), while m/z 588.4662 contained a fragment ion at m/z 350.2372. Two compounds with precursor ions at m/z 588.4298 and 686.4645 were detected in both strains. Due to a low signal intensity the peaks were not visible in the figures.

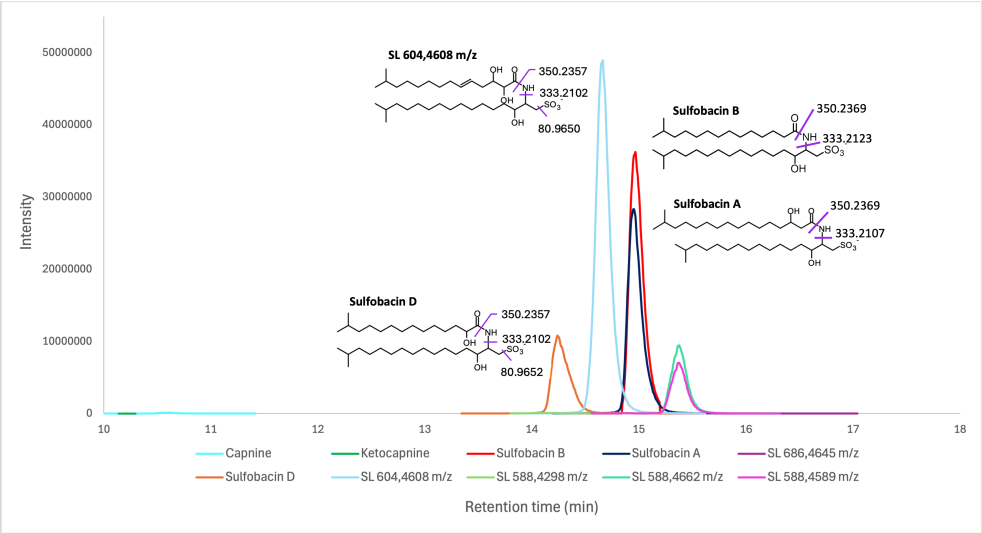

Figure 50.: **Lipidomic analysis of Δ4604.** LC–MS/MS analysis demonstrated that all sulfonolipid species identified in the wild type were also present in the Δ4604 strain. Retention times and corresponding m/z values closely matched those observed for *F. johnsoniae* wild type. MS/MS fragmentation of sulfobacins A, B, and D yielded characteristic capnine fragment ions at m/z 350.2372 and 333.2102. Sulfobacin D additionally showed a sulfonate fragment at m/z 80.9652. The sulfonolipid species m/z 604.4608 exhibited fragmentation patterns indicative of a capnine backbone. Although not shown in this figure, fragmentation of sulfonolipid species m/z 588.4662 revealed fragmentation ion at 350.2372. The sulfonolipid species at m/z 686.4645 and m/z 588.4298 were detected but exhibited a low signal and are therefore not visible in the figure.

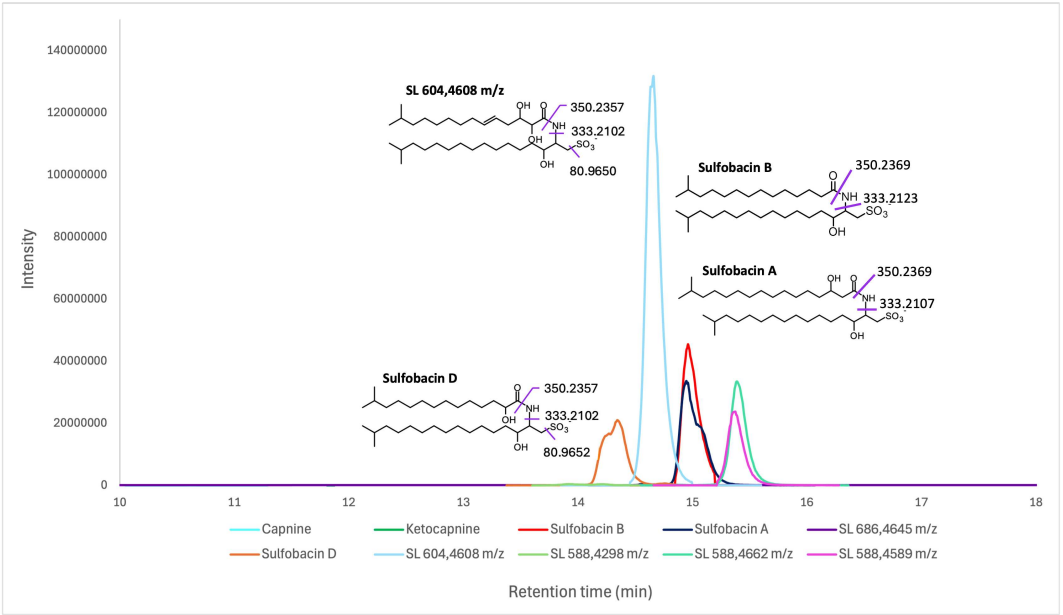

Figure 51.: **Lipidomic analysis of Δ1748.** LC-MS/MS analysis revealed the presence of all sulfonolipid species detected in the wild type with comparable retention times and m/z values. MS/MS fragmentation of sulfobacins A, B, and D yielded ions at m/z 350.2372 and 333.2102 characteristic for a capnine backbone. Sulfobacin D also exhibited a sulfonate fragment at m/z 80.9652. The sulfonolipid species m/z 604.4608 exhibited a fragmentation pattern that resembled the one of sulfobacin D. Although not shown in this figure, fragmentation of sulfonolipid species m/z 588.4662 revealed fragmentation ion at 350.2372. The sulfonolipid species at m/z 686.4645 and m/z 588.4298 were detected but due to low signal intensity are not visible in the figure.

4. Discussion

This work aimed to elucidate the sulfobacin biosynthesis pathway in *Flavobacterium johnsoniae*. Specifically, it sought to identify the genes encoding the enzymes responsible for cysteate synthesis and enzymes needed for the N-acylation of capnine to yield sulfobacin B. In addition, this work investigated whether hydroxylation of sulfobacin B to yield sulfobacin D is mediated by a monooxygenase. To answer these questions, markerless deletions and frameshift mutations of candidate genes were performed in *F. johnsoniae*. The candidate genes chosen were fjoh_1927 and fjoh_2557 as potential cysteate synthases, fjoh_2421 as a putative sulfobacin synthase, and fjoh_1748 together with fjoh_4604 as potential monooxygenases (*Figure 52*). As sulfobacins are required for gliding motility an immobile phenotype was expected for mutants deficient in sulfobacin production. Gliding phenotypes of the mutant strains were evaluated microscopically and their growth analyzed in liquid medium to ensure that impaired colony spreading was not attributable to general growth defects. We found that gliding motility was completely abolished in the putative sulfobacin synthase Δ2421 deletion mutant and in a mutant with a single crossover disruption in fjoh_1748, a potential monooxygenase gene. In the Δ4604 mutant strains, also potentially encoding a monooxygenase, gliding was impaired but not completely absent. Lipidomic analysis confirmed the absence of sulfonolipids and an accumulation of the precursor capnine in the putative sulfobacin synthase mutant strain. The two mutant strains with mutations in the potential monooxygenase genes, although exhibiting an altered gliding phenotype, still produced sulfonolipids.

These results suggest that the fjoh_2421 gene is central in sulfobacin biosynthesis, encoding a putative sulfobacin synthase, which is essential for gliding motility in *F. johnsoniae*.

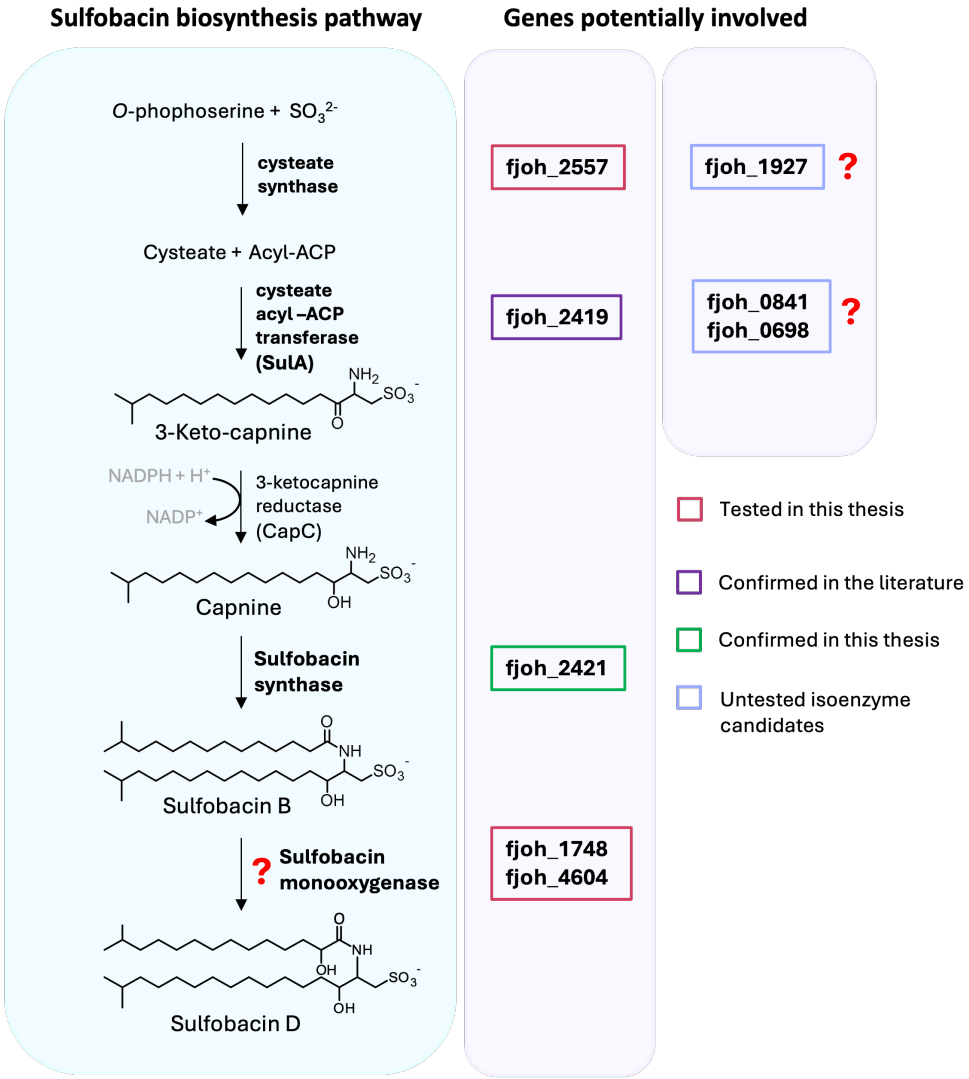

Figure 52.: **Functional assignment and validation of genes involved in sulfobacin biosynthesis in *F. johnsoniae* .** Schematic representation of the proposed sulfobacin biosynthetic pathway in *F. johnsoniae*, illustrating enzymatic steps from O-phosphoserine and sulfite to sulfabacin D. Corresponding genes are indicated next to each enzymatic step. Genes are color-coded according to their validation status. Genes shown in red were experimentally tested in this thesis, but were not essential for sulfobacin biosynthesis or modifications. Fjoh_2419 (purple) was previously confirmed in the literature to encode the cysteate acyl-ACP transferase (Vences-Guzmán et al., 2021, Radka et al., 2022). Fjoh_2421 (green) was experimentally validated to be involved in sulfobacin synthesis in this thesis and most likely encodes a sulfobacin synthase. Genes shown in blue represent potential isoenzyme candidates with proposed but unconfirmed functions. Possible candidates for reductases were not investigated, as too many candidate genes were present in the genome of *F. johnsoniae*.

4.1. Sulfonolipids and their biosynthesis in *F. johnsoniae*

The Gram negative bacterium *F. johnsoniae* is characterized not only by it's unique gliding motility but also by an unusual membrane composition in which sulfonolipids can account for up to 20% of total membrane lipids (Vences-Guzmán et al., 2021). Sulfonolipids and their precursor capnine have first been reported in the genus of *Capnocytophaga* and were later identified in several gliding bacteria within the phylum Bacteroidota, including *F. johnsoniae* (Godchaux and Leadbetter, 1980, Godchaux and Leadbetter, 1984). Early analysis of *F. johnsoniae* lipid profile detected only a small number of sulfonolipids with three species identified by Abbanat et al., 1988. Based on their proposed structure, one lipid species most likely represented sulfobacin D. In this early study, sulfonolipids were separated and detected by thin-layer chromatography and radiolabeling, followed by structural characterization of fatty acid methyl esters using gas chromatography-mass spectrometry (Abbanat et al., 1988). While these approaches enabled structural insights into the fatty acyl chain composition of sulfonolipids, they relied on prior separation and derivatization steps and did not provide high-resolution analysis of intact lipid species. This may have limited the detection of low-abundance or structurally similar sulfonolipids. Subsequent studies in related organisms, such as *Chryseobacterium sp.* and *Algoriphagus machipogonensis*, revealed a considerably broader structural diversity of sulfonolipids, including sulfobacin A-F and the rosette inducing factors RIF-1 and RIF-2 (Kamiyama et al., 1995, Beemelmanns et al., 2014, Leichnitz et al., 2022). To date, LC-MS/MS based lipidomic analysis of sulfonolipids in *F. johnsoniae* have only been mentioned by Vences-Guzmán et al., 2021, who reported solely the detection of sulfobacins A and B. However, the study did not provide LC-MS chromatograms or supporting mass spectrometric data.

In this work, LC-MS/MS based lipidomic analysis revealed a substantially broader sulfonolipid profile in *F. johnsoniae* compared to previous reports. In addition to the known Sufobacin A, B and D, five further sulfonolipid species were detected. Several of these displayed molecular masses corresponding to previously described lipids but exhibited distinct fragmentation patterns, suggesting the presence of constitutional isomers rather than identical compounds. The sulfonolipid species at m/z 604,4608 matched the reported mass of RIF-2, yet MS/MS spectra indicated an unmodified capnine backbone, which is inconsistent with the published structure and suggests an isomeric species (Leichnitz et al., 2022). Likewise, three sulfonolipids of m/z 588 exhibited the mass of sulfobacin F, but produced fragment ions, which were incompatible with the expected double bond within the capnine backbone characteristic for sulfobacin F (Peng et al., 2023). This again suggests the presence of constitutional isomers. In our analysis, although a signal for sulfobacin E was detected, no MS/MS data were obtained, which prevented definitive assignment (Leichnitz et al., 2022). The absence of these masses in the cysteate acyl-ACP transferase mutant strain and Δ2421 strain demonstrates that the detected species depend on an intact sulfonolipid biosynthetic pathway, consistent with their assignment as sulfonolipids. Together, these findings suggest that the sulfonolipid profile of *F. johnsoniae* is more diverse than previously recognized.

4.1.1. The role of fjoh_2557 in cysteate synthesis

Cysteate can be scavenged from the environment or synthesized endogenously from O-phosphoserine and sulfite by a cysteate synthase (Liu et al., 2022). Before cysteate synthases were identified in bacteria, they had only been described in methanogenic archaea (Graham et al., 2009). It is now known that there are two convergently evolved cysteate synthases in bacteria (Yang et al., 2025). The cysteate synthases of anaerobic *Bacteroidales* are homologues of archaeal cysteate synthases, whereas the cysteate synthases in aerobic bacteria are closely related to cystathionine β-synthases (Liu et al., 2022, Hou et al., 2022). Taking into account the strictly aerobic lifestyle of *F. johnsoniae*, the candidate genes fjoh_2557 and fjoh_1927 were selected based on sequence similarity to an experimentally validated cystathionine β-synthase related cysteate synthase in *Chryseobacterium gleum* (Hou et al., 2022). Previous studies reported *F. johnsoniae* mutants defective in cysteate formation were unable to synthesize sulfobacins and exhibited an immobile phenotype. Addition of the sulfonolipid precursor L-cysteate restored both sulfonolipid synthesis and motility, indicating that cysteate availability is essential for this process. However, the genomic loci affected in these mutants were not identified (Abbanat et al., 1986).

To investigate the role of fjoh_2557 in cysteate synthesis, a markerless deletion mutant was generated. Since the absence of cysteate is expected to abolish sulfonolipid production, loss of motility was anticipated if fjoh_2557 encoded an essential cysteate synthase. However, the Δ2557 mutant did not show any detectable defect in gliding motility. This observation suggests that fjoh_2557 alone is not essential for cysteate synthesis under the conditions tested. Several explanations may account for this result. First, despite sequence similarity to the cysteate synthase described in *Chryseobacterium gleum*, fjoh_2557 may not encode the functional cysteate synthase in *F. johnsoniae*. Instead, fjoh_1927 represents a more likely candidate, as it shows stronger statistical support in sequence comparisons (Hou et al., 2022). An alternative explanation is functional redundancy, where fjoh_2557 and fjoh_1927 encode isoenzymes. In this case deletion of a single gene may not abolish cysteate production. Such redundancy has been described in *Chryseobacterium gleum*, where two related enzymes independently catalyzed cysteate formation *in vitro*, albeit with different catalytic efficiencies (Hou et al., 2022). A comparable arrangement in *F. johnsoniae* would explain why deletion of a single gene did not result in a detectable gliding phenotype. To test this hypothesis, construction of a double deletion mutant would be required. In this work, attempts to generate such a strain were unsuccessful, leaving the precise genetic basis of cysteate synthesis unresolved. In addition to genetic redundancy, exogenous cysteate availability or metabolic compensation may further obscure a possible phenotype. Cysteate or related sulfur-containing compounds may have been supplied by the growth medium, allowing sulfonolipid synthesis without the action of a cysteate synthase. To minimize complex nutrient sources, LTY medium composed of 0.5% tryptone and 0.5% yeast extract was used to analyze the motility phenotype. This medium has previously been employed to analyze gliding behaviour of cysteate deficient mutant strains (Abbanat et al., 1986). However, yeast ex-

tract is a chemically undefined component and may contain sulfur-containing metabolites that support cysteate-dependent processes. Finally, cysteate may have been produced via an alternative metabolic pathway, thereby compensating for the loss of fjoh_2557. In principle, cysteine can be oxidized to cysteate. Aerobic organisms form reactive oxygen species endogenously through the reaction between molecular oxygen and univalent electron donors, such as metal centers, flavins and quinones. These cofactors are prominent electron carriers in respiratory chains, making reactive oxygen species a by-product of energy metabolism (Imlay, 2013). Due to the high reactivity of its sulfur containing thiol group (-SH), cysteine is especially susceptible to oxidation by reactive oxygen species. Oxidation of cysteine proceeds stepwise via the formation of sulfenic acid (-SOH), which can further be oxidized to sulfinic acid ($-SO_2H$) and ultimately to sulfonic acid ($-SO_3H$), corresponding to cysteate (Ezraty et al., 2017). Considering the aerobic lifestyle of *F. johnsoniae* oxidation of cysteine could possibly contribute to cysteate formation without the activity of a cysteate synthase.

4.1.2. Deletion of *sulA* and its role in the formation of 3-ketocapnine

Given that sulfonolipids and their precursor capnine are sulfur analogs of ceramides and sphinganine, the reaction steps following cysteate formation have been proposed to be analogous to bacterial ceramide synthesis (Radka et al., 2022). The next step in sulfonolipid synthesis is the condensation of cysteate with an acyl-ACP to generate 3-ketocapnine, catalyzed by a cysteate acyl-ACP transferase termed SulA (Radka et al., 2022). In *F. johnsoniae sulA* was previously proposed based on sequence similarity to serine palmitoyltransferase (Spt) in *Sphingomonas wittichii*, which catalyzes an analogous reaction in ceramide synthesis. Both enzymes belong to the α-oxoamine synthase family and catalyze a carbon-carbon bond formation between an amino acid and a fatty acyl thioester (Raman et al., 2010, Vences-Guzmán et al., 2021). In this previous study, deletion of the proposed *sulA* gene fjoh_2419 abolished sulfonolipid production and gliding motility, supporting a central role in sulfonolipid synthesis. Heterologous expression of this gene in *E. coli* led to the formation of a capnine like molecule. Based on their LC MS/MS analysis, this molecule appeared to be an unsaturated capnine without the iso-branched chain and having lost a molecule of water. This divergence from the actual 3-ketocapnine molecule was argued to be due to the absence of branched chain fatty acids in *E. coli*. While genetic evidence strongly implicated *sulA*, direct biochemical confirmation of the reaction product remained limited (Vences-Guzmán et al., 2021).

In this work a *sulA* deletion mutant was generated to serve as a sulfobacin deficient and immobile control. As expected, deletion of fjoh_2419 resulted in loss of gliding motility and sulfobacin production. Growth in liquid medium of the Δ2419 strain was not affected, indicating that neither the introduced deletion nor the absence of sulfonolipids caused a general growth defect. Given the proposed role of *sulA*, the absence of 3-ketocapnine and its downstream product capnine would be anticipated upon deletion. However, lipidomic analysis revealed detectable levels of capnine and 3-ketocapnine. At first glance, this observa-

tion appears inconsistent with disruption of the SulA-catalyzed step.

However, recent biochemical and structural characterization of SulA from *Alistipes finegoldii* provides strong evidence linking fjoh_2419 in *F. johnsoniae* to the cysteate acyl-ACP transferase. SulA was confirmed to function as a pyridoxal phosphate (PLP)-dependent α-oxoamine synthase and adpots the prototypical fold of bacterial serine palmitoyltransferases (Spt), with nearly identical active sites, supporting the annotation of fjoh_2419 based on Spt homology (Radka et al., 2022, Vences-Guzmán et al., 2021). Phylogenetic analysis further placed SulA from *Alistipes finegoldii* in close proximity to fjoh_2419 within the Spt-like branch of the α-oxoamine synthase family, supporting functional assignment of fjoh_2419 as the cysteate acyl-ACP transferase in *F. johnsoniae* (Radka et al., 2022). Additionally, the presence of residual capnine and 3-ketocapnine does not necessarily imply continued SulA-dependent synthesis. Low-level accumulation of these intermediates may arise from non-specific metabolic side reactions or from the activity of isoenzymes that catalyze analogous reactions with lower catalytic efficiency. Such activity may be insufficient to provide enough substrate for downstream sulfonolipid synthesis. In addition to fjoh_2419, two genes fjoh_0814 and fjoh_0698 were identified as candidates potentially encoding cysteate acyl-ACP transferases in *F. johnsoniae* (Vences-Guzmán et al., 2021). Both enzymes are annotated as PLP-dependent enzymes acting on amino acid-derived substrates. While their function and potential involvement in 3-ketocapnine synthesis has not been described, their predicted catalytic mechanism is conceptually compatible with formation of 3-ketocapnine (Vences-Guzmán et al., 2021). Given the high sensitivity of LC-MS/MS detection, metabolically insignificant pools of 3-ketocapnine and capnine may still be readily observed without supporting measurable sulfonolipid production. Although signal intensity for capnine was strong, LC-MS/MS analysis was performed without the use of internal standards and therefore does not allow reliable quantification. Ionization efficiency and matrix effects vary substantially between compound and sample backgrounds, such that signal intensities do not directly reflect absolute metabolite abundance in the absence of appropriate internal standards (Van Eeckhaut et al., 2009).

Overall, these findings are consistent with fjoh_2419 encoding SulA in *F. johnsoniae*, while residual 3-ketocapnine and capnine detected in the deletion mutant most likely arise from metabolically insignificant background reactions.

4.1.3. Identification of a sulfobacin synthase gene in *F. johnsoniae*

The third step of sulfonolipid synthesis is the reduction of 3-ketocapnine to capnine. A 3-ketocapnine reductase (CapC) has previously been identified in *Ornithobacterium rhinotracheale* (Liu et al., 2022). In this work, possible candidates for reductases in *F. johnsoniae* were not investigated, as 39 short-chain dehydrogenases/reductases were found as potential candidate genes (E-value < 8 x 10^{-04}), making knockout analysis impractical. Following reduction of 3-ketocapnine to capnine, the proposed pathway predicts an N-acylation step in which capnine is condensed with a branched chain C15 fatty acid to form sulfobacin

B. This reaction is conceptually analogous to ceramide synthesis, where the sphingoid base is acylated by ceramide synthases. The candidate gene fjoh_2421 was selected based on sequence homology to the ceramide synthase (bCers) identified in *Caulobacter crescentus* (Stankeviciute et al., 2022). Although overall sequence identity was modest (23.9%), the high alignment coverage (82%) and significant E-values (3×10^{-24}) supported homology. In addition, both fjoh_2421 and ceramide synthase (bCers) are annotated to the acyl-CoA N-acyltransferase (Nat) superfamily based on an UniProt classification, suggesting a shared enzymatic function.

Consistent with this, deletion of fjoh_2421 resulted in complete loss of motility, while growth in liquid medium was not affected. Lipidomic analysis revealed the absence of sulfonolipids and accumulation of the precursor capnine. Such precursor build up is consistent with interruption of the downstream acylation step. Additionally, the ceramide synthase in *Caulobacter crescentus* uses acyl-CoA substrates with varying chain lengths for the N-acylation step with the highest activity observed for C14 acyl chains and reduced activity for longer substrates (Stankeviciute et al., 2022). Similarly, sulfonolipid-producing *Alistipes finegoldii* predominantly incorporates medium-chain fatty acids ($\leq$ C16) into sulfonolipids (Radka et al., 2020). The comparable chain length preferences observed in both systems further support the idea that fjoh_2421 catalyzes a related acylation reaction during sulfonolipid biosynthesis in *F. johnsoniae*.

However, the highly similar lipidomic profiles observed for Δ2419 and Δ2421 raise the question, whether these genes encode enzymes with overlapping or identical function in sulfonolipid synthesis. Given that SulA has not been structurally and biochemically characterized in *F. johnsoniae* this cannot be ruled out. Both mutant strains produced 3-ketocapnine and capnine. However, fjoh_2419 and fjoh_2421 likely belong to different enzyme families that catalyze different reaction chemistries. Fjoh_2419 is closely related to *sulA* from *Alistipes finegoldii*, which has been biochemically and structurally characterized as a PLP-dependent α-oxoamine synthase. Members of this enzyme family catalyze the stereospecific carbon-carbon bond between the α-carbon of an amino acid and the carbonyl carbon of a fatty acyl thioester. In contrast, the ceramide synthase bCers from *Caulobacter crescentus* is independent of PLP and acts as an acyltransferase that catalyzes an amide bond formation during N-acylation of the sphingoid base. Given the homology of fjoh_2421 to bCers and its annotation to the acyl-CoA N-acyltransferase superfamily, fjoh_2421 is more likely to catalyze the N-acylation step in sulfobacin biosynthesis.

Together, these findings support fjoh_2421 encoding the sulfobacin synthase responsible for capnine N-acylation. Nevertheless, functional confirmation will require *in-tans* complementation, in which a functional copy of fjoh_2421 is expressed on a plasmid in the deletion mutant. Such *in-trans* complementations are commonly used to confirm gene function in bacterial metabolic pathways (de Maat et al., 2020, Tian et al., 2020). Additional biochemical assays will further support the proposed role.

4.1.4. Putative monooxygenase candidates are not involved in hydroxylation of sulfobacins

Sulfobacin B can further be modified by the introduction of a hydroxyl group, yielding sulfobacin D. In mammals, analogous hydroxylation reactions in sphingolipid metabolism are catalyzed by the sphingolipid delta(4)-desaturase/C4-monooxygenase (DES2). DES2 introduces a hydroxyl group at C4 of dihydroceramide to form phytoceramide (Mizutani et al., 2004). Therefore, the functional assignment of fjoh_1748 and fjoh_4604 as putative sulfobacin monooxygenases was based on shared protein family classification with the eukaryotic DES2.

Deletion of the monooxygenase candidates was not expected to completely impair gliding motility, unless hydroxylated sulfonolipids are the only species required for gliding. Deletion of fjoh_4604 resulted in an impaired gliding phenotype in *F. johnsoniae*, while growth in liquid culture was not affected. However, lipidomic analysis revealed an unchanged sulfonolipid profile compared to the wild type, indicating that this gene is not essential for sulfonolipid biosynthesis or hydroxylation. Similarly, disruption of fjoh_1748 via a frameshift mutation led to loss of motility without detectable changes in sulfonolipid composition. However, growth was strongly impaired in this mutant strain, which was observed during routine cultivation and microscopic analysis. Due to this growth deficiency, the lack of colony spreading of this strain may not be unequivocally attributed to a motility defect alone. Frameshift mutations can exert polar effects on downstream genes by disrupting transcription within operons. Since four genes located downstream of fjoh_1748 are oriented in the same direction, the observed phenotype may result from altered expression of downstream genes rather than solely from loss of fjoh_1748 function. Among these, two genes encode proteins of unknown function, fjoh_1744 is predicted to encode a peptidase, and fjoh_1747 is predicted to encode an aspartate aminotransferase. Aspartate aminotransferases have been shown to play important roles in bacterial growth and nitrogen fixation (Ledermann et al., 2024, Jansen et al., 2020). Deletion of the corresponding gene in *Rhizobium leguminosarum* resulted in impaired growth compared to the wild type (Ledermann et al., 2024). It is therefore plausible that altered expression of fjoh_1747 contributes to the growth defect observed in the fjoh_1748 mutant strain.

Although fjoh_1748 and fjoh_4604 are annotated to the same protein family of fatty acid desaturases as DES2, they do not show sequence homology to DES2, suggesting they are not closely related. In bacteria, sphingolipid hydroxylation has instead been attributed to distinct enzymes. For example, in *Caulobacter crescentus* the DesA-family fatty acid desaturase/hydroxylase CerH catalyzes a hydroxylation of dihydroceramide. Although CerH belongs to the same protein family as DES2, it belongs to a separate taxonomic sub lineage (Stankeviciute et al., 2022). Functionally, the two enzymes also differ in their modification sites. DES2 acts at C4 on the sphingoid base, whereas CerH hydroxylates C2 of the fatty acyl chain (Mizutani et al., 2004, Stankeviciute et al., 2022). Given that sulfobacin D also carries its hydroxylation at C2 of the acyl chain, the corresponding enzyme may be more closely related to bacterial ceramide hydroxylases,

rather than eukaryotic DES2 (Stankeviciute et al., 2022).

These findings suggest that neither fjoh_1748 nor fjoh_4604 is required for sulfobacin hydroxylation in *F. johnsoniae*. Instead, these genes may participate in modification of other membrane lipids or alter membrane physicochemical properties that are important for efficient gliding motility. To date, sulfonolipids are the only lipid class reported to be essential for gliding motility in *F. johnsoniae*, but the underlying mechanism remains unresolved (Abbanat et al., 1986, Vences-Guzmán et al., 2021). However, it is well known that the acyl chain composition of membrane lipids influences membrane fluidity. Together with other features like the head group identity, the presence and position of hydoxyl groups and double bonds affect lipid packing and membrane dynamics. These changes in membrane dynamics can also influence membrane protein localization and function (Renne and Ernst, 2023). Gliding motility in *F. johnsoniae* depends on the type IX secretion system, which comprises multiple membrane proteins and is essential for the secretion of motility adhesions to the cell surface (Johnston et al., 2018). Loss of lipid modifications, like hydoxylations or desaturations, following the deletion of fjoh_1748 or fjoh_4604 may increase membrane rigidity and thereby impair the localization and function of these components. Although both genes are annotated as fatty acid desaturases, their precise function and their potential role in membrane lipid remodeling or the gliding machinery remain to be elucidated.

4.2. Re-evaluation of the proposed sulfobacin biosynthesis pathway and its relevance to anaerobic model systems

Based on the results of this study and comparison with sphingolipid biosynthesis pathways in other organisms, the proposed sulfobacin biosynthesis pathway in *F. johnsoniae* can be reevaluated with respect to reaction order and its transferability to anaerobic model systems.

In bacterial sphingolipid synthesis, two alternative biosynthesis pathways have been proposed. One model follows the enzymatic reaction order of eukaryotic sphingolipid synthesis, whereas the second appears to be unique to bacteria (*Figure 2*). In the eukaryotic pathway, 3-ketosphinganine is first reduced to sphinganine by a 3-keto-sphinganine reductase, followed by N-acylation through the action of a ceramide synthase (Rabionet et al., 2014 Lee et al., 2022). In contrast, studies in Caulobacter crescentus suggest that N-acylation of the long-chain base precedes the reduction step, resulting in an oxidized dihydroceramide intermediate (Uchendu et al., 2024). This raises the question whether sulfobacin biosynthesis might follow a bacterial-specific sphingolipid pathway rather than the proposed eukaryotic reaction order.

In such a scenario, 3-ketocapnine would first undergo N-acylation to form an oxidized sulfobacin intermediate, which would subsequently be reduced to sulfobacin B. However, this reaction order seems unlikely in *F. johnsoniae*. Capnine formation has been well documented in this organism and related bacterial species (Godchaux and Leadbetter, 1984, Liu et al., 2022). Additionally, LC-MS/MS analysis performed in this work consistently identified capnine as a precursor of sulfobacin synthesis. These findings strongly

support a pathway in which reduction of 3-ketocapnine precedes the N-acylation step catalyzed by the sulfobacin synthase.

This reaction sequence is consistent with sulfonolipid biosynthesis described in anaerobic gut bacteria. In *Alistipes finegoldii* cysteate synthase activity, formation of 3-ketocapnine mediated by SulA, and subsequent reduction to capnine have been reported (Radka et al., 2022, Yang et al., 2025, Wu et al., 2024). The cysteate synthase identified in *A. finegoldii* is homologous to archaeal cysteate synthases, whereas cysteate synthases in aerobic bacteria are more closely related to cystathionine β-synthases (Yang et al., 2025). In contrast, the cysteate acyl-ACP transferase characterized in *A. finegoldii* is closely related to the corresponding enzyme in *F. johnsoniae* (Radka et al., 2022). This indicates that the reaction order of early steps in sulfobacin biosynthesis is conserved between *F. johnsoniae* and gut associated *Alistipes* species, although distinct enzyme families can catalyze analogous reactions in aerobic and anaerobic systems.

Alternative reaction sequences involving early modification of the sphingoid backbone have also been described in eukaryotic sphingolipid metabolism. In plants, sphingoid base hydroxylases introduce a hydroxyl group into sphinganine prior to acylation, generating phytosphingosine (Chen et al., 2008). Comparable early backbone modifications could contribute to the structural diversity of sulfonolipids observed in other sulfobacin producing bacteria, such as the rosette inducing fators RIF-1 and RIF-2 identified in *Algoriphagus machipongonensis* (Beemelmanns et al., 2014, Leichnitz et al., 2022).

However, in *F. johnsoniae*, the dominant sulfonolipid species detected in this work exhibit an unmodified capnine backbone, with hydroxylations occurring on the fatty acyl chain. This observation argues against early hydroxylation of capnine prior to the action of a sulfobacin synthase in this organism. Whether such modifications could occur in sulfobacin producing gut strains remains an open question. LC-MS-based analysis of sulfonolipids in the genera *Alistipes* and *Odoribacter* revealed a diverse set of sulfonolipid species, including compounds assigned to sulfobacin A and B, as well as flavochristamide A. Structural diversity among the different sulfonolipids was attributed to variations in fatty acyl chain lengh and the number of oxygen atoms. The sulfonolipids were described as sharing a capnine backbone, but modifications of the capnine backbone itself have not been reported (Walker et al., 2017).

In *F. johnsoniae*, hydroxylations of sulfonolipids, including the conversion of sulfobacin B to sulfobacin D, are more likely to represent a late modification step in sulfobacin biosynthesis. The monooxygenase candidates investigated in this work were selected based on their classification within the same protein family as the eukaryotic sphingolipid C4-monooxygenase DES2. However, deletion of these genes did not affect the sulfonolipid profile, indicating that they are not required for sulfobacin hydroxylation. Given the position of the hydroxyl group in sulfobacin D, the reaction more closely resembles a fatty acyl chain hydroxylation catalyzed by bacterial ceramide hydroxylase described in *Caulobacter crescentus* (Stankeviciute et al., 2022). Nevertheless, the enzymatic mechanism of bacterial ceramide hydroxylases has not yet been conclusively characterized, and it remains unclear whether this enzyme functions as a monooxy-

genase or whether a related enzyme mediates this reaction in *F. johnsoniae*. In anaerobic environments, oxygen-dependent monooxygenase reactions are unlikely to account for sulfobacin hydroxylation. If sulfobacin D is produced by anaerobic gut bacteria, this modification would require an alternative enzymatic mechanism that remains to be identified. Such a reaction could potentially be catalyzed by a hydroxylase or another oxygen-independent enzyme (Stankeviciute et al., 2022).

Taken together, the data presented here support a sulfobacin biosynthesis pathway in *F. johnsinae* that is catalyzed by enzymes homologous to bacterial sphingolipid biosynthetic enzymes, yet follows a reaction order resembling the eukaryotic pathway, in which reduction precedes N-acylation. Consistent with this model, key enzymatic steps preceding N-acylation have also been demonstrated in anaerobic sulfobacin-producing gut bacteria. This indicates that the proposed pathway provides a useful framework for investigating sulfobacin biosynthesis in anaerobic systems, although individual reactions may be catalyzed by distinct enzyme families in different ecological contexts (Figure 53).

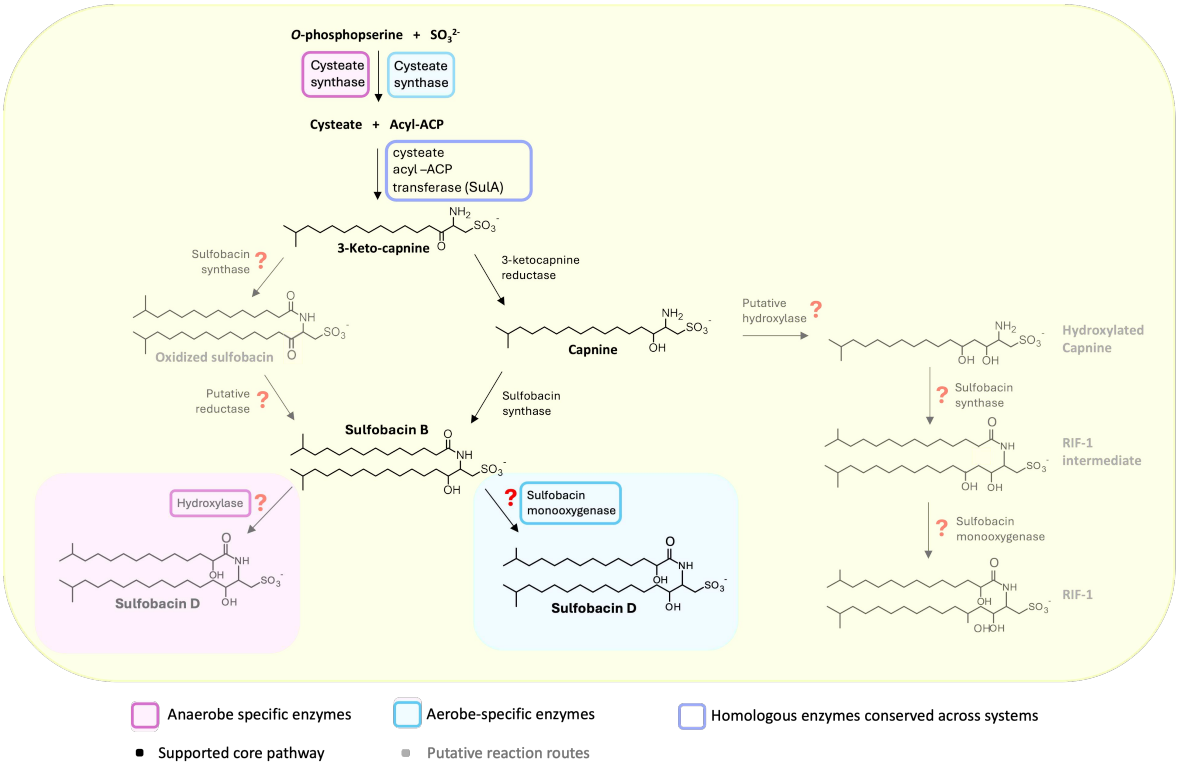

Figure 53.: **Sulfobacin biosynthesis and putative reaction routes in aerobic and anaerobic bacteria.** Reactions on a yellow background represent the conserved core pathway and putative scenarios shared between aerobic and anaerobic systems. The core pathway (black) depicts the conversion of O-phosphoserine and sulfite to cysteate, followed by condensation of cysteate with acyl-ACP to form 3-ketocapnine and its subsequent reduction to capnine. Capnine is then N-acylated to yield sulfobacin B. Putative reaction routes (grey) include a bacterial-type reaction order in which N-acylation of 3-ketocapnine precedes reduction, generating an oxidized sulfobacin intermediate and early hydroxylation of the capnine backbone prior to N-acylation, potentially yielding the rosette inducing factor RIF-1. Late hydroxylation of sulfobacin B to sulfobacin D is depicted as a terminal modification step. In aerobic bacteria, this reaction may involve an oxygen-dependent monooxygenase, whereas anaerobic systems likely require an alternative hydroxylation mechanism, potentially mediated by a hydroxylase. Colored boxes denote enzyme conservation: system-specific enzymes (blue or pink) and homologous enzymes from the same protein family present in both systems (purple) (Chen et al., 2008, Uchendu et al., 2024, Vences-Guzmán et al., 2021, Radka et al., 2022, Yang et al., 2025).

5. Conclusion and Outlook

Sulfonolipids represent an emerging class of bacterial membrane lipids that have gained increasing attention due to their bioactivity and potential role in host-microbe interactions. Sulfobacins produced by gut-associated bacteria have been shown to modulate immune responses through interactions with mammalian immune cell receptors. Several sulfonolipid producing genera have been identified. However, the distribution of this biosynthetic capacity among gut bacteria remains unclear, largely due to a limited understanding of the genetic and biochemical basis of sulfobacin biosynthesis.

This thesis aimed to elucidate the sulfobacin biosynthesis pathway in the genetically accessible model organism *F. johnsoniae*. Based on structural similarities between sulfonolipids and sphingolipids, the pathway was proposed to follow reactions analogous to bacterial ceramide biosynthesis. Through targeted mutagenesis and lipidomic analysis, this work provided new insights into several key steps of sulfobacin biosynthesis in *F. johnsoniae*.

Analysis of the pathway identified fjoh_2421 as a critical enzyme in sulfobacin biosynthesis. Deletion of this gene resulted in complete loss of sulfonolipid production and accumulation of the precursor capnine. Combined with the sequence homology to ceramide synthase described in *Caulobacter cerscentus*, these findings support fjoh_2421 as the first reported sulfobacin synthase gene. In contrast, deletion of fjoh_2557 did not impair gliding motility, indicating that this gene alone is not essential for cysteate synthesis. Instead, cysteate production likely depends on fjoh_1927 or both genes, as they potentially encode iso-enzymes. However, the functional assignment of a cysteate synthase in *F. johnsoniae* will require further investigation. Furthermore, the candidate monooxygenases fjoh_1748 and fjoh_4604 were not required for sulfobacin hydroxylation, demonstrating that functional prediction based on a shared protein family with eukaryotic sphingolipid monooxygenase DES2 was not suitable for identifying sulfonolipid-modifying enzymes.

Collectively, this work advances the mechanistic understanding of sulfobacin biosynthesis and identify fjoh_2421 as a central biosynthesis gene in *F. johnsoniae*.

Although this work clarified a critical step in sulfobacin biosynthesis, several questions remain to be answered. The genetic basis of cysteate synthesis requires further investigation, for example through generation of a double deletion mutant or biochemical characterization of fjoh_1927 and fjoh_2557.

Similarly, the enzymes responsible for the hydroxylation of sulfobacins remain unknown and will require a broader candidate screening. In addition, functional validation of fjoh_2421 by *in-trans* complementation and *in vitro* activity assays will be necessary to further substantiate its assignment as a sulfobacin synthase.

Once structurally and functionally characterized, fjoh_2421 can serve as a reference for homology based searches, enabling the identification of corresponding genes in sulfobacin producing gut strains and facilitating the discovery of unknown sulfonolipid producers in the human gut. However, transfer of these findings to gut-associated bacteria should consider metabolic and evolutionary differences between aerobic model organisms and predominantly strict anaerobic gut bacteria, as individual reactions may be catalyzed by distinct enzyme families.

Future studies combining comparative genomics, biochemical characterization, and anaerobic model systems will be essential to fully resolve the sulfobacin biosynthesis pathway. A deeper understanding of this pathway may ultimately clarify the ecological distribution and biological relevance of sulfonolipids within the human gut microbiota.

6. Disclaimer

ChatGPT Version 5.2 was used to assist with clarity and grammar corrections, to perform initial literature searches in specific topics, and to translate the abstract into German.

References

Abbanat, D. R., Godchaux, W., & Leadbetter, E. R. (1988). Surface-induced synthesis of new sulfonolipids in the gliding bacterium Cytophaga johnsonae. *Archives of Microbiology*, *149*(4), 358–364. https://doi.org/10.1007/BF00411656

Abbanat, D. R., Godchaux, W., Polychroniou, G., & Leadbetter, E. R. (1985). Biosynthesis of a sulfonolipid in gliding bacteria. *Biochemical and Biophysical Research Communications*, *130*(2), 873–878. https://doi.org/10.1016/0006-291X(85)90497-8

Abbanat, D. R., Leadbetter, E. R., Godchaux III, W., & Escher, A. (1986). Sulphonolipids are molecular determinants of gliding motility. *Letters to Nature*, *327*, 367–369.

Alegado, R. A., Brown, L. W., Cao, S., Dermenjian, R. K., Zuzow, R., Fairclough, S. R., Clardy, J., & King, N. (2012). A bacterial sulfonolipid triggers multicellular development in the closest living relatives of animals. *1*, 13. https://doi.org/10.7554/eLife.00013

An, D., Na, C., Bielawski, J., Hannun, Y. A., & Kasper, D. L. (2011). Membrane sphingolipids as essential molecular signals for Bacteroides survival in the intestine. *Proceedings of the National Academy of Sciences*, *108*(supplement_1), 4666–4671. https://doi.org/10.1073/pnas.1001501107

An, D., Oh, S. F., Olszak, T., Neves, J. F., Avci, F. Y., Erturk-Hasdemir, D., Lu, X., Zeissig, S., Blumberg, R. S., & Kasper, D. L. (2014). Sphingolipids from a Symbiotic Microbe Regulate Homeostasis of Host Intestinal Natural Killer T Cells. *Cell*, *156*(1-2), 123–133. https://doi.org/10.1016/j.cell.2013.11.042

Beemelmanns, C., Woznica, A., Alegado, R. A., Cantley, A. M., King, N., & Clardy, J. (2014). Synthesis of the rosette-inducing factor RIF-1 and analogs. *Journal of the American Chemical Society*, *136*(29), 10210–10213. https://doi.org/10.1021/ja5046692

Bertani, G. (1951). *Studies on lysogenesis. I. The mode of phage liberation by lysogenic Escherichia coli* (tech. rep.).

Bligh, E. G., & Dyer, W. J. (1959). A rapid method of total lipid extraction and purification. *Canadian Journal of Biochemistry and Physiology*, *37*(8), 911–917. https://doi.org/10.1139/o59-099

Braun, T. F., Khubbar, M. K., Saffarini, D. A., & McBride, M. J. (2005). Flavobacterium johnsoniae Gliding Motility Genes Identified by mariner Mutagenesis. *Journal of Bacteriology*, *187*(20), 6943–6952. https://doi.org/10.1128/JB.187.20.6943-6952.2005

Brown, E. M., Ke, X., Hitchcock, D., Jeanfavre, S., Avila-Pacheco, J., Nakata, T., Arthur, T. D., Fornelos, N., Heim, C., Franzosa, E. A., Watson, N., Huttenhower, C., Haiser, H. J., Dillow, G., Graham, D. B., Finlay, B. B., Kostic, A. D., Porter, J. A., Vlamakis, H., … Xavier, R. J. (2019). Bacteroides-Derived Sphingolipids Are Critical for Maintaining Intestinal Homeostasis and Symbiosis. *Cell Host & Microbe*, *25*(5), 668–680. https://doi.org/10.1016/j.chom.2019.04.002

Chen, M., Markham, J. E., Dietrich, C. R., Jaworski, J. G., & Cahoon, E. B. (2008). Sphingolipid Long-Chain Base Hydroxylation Is Important for Growth and Regulation of Sphingolipid Content and Composition in Arabidopsis. *The Plant Cell*, *20*(7), 1862–1878. https://doi.org/10.1105/tpc.107.057851

Dagert, M., & Ehrlich, D. (1979). *Prolonged incubation in calcium chloride improves the competence of Escherichia coli cells* (tech. rep.). https://doi.org/10.1016/0378-1119(79)90082-9

de Maat, V., Arredondo-Alonso, S., Willems, R. J. L., & van Schaik, W. (2020). Conditionally essential genes for survival during starvation in Enterococcus faecium E745. *BMC Genomics*, *21*(1), 568. https://doi.org/10.1186/s12864-020-06984-2

Ezraty, B., Gennaris, A., Barras, F., & Collet, J.-F. (2017). Oxidative stress, protein damage and repair in bacteria. *Nature Reviews Microbiology*, *15*(7), 385–396. https://doi.org/10.1038/nrmicro.2017.26

Ferrières, L., Hémery, G., Nham, T., Guérout, A. M., Mazel, D., Beloin, C., & Ghigo, J. M. (2010). Silent mischief: bacteriophage Mu insertions contaminate products of Escherichia coli random mutagenesis performed using suicidal transposon delivery plasmids mobilized by broad-host-range RP4 conjugative machinery. *Journal of bacteriology*, *192*(24), 6418–6427. https://doi.org/10.1128/JB.00621-10

Fitzgerald, K. A., & Kagan, J. C. (2020). Toll-like Receptors and the Control of Immunity. *Cell*, *180*(6), 1044–1066. https://doi.org/10.1016/j.cell.2020.02.041

Godchaux, W., & Leadbetter, E. R. (1980). Capnocytophaga spp. contain sulfonolipids that are novel in procaryotes. *Journal of Bacteriology*, *144*(2), 592–602. https://doi.org/10.1128/jb.144.2.592-602.1980

Godchaux, W., & Leadbetter, E. R. (1984). Sulfonolipids of gliding bacteria. Structure of the N-acylaminosulfonates. *The Journal of biological chemistry*, *259*(5), 2982–90.

Graham, D. E., Taylor, S. M., Wolf, R. Z., & Namboori, S. C. (2009). Convergent evolution of coenzyme M biosynthesis in the Methanosarcinales: cysteate synthase evolved from an ancestral threonine synthase. *Biochemical Journal*, *424*(3), 467–478. https://doi.org/10.1042/BJ20090999

Hanahan, D., Jessee, J., & Bloom, F. R. (1991). *Plasmid transformation of Escherichia coli and other bacteria* (tech. rep.). https://doi.org/10.1016/0076-6879(91)04006-a

Harrison, P. J., Dunn, T. M., & Campopiano, D. J. (2018). Sphingolipid biosynthesis in man and microbes. *Natural Product Reports*, *35*(9), 921–954. https://doi.org/10.1039/C8NP00019K

Heidler von Heilborn, D., Nover, L.-L., Weber, M., Hölzl, G., Gisch, N., Waldhans, C., Mittler, M., Kreyenschmidt, J., Woehle, C., Hüttel, B., & Lipski, A. (2022). Polar lipid characterization and descrip-

tion of Chryseobacterium capnotolerans sp. nov., isolated from high CO2-containing atmosphere and emended descriptions of the genus Chryseobacterium, and the species C. balustinum, C. daecheongense, C. formosense, C. gleum, C. indologenes, C. joostei, C. scophthalmum and C. ureilyticum. *International Journal of Systematic and Evolutionary Microbiology*, *72*(5). https://doi.org/10.1099/ijsem.0.005372

Hou, L., Tian, H. Y., Wang, L., Ferris, Z. E., Wang, J., Cai, M., Older, E. A., Raja, M. R. K., Xue, D., Sun, W., Nagarkatti, P., Nagarkatti, M., Chen, H., Fan, D., Tang, X., & Li, J. (2022). Identification and Biosynthesis of Pro-Inflammatory Sulfonolipids from an Opportunistic Pathogen Chryseobacterium gleum. *ACS Chemical Biology*, *17*(5), 1197–1206. https://doi.org/10.1021/acschembio.2c00141

Ikushiro, H., Hayashi, H., & Kagamiyama, H. (2003). Bacterial serine palmitoyltransferase: a water-soluble homodimeric prototype of the eukaryotic enzyme. *Biochimica et Biophysica Acta (BBA) - Proteins and Proteomics*, *1647*(1-2), 116–120. https://doi.org/10.1016/S1570-9639(03)00074-8

Imlay, J. A. (2013). The molecular mechanisms and physiological consequences of oxidative stress: lessons from a model bacterium. *Nature Reviews Microbiology*, *11*(7), 443–454. https://doi.org/10.1038/nrmicro3032

Jansen, R. S., Mandyoli, L., Hughes, R., Wakabayashi, S., Pinkham, J. T., Selbach, B., Guinn, K. M., Rubin, E. J., Sacchettini, J. C., & Rhee, K. Y. (2020). Aspartate aminotransferase Rv3722c governs aspartate-dependent nitrogen metabolism in Mycobacterium tuberculosis. *Nature Communications*, *11*(1), 1960. https://doi.org/10.1038/s41467-020-15876-8

Jarrell, K. F., & McBride, M. J. (2008). The surprisingly diverse ways that prokaryotes move. *Nature Reviews Microbiology*, *6*(6), 466–476. https://doi.org/10.1038/nrmicro1900

Johnston, J. J., Shrivastava, A., & McBride, M. J. (2018). Untangling Flavobacterium johnsoniae gliding motility and protein secretion. *Journal of Bacteriology*, *200*(2). https://doi.org/10.1128/JB.00362-17

Kamiyama, T., Umino, T., Satoh, T., Sawairi, S., Shirane, M., Ohshima, S., & Yokose, K. (1995). *Sulfobacins A and B, Novel von Willebrand Factor Receptor Antagonists I. Production, Isolation, Characterization and Biological Activities* (tech. rep.).

Kawahara, K., Moll, H., Knirel, Y. A., Seydel, U., & Zähringer, U. (2000). Structural analysis of two glycosphingolipids from the lipopolysaccharide-lacking bacterium Sphingomonas capsulata. *European Journal of Biochemistry*, *267*(6), 1837–1846. https://doi.org/10.1046/j.1432-1327.2000.01189.x

Kohayashi, J., Mikami, S., Shigemori, H., Takao, T., Shimonishi, Y., Izuta, S., & Yoshida, S. (1995). Flavocristamides A and B, new DNA polymerase α inhibitors from a marine bacterium Flavobacterium sp. *Tetrahedron*, *51*(38), 10487–10490. https://doi.org/10.1016/0040-4020(95)00631-H

Lavelle, A., & Sokol, H. (2020). Gut microbiota-derived metabolites as key actors in inflammatory bowel disease. *Nature Reviews Gastroenterology & Hepatology*, *17*(4), 223–237. https://doi.org/10.1038/s41575-019-0258-z

Ledermann, R., Bourdès, A., Schuller, M., Jorrin, B., Ahel, I., & Poole, P. S. (2024). Aspartate aminotransferase of Rhizobium leguminosarum has extended substrate specificity and metabolizes aspartate to enable N2 fixation in pea nodules. *Microbiology*, *170*(7). https://doi.org/10.1099/mic.0.001471

Lee, M.-T., Le, H. H., Besler, K. R., & Johnson, E. L. (2022). Identification and characterization of 3-ketosphinganine reductase activity encoded at the BT_0972 locus in Bacteroides thetaiotaomicron. *Journal of Lipid Research*, *63*(7), 100236. https://doi.org/10.1016/j.jlr.2022.100236

Leichnitz, D., Peng, C.-C., Raguž, L., Rutaganira, F. U. N., Jautzus, T., Regestein, L., King, N., & Beemelmanns, C. (2022). Structural and Functional Analysis of Bacterial Sulfonosphingolipids and Rosette-Inducing Factor 2 (RIF-2) by Mass Spectrometry-Guided Isolation and Total Synthesis. *Chemistry – A European Journal*, *28*(8). https://doi.org/10.1002/chem.202103883

Liebisch, G., Fahy, E., Aoki, J., Dennis, E. A., Durand, T., Ejsing, C. S., Fedorova, M., Feussner, I., Griffiths, W. J., Köfeler, H., Merrill, A. H., Murphy, R. C., O'Donnell, V. B., Oskolkova, O., Subramaniam, S., Wakelam, M. J., & Spener, F. (2020). Update on LIPID MAPS classification, nomenclature, and shorthand notation for MS-derived lipid structures. *Journal of Lipid Research*, *61*(12), 1539–1555. https://doi.org/10.1194/jlr.S120001025

Liu, Y., Wei, Y., Teh, T. M., Liu, D., Zhou, Y., Zhao, S., Ang, E. L., Zhao, H., & Zhang, Y. (2022). Identification and Characterization of the Biosynthetic Pathway of the Sulfonolipid Capnine. *Biochemistry*, *61*(24), 2861–2869. https://doi.org/10.1021/acs.biochem.2c00102

Maceyka, M., & Spiegel, S. (2014). Sphingolipid metabolites in inflammatory disease. *Nature*, *510*(7503), 58–67. https://doi.org/10.1038/nature13475

MacLean, B., Tomazela, D. M., Shulman, N., Chambers, M., Finney, G. L., Frewen, B., Kern, R., Tabb, D. L., Liebler, D. C., & MacCoss, M. J. (2010). Skyline: an open source document editor for creating and analyzing targeted proteomics experiments. *Bioinformatics*, *26*(7), 966–968. https://doi.org/10.1093/bioinformatics/btq054

Mcbride, M. J., & Kempf, M. J. (1996). *Development of Techniques for the Genetic Manipulation of the Gliding Bacterium Cytophaga johnsonae* (tech. rep. No. 3).

McBride, M. J. (2004). Cytophaga-Flavobacterium Gliding Motility. *Microbial Physiology*, *7*(1-2), 63–71. https://doi.org/10.1159/000077870

McBride, M. J., Xie, G., Martens, E. C., Lapidus, A., Henrissat, B., Rhodes, R. G., Goltsman, E., Wang, W., Xu, J., Hunnicutt, D. W., Staroscik, A. M., Hoover, T. R., Cheng, Y.-Q., & Stein, J. L. (2009). Novel features of the polysaccharide-digesting gliding bacterium Flavobacterium johnsoniae as revealed

by genome sequence analysis. *Applied and Environmental Microbiology*, *75*(21), 6864–6875. https://doi.org/10.1128/AEM.01495-09

Mizutani, Y., Kihara, A., & Igarashi, Y. (2004). Identification of the human sphingolipid C4-hydroxylase, hDES2, and its up-regulation during keratinocyte differentiation. *FEBS Letters*, *563*(1-3), 93–97. https://doi.org/10.1016/S0014-5793(04)00274-1

Mullis, K., Faloona, F., Scharf, S., Saiki, R., Horn, G., & Erlich, H. (1986). Specific Enzymatic Amplification of DNA In Vitro: The Polymerase Chain Reaction. *Cold Spring Harbor Symposia on Quantitative Biology*, *51*(0), 263–273. https://doi.org/10.1101/SQB.1986.051.01.032

Nelson, S. S., Bollampalli, S., & McBride, M. J. (2008). SprB Is a Cell Surface Component of the Flavobacterium johnsoniae Gliding Motility Machinery. *Journal of Bacteriology*, *190*(8), 2851–2857. https://doi.org/10.1128/JB.01904-07

Older, E. A., Mitchell, M. K., Campbell, A., Lian, X., Madden, M., Wang, Y., van de Wal, L. E., Zaw, T., VanderVeen, B. N., Tatum, R., Murphy, E. A., Chen, Y.-H., Fan, D., Ellermann, M., & Li, J. (2025). Human gut commensal Alistipes timonensis modulates the host lipidome and delivers anti-inflammatory outer membrane vesicles to suppress colitis in an Il10-deficient mouse model. *Gut Microbes*, *17*(1). https://doi.org/10.1080/19490976.2025.2517380

Older, E. A., Zhang, J., Ferris, Z. E., Xue, D., Zhong, Z., Mitchell, M. K., Madden, M., Wang, Y., Chen, H., Nagarkatti, P., Nagarkatti, M., Fan, D., Ellermann, M., Li, Y. X., & Li, J. (2024). Biosynthetic enzyme analysis identifies a protective role for TLR4-acting gut microbial sulfonolipids in inflammatory bowel disease. *Nature Communications*, *15*(1). https://doi.org/10.1038/s41467-024-53670-y

Peng, C.-C., Dormanns, N., Regestein, L., & Beemelmanns, C. (2023). Isolation of sulfonosphingolipids from the rosette-inducing bacterium Zobellia uliginosa and evaluation of their rosette-inducing activity. *RSC Advances*, *13*(39), 27520–27524. https://doi.org/10.1039/D3RA04314B

Rabionet, M., Gorgas, K., & Sandhoff, R. (2014). Ceramide synthesis in the epidermis. *Biochimica et Biophysica Acta (BBA) - Molecular and Cell Biology of Lipids*, *1841*(3), 422–434. https://doi.org/10.1016/j.bbalip.2013.08.011

Radka, C. D., Frank, M. W., Rock, C. O., & Yao, J. (2020). Fatty acid activation and utilization by Alistipes finegoldii, a representative Bacteroidetes resident of the human gut microbiome. *Molecular Microbiology*, *113*(4), 807–825. https://doi.org/10.1111/mmi.14445

Radka, C. D., Miller, D. J., Frank, M. W., & Rock, C. O. (2022). Biochemical characterization of the first step in sulfonolipid biosynthesis in Alistipes finegoldii. *Journal of Biological Chemistry*, *298*(8), 102195. https://doi.org/10.1016/j.jbc.2022.102195

Raetz, C. R., & Dowhan, W. (1990). Biosynthesis and function of phospholipids in Escherichia coli. *The Journal of biological chemistry*, *265*(3), 1235–8.

Raman, M. C. C., Johnson, K. A., Clarke, D. J., Naismith, J. H., & Campopiano, D. J. (2010). The serine palmitoyltransferase from Sphingomonas wittichii RW1: An interesting link to an unusual acyl carrier protein. *Biopolymers*, *93*(9), 811–822. https://doi.org/10.1002/bip.21482

Renne, M. F., & Ernst, R. (2023). Membrane homeostasis beyond fluidity: control of membrane compressibility. *Trends in Biochemical Sciences*, *48*(11), 963–977. https://doi.org/10.1016/j.tibs.2023.08.004

Ros-Rocher, N., Pérez-Posada, A., Leger, M. M., & Ruiz-Trillo, I. (2021). The origin of animals: an ancestral reconstruction of the unicellular-to-multicellular transition. *Open Biology*, *11*(2). https://doi.org/10.1098/rsob.200359

Ryan, E., Joyce, S. A., & Clarke, D. J. (2023). Membrane lipids from gut microbiome-associated bacteria as structural and signalling molecules. *Microbiology*, *169*(3). https://doi.org/10.1099/mic.0.001315

Safarchi, A., Al-Qadami, G., Tran, C. D., & Conlon, M. (2025). Understanding dysbiosis and resilience in the human gut microbiome: biomarkers, interventions, and challenges. *Frontiers in Microbiology*, *16*. https://doi.org/10.3389/fmicb.2025.1559521

Sato, K., Naya, M., Hatano, Y., Kondo, Y., Sato, M., Narita, Y., Nagano, K., Naito, M., Nakayama, K., & Sato, C. (2021). Colony spreading of the gliding bacterium Flavobacterium johnsoniae in the absence of the motility adhesin SprB. *Scientific Reports*, *11*(1), 967. https://doi.org/10.1038/s41598-020-79762-5

Sender, R., Fuchs, S., & Milo, R. (2016). Are We Really Vastly Outnumbered? Revisiting the Ratio of Bacterial to Host Cells in Humans. *Cell*, *164*(3), 337–340. https://doi.org/10.1016/j.cell.2016.01.013

Shrivastava, A., Lele, P. P., & Berg, H. C. (2015). A Rotary Motor Drives Flavobacterium Gliding. *Current Biology*, *25*(3), 338–341. https://doi.org/10.1016/j.cub.2014.11.045

Shrivastava, A., Rhodes, R. G., Pochiraju, S., Nakane, D., & McBride, M. J. (2012). Flavobacterium johnsoniae RemA Is a Mobile Cell Surface Lectin Involved in Gliding. *Journal of Bacteriology*, *194*(14), 3678–3688. https://doi.org/10.1128/JB.00588-12

Stankeviciute, G., Tang, P., Ashley, B., Chamberlain, J. D., Hansen, M. E., Coleman, A., D'Emilia, R., Fu, L., Mohan, E. C., Nguyen, H., Guan, Z., Campopiano, D. J., & Klein, E. A. (2022). Convergent evolution of bacterial ceramide synthesis. *Nature Chemical Biology*, *18*(3), 305–312. https://doi.org/10.1038/s41589-021-00948-7

Steinmetz, M., Le Coq, D., Djemia, H. B., & Gay, P. (1983). Analyse génétique de sacB, gène de structure d'une enzyme secrétée, la lévane-saccharase de Bacillus subtilis Marburg. *MGG Molecular & General Genetics*, *191*(1), 138–144. https://doi.org/10.1007/BF00330901/METRICS

Tian, X., Auger, R., Manat, G., Kerff, F., Mengin-Lecreulx, D., & Touzé, T. (2020). Insight into the dual function of lipid phosphate phosphatase PgpB involved in two essential cell-envelope metabolic pathways in Escherichia coli. *Scientific Reports*, *10*(1), 13209. https://doi.org/10.1038/s41598-020-70047-5

Uchendu, C. G., Guan, Z., & Klein, E. A. (2024). Spatial organization of bacterial sphingolipid synthesis enzymes. *Journal of Biological Chemistry*, *300*(5). https://doi.org/10.1016/j.jbc.2024.107276

Van Eeckhaut, A., Lanckmans, K., Sarre, S., Smolders, I., & Michotte, Y. (2009). Validation of bioanalytical LC–MS/MS assays: Evaluation of matrix effects. *Journal of Chromatography B*, *877*(23), 2198–2207. https://doi.org/10.1016/j.jchromb.2009.01.003

Vences-Guzmán, M. Á., Peña-Miller, R., Hidalgo-Aguilar, N. A., Vences-Guzmán, M. L., Guan, Z., & Sohlenkamp, C. (2021). Identification of the Flavobacterium johnsoniae cysteate-fatty acyl transferase required for capnine synthesis and for efficient gliding motility. *Environmental Microbiology*, *23*(5), 2448–2460. https://doi.org/10.1111/1462-2920.15445

Vogelstein, B., & Gillespie, D. (1979). Preparative and analytical purification of DNA from agarose. *Proceedings of the National Academy of Sciences*, *76*(2), 615–619. https://doi.org/10.1073/pnas.76.2.615

Walker, A., Pfitzner, B., Harir, M., Schaubeck, M., Calasan, J., Heinzmann, S. S., Turaev, D., Rattei, T., Endesfelder, D., Castell, W. z., Haller, D., Schmid, M., Hartmann, A., & Schmitt-Kopplin, P. (2017). Sulfonolipids as novel metabolite markers of Alistipes and Odoribacter affected by high-fat diets. *Scientific Reports*, *7*(1), 11047. https://doi.org/10.1038/s41598-017-10369-z

White, R. H. (1984). Biosynthesis of the sulfonolipid 2-amino-3-hydroxy-15-methylhexadecane-1-sulfonic acid in the gliding bacterium Cytophaga johnsonae. *Journal of Bacteriology*, *159*(1), 42–46. https://doi.org/10.1128/jb.159.1.42-46.1984

Wilkinson, T. G., Kedar, G. C., Lee, C., Guzmán, E. C., Smith, D. W., & Zyskind, J. W. (2006). The Synchrony Phenotype Persists after Elimination of Multiple GATC Sites from the dnaA Promoter of Escherichia coli. *Journal of Bacteriology*, *188*(12), 4573–4576. https://doi.org/10.1128/JB.00089-06

Wu, X., Hou, L., Zhang, H., Ma, Y., Wang, J., Cai, M., & Tang, X. (2024). Identification of 3-ketocapnine reductase activity within the human microbiota. *mLife*, *3*(2), 307–316. https://doi.org/10.1002/mlf2.12134

Yang, S., Wang, K., Hu, Y., Zhang, L., Zhang, C., Liu, Y., Li, Z., Jiang, L., Han, Y., Naowarojna, N., Wei, Y., & Zhang, Y. (2025). Studies on Two Convergently Evolved Cysteate Synthases in Sulfonolipid Biosynthesis. *ACS Chemical Biology*, *20*(11), 2560–2573. https://doi.org/10.1021/acschembio.5c00142

Zhu, Y., Thomas, F., Larocque, R., Li, N., Duffieux, D., Cladière, L., Souchaud, F., Michel, G., & McBride, M. J. (2017). Genetic analyses unravel the crucial role of a horizontally acquired alginate lyase for brown algal biomass degradation by Zobellia galactanivorans. *Environmental Microbiology*, *19*(6), 2164–2181. https://doi.org/10.1111/1462-2920.13699

A. Zusammenfassung

Sulfobacine sind bakterielle, bioaktive Sulfonolipide, die Entzündungsprozesse im Darm von Säugetieren hemmen und die Polarisation von Makrophagen unterdrücken, was auf eine immunmodulatorische Funktion hinweist. Darüber hinaus sind sie essenziell für die Motilität von *Flavobacterium johnsoniae* und induzieren Multizellularität bei Choanoflagellaten. Strukturell sind Sulfobacine mit Ceramiden verwandt, einer Unterklasse der Sphingolipide. Diese besitzen ein von Serin abgeleitetes Aminoalkohol-Rückgrat (Sphinganin), das über eine N-Acylierung mit einer Fettsäure verknüpft ist. Ceramide fungieren in Eukaryoten als bioaktive Signalmoleküle, und verwandte Sphingolipide werden auch von bestimmten Darmbakterien synthetisiert. Die Biosynthese der Sulfobacine erfolgt durch die N-Acylierung von Capnin, dem sulfonierten Analogon des Sphinganins. Zu den ersten Schritten dieses Synthesewegs zählen die Kondensation von Cysteat mit einem Acyl-Carrier-Protein, katalysiert durch die Cysteat-Acyl-ACP-Transferase (SulA), sowie die anschließende Reduktion von 3-Ketocapnin zu Capnin durch eine Dehydrocapnin-Reduktase. Die Enzyme, die die weitere Umwandlung von Capnin zu Sulfobacinen katalysieren, sind bislang jedoch nicht bekannt. Ziel dieser Arbeit war es, bislang unbekannte Gene der Sulfobacin-Biosynthese mithilfe von *Flavobacterium johnsoniae* als genetisch gut zugänglichem Modellorganismus zu charakterisieren. Vergleichende Genomanalysen bakterieller Ceramid-Biosynthesewege deuteten auf zwei Gene für Cysteat-Synthasen sowie auf ein potenzielles Sulfobacin-Synthase-Gen hin, das für die N-Acylierung von Capnin verantwortlich sein könnte. Darüber hinaus wurden zwei mutmaßliche Monooxygenasen als Kandidaten für die Biosynthese einer hydroxylierten Sulfobacin-Variante identifiziert. Zur funktionellen Analyse wurden markerlose Deletionsmutanten sowie Mutanten mit Verschiebung des Leserasters von *F. johnsoniae* erzeugt. Die Lipidzusammensetzung der Mutanten wurde mittels Tandem-Massenspektrometrie (LC-MS/MS) untersucht, während die Motilität mikroskopisch analysiert wurde. Im Mutantenstamm mit Deletion des potenziellen Sulfobacin-Synthase-Gens ging die Motilität vollständig verloren. LC-MS/MS-Analysen zeigten das vollständige Fehlen von Sulfobacinen sowie eine Akkumulation des Vorläufers Capnin und bestätigten damit die zentrale Rolle des deletierten Gens in der Sulfobacin-Biosynthese. Im Gegensatz dazu produzierten die Monooxygenase-Mutanten weiterhin Sulfonolipide, obwohl ihre Motilität beeinträchtigt war. Zusammenfassend identifiziert diese Arbeit ein bislang unbekanntes Schlüsselenzym der Sulfobacin-Biosynthese, eine mutmaßliche Sulfobacin-Synthase, die essenziell für die Motilität von *F. johnsoniae* ist.